ACHIEVING EVEN FROSTING ON THE OUTDOOR COIL ALONG THE AIRFLOW DIRECTION IN A SPACE HEATING AIR SOURCE HEAT PUMP FOR IMPROVED ENERGY EFFICIENCY AND OCCUPANT THERMAL COMFORT

BAI XIAOXIA

PhD

The Hong Kong Polytechnic University

2023

The Hong Kong Polytechnic University

Department of Building Environment and Energy Engineering

Achieving even frosting on the outdoor coil along the airflow direction in a space heating air source heat pump for improved energy efficiency and occupant thermal comfort

BAI Xiaoxia

A thesis submitted in partial fulfillment of the requirements for the Degree of Doctor of Philosophy

March 2023

Certificate of Originality

I hereby declare that this thesis is my own work and that, to the best of my knowledge and belief, it reproduces no material previously published or written, nor material that has been accepted for the award of any other degree or diploma, except where due acknowledgement has been made in the text.

_____ (Signed)

BAI Xiaoxia (Name of student)

Abstract

Air source heat pump (ASHP) is an important clean energy technology for building space heating and cooling. ASHP systems are widely accepted because of high energy efficiency and low initial and operating costs. Over the past decades, a growing number of countries have promoted the development and / or a wider application of ASHP technology by introducing favourable policies, so as to alleviate the energy crisis and environmental degradation. Therefore, with the continuous technology developments, future extensive applications of ASHP systems can be expected.

However, frosting on the surface of the outdoor coil in an ASHP unit significantly limits its efficient operation. It is well understood that when the surface temperature of an outdoor coil in an ASHP unit is lower than the dew point of humid ambient air and freezing point of water, frost will form on the outdoor coil surface. Frosting may lead to a series of negative impacts on the operation of ASHP units, including increased heat transfer resistance between ambient air and refrigerant, increased air pressure drop in an outdoor coil, reduced output heating capacity and coefficient of performance (COP) of the ASHP unit and the necessity of periodical defrosting operations. Therefore, frosting is an unwanted phenomenon that should be suppressed as much as possible for a higher heating operating efficiency and better indoor thermal comfort. Up to date, a great number of studies have focused on developing effective frosting-suppression technologies and efficient defrosting methods, with however inadequate attentions paid to the uneven frosting of outdoor coils, a commonly seen phenomenon for space heating ASHPs. In

particular, uneven frosting along the airflow direction, i.e., more frost deposited on the windward side than that on the leeward side in a traditional single-fan outdoor coil, has been commonly observed. As a result, frost deposited on the windward side may rapidly block the airflow path, causing a rapid deterioration in the heating performances of an ASHP unit, the energy waste during defrosting, and frequent defrosting operations. Although there have been efforts to deal with uneven frosting along the airflow direction, it cannot be effectively avoided in ASHP units where traditional single-fan outdoor coils with a fixed airflow direction are used. To effectively alleviate uneven frosting along airflow direction, a novel dual-fan outdoor coil (DFOC) that can alternately reverse the airflow direction has been proposed and studied, experimentally and by modelling, in the research project reported in this Thesis.

This Thesis begins with reporting the development of an experimental novel DFOC having two identical fans, and an experimental ASHP unit using the DFOC (ASHP / DFOC). The two fans, Fan A and Fan B, may operate alternately to reverse airflow direction based on a pre-set value of time interval for alternate operation (t_{TIAO}). An experimental ASHP / DFOC setup was established. The setup included the experimental ASHP / DFOC unit and an environmental chamber where there were two rooms, one for a simulated indoor space and the other for simulated outdoor environment. A computerised measuring and monitoring system that can collect real-time data for all key operating parameters in the experimental setup has been installed. The availability of the setup would facilitate all the experimental work required in the research project reported in this Thesis.

Secondly, the Thesis presents an experimental study on even frosting characteristics of the experimental ASHP / DFOC unit in terms of the frosting / defrosting duration, the total output heating capacity and COP at different dual-fan operating modes. There were seven experimental cases including both single and multiple frosting-defrosting operation cycles. The experimental results demonstrated that when using the experimental DFOC in Cases 3, 4 and 7, the heating / frosting duration was lengthened by 23.6%, 34.5% and 46.4%, and the averaged output heating capacity, $\bar{q}$, was increased by 5.5%, 9.5% and 9.6 %, and averaged *COP*, $\overline{COP}$ by 6.7%, 10.5% and 11.1% respectively, and the defrosting frequency was decreased by 33.3% in Case 7, when compared to using the traditional single-fan outdoor coil in other cases. Besides, as t_{TIAO} values were decreased from 15 mins to 10 mins for both fans, and to 6 mins for Fan A and 8 mins for Fan B, heating / frosting operation duration was increased by 8.9% and 19.4%, respectively, at a higher $\bar{q}$ and $\overline{COP}$, as compared to those using the traditional single-fan outdoor coil. The experimental results clearly demonstrated that the use of the experimental DFOC can help achieve evener frosting along airflow direction, and hence a longer heating operation duration and a higher operating efficiency and output heating capacity.

Thirdly, the Thesis reports on the development and experimental validation of a dynamic mathematical model for the experimental ASHP / DFOC unit, in order to more effectively and comprehensively study the operating characteristics of the ASHP / DFOC unit at different fan operating modes, with different configurations and under different operating ambient conditions. With the validated model, a follow-up modelling study for different operating modes of the two fans, fin pitches and operating ambient conditions was carried out. The modelling results

demonstrated that by optimizing fan operating mode, the difference in frost thickness between the windward and leeward sides of DFOC can be reduced by up to 77.3 %, the averaged output heating capacity and COP improved by up to 11.1 % and 12.7 %, respectively, and the number of switching operation of the two fans decreased by 55.6 %. Besides, the recommendations for using the DFOC at different operating modes of the two fans, different fin pitches and operating ambient conditions were also made.

Finally, the Thesis presents the development of a GRNN model-based optimal control strategy that enables the efficient operation of the experimental ASHP / DFOC unit at varying ambient conditions. A database for developing the GRNN model was established first, and a new coefficient of performance-related index, which was the change rate of averaged COP (CRAC), was proposed after analysing the database. Then, based on the developed database and CRAC, a GRNN model was developed and validated, and then used to predict and search the optimal dual-fan operating modes when the experimental ASHP / DFOC unit was operated at different ambient air conditions. Lastly, an optimal control strategy for the experimental ASHP / DFOC unit based on those identified optimal dual-fan operating modes was developed and experimentally validated. The experimental results demonstrated that the use of the developed optimal control strategy led to a higher heating efficiency, a longer frosting - defrosting duration and a fewer number of dual-fan switching for the experimental ASHP / DFOC unit, with its averaged COP improved by 9.9 % and 6.8 %, CRAC decreased by 17.1 % and 10.5 %, defrosting frequency reduced by 22.2 % and 12.5 %, and averaged frosting - defrosting duration

extended by 32.8 % and 19.4 %, respectively, when compared to the use of traditional single-fan operating mode and a fixed dual-fan operating mode at varying ambient conditions.

Publications arising from the Thesis

Journal Papers

- **Bai Xiaoxia**, Liu Shengnan, Deng Shiming, Zhang Long, Wei Mincheng. (2022). An experimental study on achieving even-frosting for an air source heat pump using a novel dual-fan outdoor coil. Energy and Buildings, 255, 111695. (Based on Chapter 5).

- **Bai Xiaoxia**, Liu Shengnan, Deng Shiming, Zhang Long, Wei Mincheng. (2023). A modelling study on the frosting characteristics of a novel dual-fan outdoor coil in an Air Source Heat Pump unit. Applied Thermal Engineering, 222, 119933. (Based on Chapter 6).

- **Bai Xiaoxia**, Liu Shengnan, Deng Shiming, Zhang Long, Wei Mincheng. (2023). An optimal control strategy for ASHP units with a novel dual-fan outdoor coil for evener frosting along airflow direction based on GRNN modelling. Energy and Buildings, 292 113136. (Based on Chapter 7).

Acknowledgements

I must express my sincere grateful thanks to my Chief Supervisor, Prof. Wei Minchen, and my Co-Supervisor, Dr. You Ruoyu, both from the Department of Building Environment and Energy Engineering, The Hong Kong Polytechnic University (HKPU), for their continuous helps and valuable advices during my doctoral study.

Secondly, my special thanks must go to Prof. Deng Shiming, my former chief supervisor at HKPU, now from Qatar University, for providing me with the precious opportunity to pursue my PhD study. During my doctoral study, he has provided efficient guidance to my academic papers and PhD thesis. As a student, I always kept making the same mistake over and over again, but he always took the trouble to help me correct the mistake, giving me a constant inner strength: you should do better to be excellent. Words are far from being able to describe my gratitude to Prof. Deng. Furthermore, I would also like to express my gratitude to Dr. Zhang Long, from the Beijing Institute of Technology, for generously sharing his professional knowledge and experience with me, which was of great help to my research.

Thirdly, I would like to thank my colleagues in HKPU, Dr. Yan Huaxia, Dr. Fang Guanyu, Dr. Yang Liu, Dr. Fang Yibo and Miss Liu Shengnan for their supports to my PhD. study, and friends from Beijing University of Technology, Dr. Wang Dan, Mr. Lin Yao and Mr. Chen Ran and Dr. Liang Shiming from Qingdao University of Technology, for their online companionship in difficulty times. During my doctoral study in HKPU, I also gained new friendships, so I would express my gratitude to Dr. Niu Ben, Dr. Yang Su, Dr. Hu Lingquan, Dr. Yu Jiali, Dr. Zhang

Yingbo, and Dr. Wei Zhengyao, for those passionate and happy moments on badminton courts and wonderful dinners in our secret base. I wish you good health and all your wishes to come true.

Finally, my deepest gratitude would go to my family for their silence supports and encouragement over the last three years. ‘Seize the day and live it to the full’, all thanks will turn into my motivation to pursue the truth and faith.

Table of Contents

Page

List of Figures

List of Tables

Nomenclature

A	surface area [m^2]
$c_{p,a}$	air specific heat at constant pressure [kJ/(kg•K)]
C	empirical water vapor absorbed coefficient [1/s]
COP	coefficient of performance
$\overline{COP}$	averaged coefficient of performance
D_c	collar diameter (= tube external diameter + fin thickness) [m]
D_{eff}	effective water vapor diffusion coefficient [m^2/s]
D_h	hydraulic diameter of finned tube heat exchanger [m]
D_{std}	standard water vapor diffusion coefficient [m^2/s]
ΔE	heating energy loss [kJ]
F_p	Fin pitch [m]
F_s	Fin spacing (= fin pitch - fin thickness) [m]
h	convective heat transfer coefficient [W/(m^2•K)]
h_{eff}	effective convective heat transfer coefficient [W/(m^2•K)]
h_r	refrigerant enthalpy [J/kg]
h_m	convective mass transfer coefficient [m/s]
i	i^{th} moment [s]
j	j^{th} parameter
j_{dry}	Colburn heat transfer factor at dry condition
k	thermal conductivity [W/(m•K)]
l_{sv}	latent heat of ablimation for water vapor [kJ/kg]
m	mass flow rate [kg/s]
$\dot{m}$	water vapor mass flux [kg/(m^2•s)]
m_r	refrigerant mass flow rate [kg/s]

M	mass [kg]
N	Number of tube row
P_t	transverse tube spacing [m]
P_l	longitudinal tube spacing [m]
P	Pearson Correlation Coefficient
$\|P\|$	absolute value of Pearson Correlation Coefficient
ΔP	air pressure difference [Pa]
$\dot{q}$	heat flux [W/m^2]
q	output heating capacity [kW]
$\bar{q}$	averaged output heating capacity [kW]
Q	output heating capacity [kW]
$\dot{Q}$	instantaneous output heating capacity [kW]
Re	Reynolds number
Rem_t	periodic function for calculating fan status
RH	relative humidity [%]
t	time [s]
t_A	running duration of Fan A [min]
t_B	running duration of Fan B [min]
t_{defn}	defrosting duration at the n^{th} cycle
t_{end}	the end of multiple frosting - defrosting cycles [s]
t_{fn}	frosting duration at the n^{th} cycle
t_FanA	running time duration of Fan A [min]
t_FanB	running time duration of Fan B [min]
T	Temperature [K]
T_a	air temperature [˚C]

$\overline{T}$	average temperature [K]
V	velocity [m/s]
V_a	air velocity [m/s]
w	water vapor moisture content [kg/kg]
$\overline{w}$	average water vapor moisture content [kg/kg]
W	power input [kW]
x	input parameter
y	measured value on output side
$\hat{y}$	predicted value on output side
η	efficiency [-]
ρ	density [kg/m^3]
δ	thickness [mm]
δ_f	frost thickness [mm]
δ_{fin}	fin thickness [m]
θ	fin inclination angle [°]
κ	heating capacity loss efficient [%/min]
$\overline{\kappa}$	average heating capacity loss efficient [%/min]
σ	smooth factor
ε	relative evenness degree of frost [%]

List of Abbreviations

a	air
a,in	inlet air
a,out	outlet air
ave	average
ASHP	Air Source Heat Pump
ASHP / DFOC	Air Source Heat Pump unit having the novel Dual-Fan Outdoor Coil
CF	Counter Flow
def	defrosting
DFOC	Dual-Fan Outdoor Coil
eff	effective
EEP	Expected Error Percentage
f	frost
f,a	frosting rate
fin	fin
fs	frost surface
f-d	frosting - defrosting
FC	Fully Closed
FO	Fully Opened
FTHX	Finned Tube Heat Exchanger
GRNN	Generalized Regression Neural Network
HGBD	Hot Gas Bypass Defrosting
HVAC	Heating, Ventilation and Air Conditioning

i	ice
lat,fs	latent at the frost surface
MAE	Mean Absolute Error
OPT	Optimal dual-fan operating mode
OP	Operated
PF	Parallel Flow
RE	Relative error
RCD	Reverse Cycle Defrosting
sat	saturated
sens,a	air side sensible
sens,fs	sensible at the frost surface
surf	surface
sys	system
SD	Shut Down
tot	total
tot,a	air side total
tot,fs	total at the frost surface
tube	tube
TEPS	Tube-Encircled Photoelectric Sensor
TES	Thermal Energy Storage
T-H-T	Temperature-Humidity-Time
TIAO	Time Interval for Alternate Operation
T-T	Time-Temperature
TMYD	Typical Meteorological Year Database

VRF	Variable Refrigerant Flow
δ, f	for increasing frost thickness
ρ, f	for increasing frost density

Chapter 1

Introduction

Air Source Heat Pump (ASHP) is an important energy-saving technology for its merits of high operating energy efficiency, environmentally friendliness and ease of installation [Bai et al., 2018]. The applications of ASHP technology have actually been very diversified, including drying industry, food preservation and storage, hot water supply and building space cooling and heating, etc. Among those, using ASHP technology for building space heating and cooling has become increasingly important. In 2015, The Technology Center of the Ministry of Housing and Urban-rural Development of the Peoples' Republic of China issued an application manual on classifying air thermal energy as a kind of renewable energy. Since then, increasing the use of ASHP units has been promoted by relevant national policies and with strong supports from relevant industry.

However, frosting on the outdoor coil surface of an ASHP unit was one of the issues that limit the further wider application of ASHP units. When the temperature of an outdoor coil surface was lower than both the dew point of moist air and the freezing point of water, frost will form on the outdoor coil surface [Yao et al., 2004]. Frosting on a cold surface is an unwanted phenomenon that hinders the heat transfer efficiency of an outdoor coil. It would cause the deterioration in output heating capacity and COP, leading to an unstable heating process and requiring periodic defrosting operation [Özkan and Özil, 2006]. Therefore, a great number of experimental and mathematical studies on frosting suppression have been carried out in the past decades, covering frosting mechanism [da Silva et al., 2011; Piucco et al., 2008], developing frosting suppression technology [Liang et al., 2020; Song et al., 2016b]and novel

defrosting methods [Huang et al., 2009], defrosting initiation methods [Zhu et al., 2015], and effective melted frost drainage methods [Song et al., 2016a] following a defrosting operation.

One of the problems associated with frosting was uneven frosting along the airflow direction in an outdoor coil, which has been observed in many previous studies [Breque and Nemer, 2017; Carlson et al., 2001; Yao et al., 2004]. It normally occurred in a traditional single-fan outdoor coil, where airflow direction was usually fixed from windward side to leeward side. As a result, frost deposited on the windward side was always more than that on the leeward side of the outdoor coil. Basically, uneven frosting along the airflow direction was inevitable when such a traditional single-fan outdoor coil was used. Uneven frosting along the airflow direction would further lead to a lower operating efficiency during frosting operation, an even shorter frosting duration or more frequent defrosting operation, and a poorer defrosting efficiency. This therefore further negatively affected indoor thermal comfort for occupants and penalized the operating efficiency of an ASHP during both frosting and defrosting operations. However, uneven frosting along the airflow direction has been inadequately studied, and only a very limited methods were proposed for alleviating the uneven frosting between windward and leeward sides of a traditional single-fan outdoor coil. In fact, uneven frosting along the airflow direction cannot be fundamentally avoided in such a traditional single-fan outdoor coil due to its fixed airflow direction.

Therefore, to achieve evener frosting along the airflow direction in outdoor coils of ASHP units for improving their operating performances as well as indoor thermal comfort levels under frosting conditions, a novel outdoor coil with two identical fans, which was able to alternately reverse airflow direction, was proposed. Based on the proposed novel dual fan outdoor coil (DFOC), a research project to develop an experimental ASHP unit having an experimental

novel dual-fan outdoor coil (ASHP / DFOC) through experiments and mathematical modelling has been carried out and the project results are presented in this Thesis.

In this Thesis, to begin with, a detailed literature review related to the frosting and defrosting issues in ASHP units is presented in Chapter 2. The reviewed literature covered: firstly, frosting mechanism and its impacts on the operating performances of ASHP units are reported; secondly, the investigated frosting mitigation methods are presented, with particular reference to summarising uneven frosting mechanism and discussing reasons for uneven frosting; thirdly, existing modelling studies on frosting characteristics are reviewed; and this is followed by reporting previous studies related to defrosting for ASHP units; fourthly, intelligent control optimization methods for building heating, ventilation and air conditioning (HVAC) systems are reviewed. Finally, the identified research gaps are presented based on the literature review.

Chapter 3 presents the research proposal, which covers the backgrounds, project title, objectives and research methodologies for the research project reported in this Thesis.

In Chapter 4, a detailed description on an experimental setup used to facilitate carrying out the research project reported in this Thesis is presented. Firstly, an experimental novel DFOC is described in great detail. Secondly, a complete experimental ASHP / DFOC unit is detailed. Finally, the experimental setup including the experimental ASHP / DFOC unit, an environmental chamber, sensors / transducers and a computerised data collecting system, are reported. The availability of the complete experimental setup including the experimental ASHP / DFOC unit and the environmental chamber is expected to be essential in successfully carrying out the research project reported in this Thesis.

Chapter 5 reports an experimental study on even frosting characteristics for the experimental ASHP / DFOC unit in terms of frosting / defrosting duration, the total output heating capacity and COP at different dual-fan operating modes. In this experiment study, seven experimental cases with both single-fan operating modes and dual-fan operating modes were investigated under the standard frosting ambient condition. The frosting performances in terms of frost thickness on the leeward and windward sides of the finned tube heat exchanger (FTHX) in the experimental DFOC and frosting duration in the seven cases were studied in detail and compared. The experimental results demonstrated that the use of the experimental DFOC can help achieve evener frosting along airflow direction, and hence a longer heating operating duration and a higher operating efficiency and output heating capacity.

In Chapter 6, to more comprehensively study the operating characteristics of an ASHP / DFOC unit at different fan operating modes, with different configurations of the FTHXs and under different operating ambient conditions, the development and experimental validation of a dynamic module-based mathematical model for the experimental ASHP / DFOC unit is presented. Using the validated model, a follow-up modelling study on the frosting performances of the experimental ASHP / DFOC unit in terms of different operating modes of the two fans, different fin pitches and operating ambient conditions was carried out. The mathematical model was proved to be capable of simulating the frosting performances of the experimental ASHP / DFOC unit at non-experimental DFOC configuration and operating ambient conditions, which is helpful for the design and control strategy development of an ASHP / DFOC unit.

Chapter 7 reports the development of a GRNN model-based optimal control strategy that enables the efficient operation of the experimental ASHP / DFOC unit at varying ambient

conditions. To develop the optimal control strategy, a database for developing the GRNN model was established first, and a new coefficient of performance related index, which was the change rate of averaged COP (CRAC), was proposed after analysing the database. Then, based on the developed database and CRAC, a GRNN model was developed and validated, and thereafter used to predict and search for the optimal dual-fan operating modes when the experimental ASHP / DFOC unit was operated at different ambient air conditions. Lastly, an optimal control strategy for the experimental ASHP / DFOC unit based on those identified optimal dual-fan operating modes was developed and experimentally validated. The experimental results demonstrated that the use of the developed optimal control strategy led to a higher heating operating efficiency, a longer frosting - defrosting duration and a fewer number of dual-fan switching for the experimental ASHP / DFOC unit.

Finally, the Conclusions of the Thesis and the proposed future work are given in Chapter 8.

Chapter 2

Literature review

2.1 Introduction

In recent years, the energy use for building heating, ventilation and air conditioning (HVAC) systems has taken a large part at ~ 40 % - 60 % of the total building energy consumption [Akram et al., 2022], as a result of achieving an improved working / living standard in buildings. To reduce the fossil fuel based energy use for the operation of HVAC systems, renewable energy has been widely applied or building space heating and cooling, including solar energy and ambient air for ASHP units. As one of the most popular green energy technologies, an ASHP unit is a reliable and efficient device for building heating and cooling. With the energy crisis being at the forefront of world attention, and given the Carbon Neutrality Target set by China government, there has been an increased interest in ASHP technology due to its merits in energy saving, low initial cost and ease of installation and use. Over the past decades, the European Union [2009] and China [2015] respectively classified ASHP as a renewable energy source technology. Since then, ASHP units have been increasingly used in many countries for building heating / cooling, food preservation and drying industry, etc., leading to a growing market share of ASHP units in the global HVAC equipment market on a year by year basis. In 2021, t more than 50% of the global ASHP products were sold in China, 30% in Europe, and 10 % in Japan. Therefore, ASHP technology plays an important role in mitigating the energy shortage worldwide.

An ASHP unit can be used for both space heating and cooling. During heating seasons, an ASHP unit can be used to extract heat from outdoor ambient air and transfer the extracted heat to an indoor space for thermal comfort. However, when an ASHP unit operates in a humid and cold climate region, frost may deposit on its outdoor coil surface and thus hinder its high-efficient heating operating performances. Frosting is an unwanted but inevitable phenomenon, which may result in a series of negative impacts on the operating performances of ASHP units [Brian et al., 2002; Wang et al., 2011], such as decreased output heating capacity and coefficient of performance (COP), as well as requiring periodic defrosting. Therefore, a great number of studies have been carried out to alleviate frosting as much as possible, so as to achieve a more stable operation and higher heating performances of ASHP units under frosting conditions.

In this Chapter, a comprehensive literature review on the frosting / defrosting problems of ASHP units and other related issues is presented. Firstly, the frosting mechanism and its impacts on the operating performances of ASHP units are reported. Secondly, a review of various existing frosting mitigation methods is presented, including anti-frosting methods, and even frosting methods, with a particular emphasis on uneven frosting and its underlying reasons. Thirdly, previous modelling studies on frosting characteristics based on a simple geometry / standalone exchanger and a complete ASHP unit, are reviewed. This is followed by reporting the studies on defrosting-related issues of ASHP units. Then, intelligent optimization methods used in the control of HVAC system / ASHP units, are reviewed and presented. Finally, a number of key issues that call for additional research have been identified and summarised. It is expected that successful studying of these issues will help improve the operating / heating performances of ASHP units under frosting / defrosting conditions, so as to contribute to the advances of ASHP technology.

2.2 Frosting mechanism and impacts on the operating performances of ASHP units

In this Section, the factors affecting frost formation, a frost formation process, and the impacts of frosting on the operating performances of ASHP units, are reviewed respectively.

2.2.1 Factors affecting frosting

When a cold surface temperature was lower than the dew point of surrounding moist air and the freezing point of water, frost will form and deposit on the cold surface. Frosting is a complex heat and mass transfer process, which is actually dominated by a number of factors. In the past decades, both experimental and mathematical studies have been carried out to investigate different factors that impact frosting on a cold surface. According to the outcomes of these studies, there are main six factors that significantly impact frosting, i.e., the ambient air temperature, ambient air humidity, air velocity, cold surface temperature, surface roughness and wettability of the cold surface [Kondepudi and O'Neal, 1989; Lee and Ro, 2002]. The way each of these factors affecting frost formation on a cold surface is as follows:

Firstly, ambient air temperature and humidity are the two fundamental factors that determine a frosting process. Trammell et al [1968] experimentally found that air temperature had a smaller effect than other parameters on the growth rate of frost thickness on a flat plate. Brian et al [1970] indicated that frost thickness decreased with an increase in air temperature based on a series of experiments. Han and Ro [1999] believed that for parallel plates, frost thickness was increased with an increase in air temperature when the dew point was below 0 °C. Rite and

Crawford [1990] experimentally investigated the effects of various parameters on frost formation and performance of a domestic refrigerator-freezer with a finned tube evaporator coil. Their results suggested that the frosting rate was increased at a higher air humidity, temperature, flow rate and lower refrigerant temperature. R.Östin and Andersson [1991] experimentally indicated that both the surface temperature of plates and air relative humidity were found to have important effects on frost thickness. Frost density was found to increase with an increase in relative humidity and in particular in air velocity. Yan et al [2003] experimentally proved that the rate of pressure drop in outdoor coil was increased rapidly as air relative humidity was increased. Amer and Wang [2020] showed that increasing air relative humidity would not only increase frost thickness, but also affect frost property, such as density.

Secondly, related studies have shown mixed results on the effects of air face velocity on frost growth. Some believed that a lower air velocity would facilitate a fast frost formation. Yan et al [2003] experimentally studied the performance of FTHXs operating under frosting conditions, and the study results demonstrated that the rate of frost formation was greater at a lower air flow rate. Similarly, Lee and Ro [2002] found that with lower air velocities, a frost layer became slightly thicker. However, others concluded that air velocity may have a positive impact on the frosting process. For example, O'Neal and Tree [1984] and Yamakawa et al [1972] showed that frost thickness was increased with an increase in Reynolds number. Furthermore, there were also experimental results demonstrating that the impact of air velocity on frosting was insignificant. Tokura et al [1988], and Yonko and Sepsy [1967] believed that air velocity had no significant influence on frost growth rate based on experimental study results. Yang et al [2006] found that increasing air velocity had little effect on mass transfer under turbulent flow, while frost growth under laminar flow was influenced by air velocity. Besides, a modelling study conducted by Kandula [2011] found that air velocity did not have

an appreciable effect on frost thickness, even though frost density was increased significantly as a result of an increased air velocity.

Thirdly, cold surface temperature is another dominant factor affecting a frosting process. The lower the cold surface temperature, the faster the frost grows. This conclusion has been seen in many previous studies. For example, Lüer and Beer [2000] theoretically and experimentally studied the frost formation on cooled parallel plates under laminar forced convection, and found that cold surface temperature significantly affected the averaged frost thickness and density. Besides, Lee and Lee [2018] demonstrated that as cooling surface temperature was decreased, the increase in the amount of frost was insignificant in the frosting initiation stage. Lei et al [2022] also proved that as surface temperature was decreased, frost thickness increased and surface roughness became more remarkable, based on their experimental results.

Moreover, when different fin material was used, or the surface treatment process of fins was different, cold surface roughness and wettability would be changed as well. Therefore, a series of studies on the impacts of cold surface roughness and wettability on frosting were carried out based on different fin materials [Abbas and Park, 2021] or different surface treatment processes, such as using surface coating technology to obtain those fins having different surface energy and contact angles. Normally, the lower the surface energy, the higher the contact angle of the surface, and vice versa [Sanders, 1974]. Surface energy was believed to only affect the nucleation stage of a frosting process [Na and Webb, 2003]. However, different contact angles for different cold surfaces show different frosting and defrosting properties, such as the hydrophobic surface, hydrophilic surface, super-hydrophobic and super-hydrophilic surfaces [Boyina et al., 2019]. Zuo et al [2017] experimentally studied an aluminate coupling agent on an aluminium (Al) surface with a hydrophobic coating having a static contact angle of 147 °,

and their results indicated that the hydrophobic coating surface obviously restrained frost growth. Kim and Lee [2011b, 2011a] investigated the effect of fin surface with different contact angles on the frosting / defrosting performances of a heat pump unit, and they found that on the hydrophobic surface, the degree of super-cooling required for the onset of frost nucleation was affected, but its frost suppression ability was not significant. Besides, the frost layer on a hydrophilic fin was thinner and had a greater average density. For defrosting performance, Jing et al [Jing et al., 2013] investigated the frosting and defrosting characteristics on a rigid super-hydrophobic surface, and their study results demonstrated that both flexible and rigid super-hydrophobic surfaces were conducive to frosting suppression, and only on the rigid superhydrophobic surface was defrosting effective without any water droplets. Besides, Sommers et al [2018] experimentally compared the frosting characteristics of surfaces having different wettability to determine the effects of surface energy on frost mass, thickness and density. It was found that a frost layer on a hydrophobic surface was "thicker and fluffier", resulting in a less-dense frost layer, but the frost thickness of a frost layer on a hydrophilic surface was relatively thinner.

2.2.2 Frost formation process on a cold surface

An entire frosting process on a cold surface may have different characteristics at different frosting stages. In an earlier study, Hayashi et al [1977] classified a frost growth process into three stages: crystal growth, frost layer growth, and frost layer full growth, as shown in Fig. 2.5. Up to now, this classification has received the highest degree of recognition. Based on this classification, others later further divided the crystal growth stage into two sub-stages: droplet condensing and solidified liquid tip growth [Song and Dang, 2018; Tao et al., 1993]. Therefore, they suggested four stages for a complete entire frost formation process.

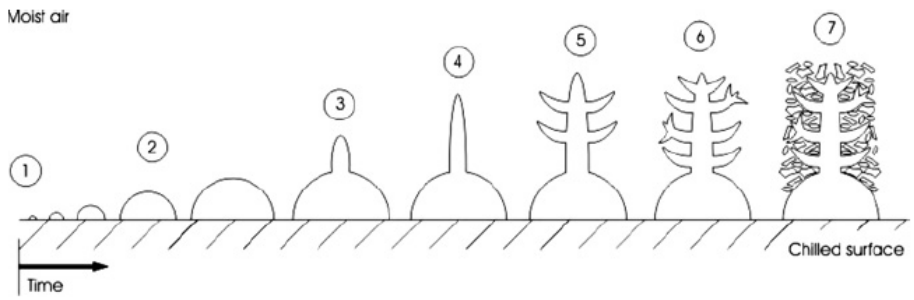

Fig. 2.5 Definition of early stages of frost growth on a cold plate - Tao, Besant, and Mao [HAYASHI et al., 1977; Tao et al., 1993].

The three-staged frosting process is detailed as follows,

***Crystal growth stage*:** As mentioned above, a crystal growth stage includes two periods: droplet condensing and solidified liquid tip growth. The form is shown in Fig. 2.6. As seen, moist air at state point A is first cooled to its dew point A', which takes place within its thermal boundary layer. Then, because of free surface energy, nucleation would be initiated only when an energy barrier is overcome, which depends on an additional cooling from point A' to point B. When the energy barrier is surpassed, a phase change process takes place from point B to point C.

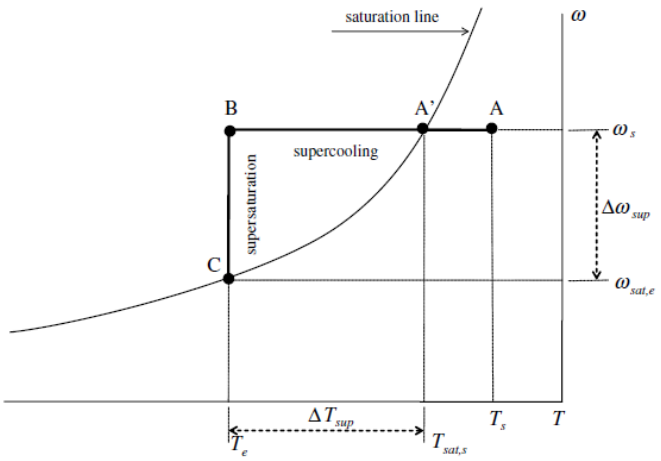

Fig. 2.6 Psychrometric representation of a frost nucleation process [Kim et al., 2017; Liang and Wu, 2022; Piucco et al., 2008; Tao et al., 1993]

A number of previous studies focused on the nucleation process from point A' to point C as shown in Fig 2.2. Na and Webb [Na and Webb, 2003] presented a fundamental description for a frost nucleation process on flat surfaces using several parameters, and modelled different types of water vapour phase change phenomena, i.e., condensation and freezing, and de-sublimation based on the specific criteria for each phase transition. The authors classified frost formation as a heterogeneous nucleation process mainly influenced by contact angle, and experimentally evaluated the frost nucleation on aluminium sheets covered with different types of coating, so as to predict the influence of contact angle. Wu et al [2007] tested two different surfaces with contact angles of 56˚ (hydrophilic) and 110˚ (hydrophobic) under supercooling degrees of up to 40 ˚C. The test results demonstrated that the hydrophobic surface (110˚) had a sparser distribution of condensate droplets, with larger droplet sizes and smaller droplet heights, which delayed droplet freezing and frost formation. Liu et al [2006, 2007b] indicated that frost nucleation did not occur when super-saturation degree was low, and the frost formed on a hydrophobic surface can be easily removed when compared with a hydrophilic surface. Piucco et al [2008] theoretically and experimentally investigated frost nucleation on flat surfaces. A mathematical model for the heterogeneous frost nucleation on smooth surfaces was developed.

***Frost growth stage*:** This stage is characterized by the densification of porous frost layer. The gaps among the ice branches or icicles were filled up by small liquid droplets, ice crystals and air molecules. In this stage, most of the mass transfer from moist air to a frost layer contributed to density increase while the variation in frost thickness was not notable as that in the first stage [Liang and Wu, 2022].

***Full development stage*:** In this stage, as a frost layer grows, surface temperature will increase due to the release of latent heat. When frost surface temperature reaches the melting point, the full development stage commences. The deposited frost would partly be melted and seep through the pores of a porous frost layer until it reaches an icy surface, where the melted frost is solidified into ice. When the thermal equilibrium is reached, this cyclical process of condensing / de-sublimating, melting, and re-freezing may take place continuously. This will lead to additional densification of a frost layer and the augmentation of frost thermal conductivity. The surface of a frost layer may gradually smoothen over the time span of this stage.

2.2.3 Impacts of frosting on the operating performances of ASHP units

Frosting may result in a series of negative impacts on the operating performances of ASHP units, as follows.

2.2.3.1 The impacts on operating parameters

Many operating parameters may be used to indicate the effects of frost formation on the operating performance of ASHP units. These parameters include: a) parameters on the refrigerant side, such as refrigerant temperatures and pressures at compressor's outlet and inlet, degree of superheat at compressor inlet, compression ratio, surface temperatures of an outdoor coil and the opening degree of a throttle valve, etc.; b) parameters on the air side of an outdoor coil, including air pressure difference, effective airflow area, actual airflow volume, and the block ratio of a FTHX; c) parameters at a terminate unit of a heating system, such as indoor air supply / return temperature for air to air ASHP units, or supply / return water temperature for

air to water ASHP units, etc. All these parameters can be used to indirectly reflect level of frosting, and many of those parameters have therefore been used when developing defrosting initiation methods and defrosting control strategies.

Changes in above parameters during a frosting process are as follows: with the frost being accumulated on outdoor coil surface in an ASHP unit, an increasingly thicker frost layer would gradually block the airflow channel of heat exchangers, causing an increase in both air pressure difference, and an increase in the effective airflow area, of the outdoor coil. As a result, the volumetric airflow rate would decrease gradually. Besides, the overall thermal resistance of outdoor coil keeps increasing with an increasingly thicker frost layer. These changes in volumetric airflow rate and the thermal resistance on the air side further lead to a continuous degradation of thermal energy being absorbed from ambient air. To maintain a stable suction degree of superheat at compressor inlet, at a lower level of absorbed thermal energy, the throttle valve in the ASHP unit inevitably needs to reduce its degree of opening, causing decreases in refrigerant evaporating pressure and temperature in outdoor coils, as well as in compressor suction pressure and refrigerant mass flow rate. At the same time, compressor discharge temperature and pressure may increase gradually due to the reduction in refrigerant mass flow rate. Hence, the temperature of indoor supply air or water will be reduced too.

The changes in these parameters described above have been observed in previous experimental and mathematical studies. For example, the experimental results by Brian et al [1970] indicated that a frosting surface can reduce the heat flux by up to 40%. Qu et al [2020] observed that frosting can lead to a high compressor discharge temperature. In some worst cases, an ASHP unit could even shut down because of a high discharge temperature [Su et al., 2017]. Yao et al [2004] numerically studied the frosting characteristics of an ASHP water heater / chiller. Their

study results indicated that airside pressure drop was increased rapidly with an increased frost accumulation. Besides, in some other studies, it was observed that accumulated frost can also obstruct the air flow passages of an FTHX, and increase the refrigerant pressure drop through an evaporator and may even lead to the shutdown of an ASHP unit [Hwang and Cho, 2014; Yan et al., 2003].

2.2.3.2 Impacts on the heating performances of ASHP units

In the existing literature, two important indexes have been widely used to reflect the heating performances of space heating ASHP units, namely, the total output heating capacity and COP. A severely frosted outdoor coil surface would cause a greater reduction in these two indexes. The studies by Kwak and Bai [2010] and Wang et al [2017] indicated that the total output heating capacity of ASHP units under frosting conditions can be decreased by 20 % - 40 %. The experimental results of Sanders [1974] demonstrated that the heating performance of an ASHP unit was decreased by 35% under frosting conditions. Wang et al [2011] conducted a series of field studies on the heating performances of ASHP units under frosting conditions and their results indicated that the total output heating capacity of ASHP units may decrease by up to 29% under a severe frosting condition.

All the above studies have demonstrated that frosting had a significantly negative effect on the heating performances of ASHP units, resulting in a lower heating efficiency, an unstable heating process and a poorer thermal comfort for building occupants. Therefore, it is highly necessary to mitigate frosting of ASHP units.

2.3 Frosting mitigation measures of ASHP units

Developing frosting mitigation methods is an important and effective approach for achieving the efficient operation of a space heating ASHP unit under frosting conditions. Currently, to mitigate frosting efficiently, a great number of studies have mainly focused on developing anti-frost methods, to suppress the frost formation on the surface of an outdoor coil in ASHP units. However, insufficient attention has been paid to other promising frosting mitigation measures, such as even frosting for an outdoor coil. Therefore, in this Section, a review of the existing literature about even frosting of outdoor coils in ASHP units is firstly presented, and this is followed by reporting other frosting suppression technologies.

2.3.1 Even frosting

Ideal even frosting for an outdoor coil in an ASHP unit is to achieve frost distributing evenly at any point of the surface of the outdoor coil at the same or similar frost thickness and density, so as to make the full use of the entire heat transfer surface area of the outdoor coil and thus lengthen a heating operation duration. Different from frosting suppression, even frosting focuses on achieving an efficient utilization of outdoor coil surface area as much as possible, rather than preventing frost from forming on outdoor coil surface.

2.3.1.1 Uneven frosting phenomenon

As a norm, frost is distributed unevenly in different parts of outdoor coil surface, with different frost thicknesses and densities. There can be grossly three types of uneven frosting: (a) along the refrigerant flow direction in an outdoor coil, (b) on the windward side among circuits in a

multi-circuit outdoor coil, and (c) between the windward and leeward sides along the airflow direction of an outdoor coil. For the first one, uneven frosting along refrigerant flow direction appears only when a non-evaporative refrigerant, such as ethylene glycol, is used and therefore, is not an issue when a direct expansion (DX) ASHP is used. For the second and third ones, in a number of related experimental and modelling studies, these two types of uneven frosting have been observed.

Song et al [2016] experimentally studied the effects of even frosting on the windward side of an outdoor coil on the frosting and defrosting performances of an ASHP unit. For a three-circuit outdoor coil, Song et al [2016a] defined a frosting evenness value (FEV), which was a ratio of the minimum mass of frost accumulated on all the surface area of a circuit to the maximum one among the three circuits. The experimental results demonstrated that COP could be increased from 4.10 to 4.26 when FEV was increased from 75.7% to 90.5% for an ASHP with a three-circuit outdoor coil within a 60-min frosting operation period. In addition, defrosting duration could also be shortened by ~ 11.2% and defrosting efficiency increased by ~ 5.7% as FEV was increased from 79.4% to 96.6%. This was because at a higher FEV, defrosting durations for different circuits will be closer to one another. Song et al also [2016c, 2016d, 2016b, 2017] comprehensively studied the uneven frosting / defrosting problems on the windward side based on a multi-circuit outdoor coil.

With regard to the studies on the uneven frosting on an outdoor coil along the airflow direction, Moallem et al [2012a, 2012b] experimentally investigated the impacts of surface coating, temperature and water retention on the frosting performance of a microchannel heat exchanger. In their studies, it was stated that when frost thickness on the windward side of a frosted heat exchanger was evaluated based on camera images, little frost accumulated on the leeward side

of the heat exchanger according to their experimental observations. Kim et al [2013] experimentally investigated local frosting behavior on a two-row outdoor coil with respect to refrigerant flow direction and surface treatment. Images of the windward and leeward sides of the frosted outdoor coil showed that there was a significant difference in the amount of deposited frost between the two sides at 36 mm apart. For a counter-flow (refrigerant-air) outdoor coil, at an evaporating temperature of -12 °C and 1.5 m/s face velocity, after 40 minutes into a frosting operation, the block ratio (BR) for its windward side was 94% but that for its leeward side only 77%. However, for a parallel-flow outdoor coil, at the same test condition, the BR for the windward side was 98% but for its leeward side only 67%. It was suggested that the driving potential for frost growth along the airflow direction of 36 mm long was reduced, because as the air passed through a frosted outdoor coil, its temperature, humidity and velocity were decreased. With regard to surface treatment, the study results suggested that the use of a hydrophilic surface for an outdoor coil would lead to a faster blockage of the windward side, when compared to the use of a hydrophobic or hybrid surface. Furthermore, Kim and Lee [2013] experimentally investigated the frosting and defrosting characteristics of surface-treated louvered-fin heat exchangers with two tube rows. Images of windward and leeward sides of the frosted heat exchangers also demonstrated that there was a significant difference in the amount of deposited frost between the two sides. However, the difference may decrease with increased refrigerant temperature, fin pitch and air velocity. It was suggested that the reason for the difference was that the active frost growth at the first row caused air humidity at the second row to decrease more intensely, thus reducing the driving force for frosting growth, leading to less frost on the leeward side. In addition, Park et al [2016] experimentally studied the frosting behavior of a heat exchanger made of a series of parallel louvered fins with unequal fin pitch, and found out that using unequal fins helped delay total frost blockage at the windward side and thus improved the thermal performance by 21 %, when compared to using

equal louver pitch. Recently, Zhang et al [2018] carried out an experimental study on frost distribution and growth on FTHXs used in ASHP units. An experimental system with visualization provisions was established, and the detailed characteristics of frost distribution and growth on, and the airside performances for, two different single-row experimental FTHXs with two different fin pitches, at 2 mm and 3.2 mm, respectively, were experimentally investigated. Significant uneven frosting on the windward and leeward sides at 22 mm apart for both FTHXs can be clearly observed, at the same experimental ambient air conditions at 2.0 °C, 85% relative humidity, 1.2 m/s face velocity and -10 °C evaporating temperature. The study results suggested that the use of a larger fin pitch can help improve the frosting evenness between the two sides.

Apart from experimental studies, numerical / modelling studies on the uneven frosting for outdoor coils / heat exchangers along the airflow direction have also been reported. Yao et al [2004] developed a distributed dynamic mathematical model to predict frost growth on a four-row outdoor coil. The model comprised a frosting sub-model and a heat exchanger sub-model, and was validated using the experimental data published by others. Using the validated model, modelling results suggested significant uneven frosting of the outdoor coil along the airflow direction, as frost accumulation occurred mainly on the first and second rows at ~ 40 % and ~ 35% of the total frost mass, respectively, but that on the fourth row only at ~3 %. Therefore, it was suggested that a heat exchanger of staged-fin pitch was superior to that of a constant fin pitch under frosting conditions, i.e., a larger fin pitch on the windward side and smaller on the leeward side. da Silva et al [2011] further developed an experimentally validated mathematical model, to predict frost growth on an outdoor coil with two tube rows. Modelling results showed that frost thickness on the first tube row was 35% greater than that on the second row. It was hence also suggested that the fin pitch on the first row should be larger than that of the second

row to improve frosting evenness. Gao and Gong [2011] developed a distributed dynamic mathematical model to predict frost growth on an outdoor coil with four tube rows, taking into account the effects of water vapor diffusion and uneven fin temperature distribution. Numerical results showed that the frost thickness on the first tube row was approximately three times as much as that on the fourth tube row. It was believed that the main reason for the uneven frost distribution was the reduced temperature difference between air and tube surface along the airflow direction. Hwang and Cho [2014] also developed an experimentally validated mathematical model to predict frost properties and airside performances of a single-row outdoor coil. Modelling results indicated that there was a significant difference in frost thickness between the windward and leeward sides of the outdoor coil, without however providing explanations for uneven frosting. Qin et al [2014] numerically and experimentally demonstrated that under frosting operational conditions, the use of a heat exchanger with a variable fin pitch can lead to a longer frosting-defrosting cycle duration and better heat transfer than that with a constant fin pitch.

Therefore, uneven frosting along the airflow direction has been widely observed. It has been also noted that uneven frosting along air flow direction has many side effects, such as reducing the usable surface area of heat exchangers, shortening a frosting operation duration. It also led to energy waste and a lower efficiency during defrosting, because when defrosting, certain energy was used to merely heat ambient air rather than to melt frost. Therefore, uneven frosting cannot be ignored when improving the operating performance of ASHP units.

Although uneven frosting along the airflow direction was observed in both experimental and numerical studies, most of those studies merely reported what were observed without a thorough investigation into how to mitigate the uneven frosting. Therefore, to alleviate uneven

frosting along the airflow direction passing through an outdoor coil in ASHP units, further detailed studies should be carried out.

2.3.1.2 Reasons for uneven frosting along the airflow direction

To alleviate uneven frosting along the airflow direction, it is necessary to understand the underlying reasons for this problem. Carlsen et al [2001] experimentally and numerically investigated the non-uniform distribution of frost on the evaporator used in a supermarket display case. In their study, the impacts of environmental parameters, including air temperature and relative humidity, refrigerant temperature, and air and refrigerant mass flow rates, on the deposition and distribution of frost on the evaporator surface of the refrigeration display case were evaluated. The evaluating results suggested that refrigerant temperature and air velocity strongly affected the uneven frosting along the airflow direction. When operated at face velocities above 5 m/s, frost might deposit near the back of the evaporator. Besides, air humidity was reduced along the airflow direction, and a higher water vapor content on the windward side led to more frost on the windward side than on the leeward side of the evaporator. Breque and Nemer [2017] developed a model of a fan-supplied flat-tube heat exchanger to study its non-uniform frost growth. The impacts of fin pitch and air velocity on uneven frosting were also investigated.

Although environmental factors causing uneven frosting along airflow direction have been studied, it is noted that the majority of experimental and numerical studies on the frosting / defrosting were only carried out based on traditional outdoor coils having only a single fan with a fixed one-way airflow direction. As a result, the impact of the configuration of such traditional outdoor coils on uneven frosting along airflow direction has been overlooked in

existing studies. The configurations of two types of traditional outdoor coils, Type 1 and Type 2, are shown in Fig. 2.7. As seen, for both types, one or two FTHXs were placed on the suction side of an outdoor air fan. During operation, given the fixed relative position of the fan and FTHXs, along airflow direction, there always existed a windward side and a leeward side for the FTHXs [Shapiro et al., 2012]. Such a fixed airflow direction led to that more frost was always deposited on the windward side, and less on the leeward side in a FTHX.

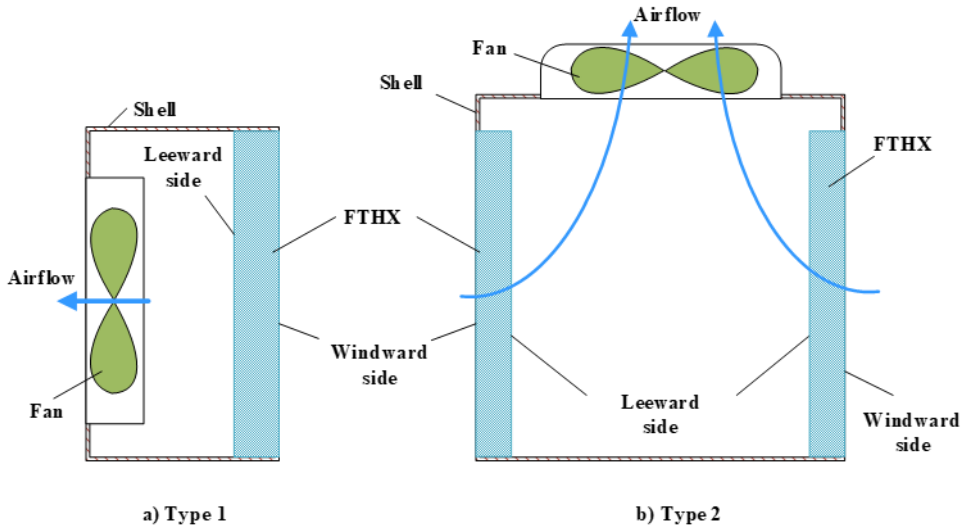

Fig. 2.7 The schematics for the two types of the configurations of traditional outdoor coils used in ASHP units

The ASHP units having the above traditionally configured outdoor coils have been widely studied. For example, Wang et al [2013a] and Bai et al [2018] conducted a number of field studies on ASHP units used in office buildings located in different climate zones of China, such as Beijing, Guizhou and Litang Zong in Tibet. In their studies, all the field ASHP units used the above two types of outdoor coils [Lin et al., 2019; Bai et al., 2018]. Song et al [2016e, 2017] experimentally investigated uneven frosting performances of ASHP units using Type 1 outdoor coil. Almost in all these studies, outdoor coils having a traditional single-fan configuration with hence a fixed airflow direction, were adopted. Therefore, as the moisture content of air on the

windward side was always higher than that on the leeward side, uneven frosting along the airflow direction in such a traditional outdoor coil became inevitable.

Therefore, it becomes clear that the configuration of a traditional single-fan outdoor coil used in ASHP units is the main reason causing uneven frosting along the airflow direction. However, studies on modifying such a traditional single-fan configuration to mitigate uneven frosting along the airflow direction have not been found in the existing literature.

2.3.1.3 Existing measures for mitigating uneven frosting along the airflow direction

Although uneven frosting along the airflow direction has significantly impacted the frosting and defrosting operating performances of ASHP units, it did not receive adequate attention for possible modification, and only in very limited studies, this issue was addressed. For example, in order to alleviate the uneven frosting along the airflow direction, Zhang et al [2018] experimentally studied the heat exchangers with single-row finned tubes having different fin pitches, and the study results demonstrated that the finned tube heat exchanger having a larger fin pitch was able to better alleviate uneven frosting along the airflow direction than that having a smaller fin pitch. However, using a larger fin pitch of FTHXs may result in a reduction in both the heat transfer area of FTHXs and the output heating capacity of ASHP units. Ultimately, it cannot fundamentally avoid uneven frosting along the airflow direction, when a traditional single-fan outdoor coil with a fixed airflow direction was used. As a result, the frost deposited on the windward side of FTHXs was always more than that on the leeward side.

Therefore, limited existing solutions for alleviating uneven frosting along the airflow direction were ineffective. Therefore, it became highly necessary to develop new methods for achieving

even frosting along the airflow direction for ASHP units, by modifying the configuration of traditional single-fan outdoor coils.

2.3.2 Frosting suppression methods

The use of various frosting suppression methods is another important approach to mitigate frosting by preventing frost from being deposited on cold surfaces under frosting conditions. So far, frosting suppression strategies can be grossly classified into three categories: cold surface treatment, dehumidifying inlet air to outdoor coils and configuration optimization of ASHP units. In this section, these three categories of frosting suppression methods are reviewed, as follows:

2.3.1.1 Cold surface treatment

Frosting suppression may be achieved by specially treating a cold surface. As seen in Section 2.2.1, different surface treatments can lead to different roughness and wettability for a cold surface. Therefore, there have been studies focusing on developing special coating materials for achieving frosting suppression. For example, Liu et al [2006] and Huang et al [2009b] applied different paints on a cold metal surface. They found that frost formation may be delayed significantly and that frost deposition was reduced, as compared to uncoated surfaces. Meanwhile, cold surfaces with different hydrophilic characteristics at different contact angles also showed different frosting suppression performances [Lee et al., 2004]. Liu et al [2007b], and Okoroafor and Newborough [2000] reported that increasing the contact angle can increase the potential barrier and restrain crystal nucleation and growth and thus frost deposition. Okoroafor and Newborough [2000] also pointed out that a hydrophobic surface could help delay frost formation to a certain extent and result in a looser frost layer but was not able to

suppress the growth of the frost layer. Besides, a new cross-linked hydrophilic polymeric coating may accelerate re-frosting during the next frosting-defrosting cycle due to its poor drainage property. Similar conclusions were also found in other studies [Na and Webb, 2003; Zuo et al., 2017]. Moreover, Kim et al [2015a] found that the effect of frost suppression can be changed with changes in refrigerant temperature. For example, frosting suppression effect was increased remarkably with a super-hydrophobic surface when refrigerant temperature was at -10 °C or -12 °C, but diminished when it was at -8 °C.

It should be noted that the durability of a treated surface is compromised in real applications, so its frosting suppression ability may no longer be available due to ageing and corrosion problems [Min et al., 2000]. Therefore, improving the durability of these treated surfaces is necessary to achieve the desired frosting suppression.

2.3.1.2 Dehumidifying outdoor air

Frost comes from the water vapor in ambient air. Hence, another frosting suppression measure to prevent water vapor from being condensed on a cold surface is to dry the inlet humid air to an outdoor coil. So far, many methods of dehumidifying air have been developed [Jia et al., 2006, 2007]. Kondepudi et al [1995] investigated the frosting duration for an outdoor coil, with and without solid desiccant placed upstream of the outdoor coil. Their results suggested that the use of desiccant can significantly reduce the frosting rate of the outdoor coil. Wang and Liu [2005] used the solid absorbent to dehumidify the inlet air to an outdoor coil, and the frosting on the outdoor coil of ASHP units can be significantly reduced. Zhang et al [2010, 2012a, 2012b] developed both a liquid dehumidification system and a solid desiccant system for dehumidifying inlet air to outdoor coils. They applied liquid dehumidification using a

lithium chloride solution as a desiccant to an ASHP unit to remove the latent heat of humid air. By decreasing the dew point of the air passing through the outdoor coil of the ASHP, no frost was formed on the outdoor coil surface. However, the adsorption capacity of desiccant in low-temperature regions was limited.

2.3.1.3 Optimizing the configurations of ASHP units

Optimizing the configurational parameters of an ASHP unit, such as the heat transfer area of outdoor coil, or the arrangement of fins and tubes, can also help achieve frosting suppression. For example, Barbosa et al [2009] investigated the thermal-hydraulic performances of commercial frost-free tube-fin evaporators, which had a smaller frontal (or face) area and a larger evaporator length than conventional evaporators. As shown in Fig. 2.8, its fin spacing was non-uniform along airflow direction and was also significantly larger than that used in conventional tube-fin exchangers. Their experimental results proved that the evaporator had a good frosting suppression ability. Moreover, Liang et al [2020] developed a new method to improve the frosting suppression performance of ASHP units by optimizing the outdoor airflow rate and the surface area of outdoor coils, which was twice as much as those in conventional ASHP units. Experimental results demonstrated that frosting rate and frosting-defrosting loss efficiency of ASHP units using the optimized configurations could be reduced from 37.2% and 39.6% to 31% and 34.2%, respectively. In addition, Yao et al [2004] indicated that increasing the airflow rate can help reduce the temperature difference for the heat transfer between the refrigerant and ambient air, thus effectively suppressing frosting on the outdoor coil surface. Similar conclusions were also obtained by Wang et al [2018] based on their experimental study. Moreover, other methods have also been developed to suppress frosting on outdoor coils, such

as mixing exhaust air with outdoor air before entering an evaporator [Liu et al., 2007a] or applying the electric fields [Tudor and Ohadi, 2006] and [Joppolo et al., 2012].

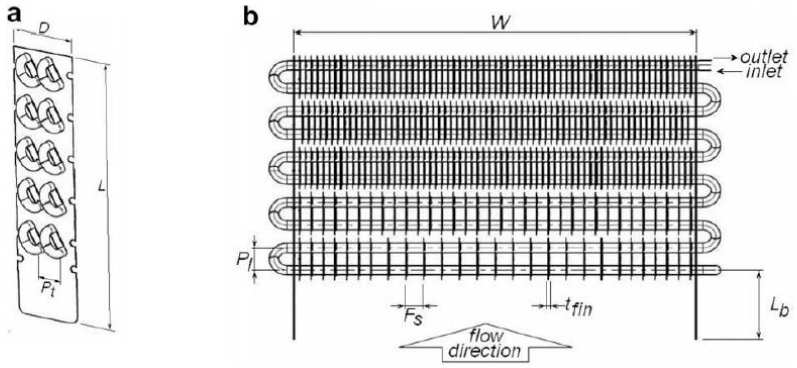

Fig. 2.8 Frost-free evaporator [Barbosa et al., 2009]

2.4 Modelling studies on the frosting characteristics

Over the past few decades, mathematical modelling study has become an important and efficient approach for investigating frosting - defrosting characteristics for ASHP units, due to its cost-effectiveness compared to using an experimental approach [Choi and Kim, 2003]. Modelling studies on frosting issues in existing literature can be classified into two groups: a) numerical studies based on a simplified geometry or a standalone heat exchanger; b) numerical studies based on a complete ASHP unit. Therefore, related modelling studies for the two groups are respectively reviewed, as follows.

2.4.1 Modelling studies based on a simplified geometry and a standalone heat exchanger

Modelling studies of frosting phenomenon based on a simplified geometry have greatly promoted the development of frosting theories, due to its merits in simplified modelling techniques and easy observation of frost built-up. Existing studies in general focused on

revealing the heat and mass transfer characteristics and growth process in a frost layer on a simplified flat surface or tube. For example, based on a cold plate, Hermes et al [2014] developed a semi-empirical correlation for frost density by advancing a first-principles model for predicting the evolution of the porosity of a frost layer over time. Ismail et al [1997] developed a two-dimensional model to predict the local frost properties around a cylinder, including frost density, thickness and temperature. Besides, Ismail and Salinas [1999] also simulated the process of frost formation on flat cold surfaces subject to humid airflow, and related frosting parameters, i.e., frost temperature, density and thickness distribution along flow direction and void fraction. Kandula [2011] investigated the frost growth and densification process in laminar flow over flat surfaces by considering the heat and mass diffusion in the frost layer using a one-dimensional model. Simulation results demonstrated that, for flat surfaces, increasing air velocity had no appreciable effect on frost thickness but contributed to significant frost densification. Le Gall et al [1997] also conducted a similar modelling study on frost growth and densification using a one-dimensional transient model, and put forward a new index called diffusion resistance factor. Lee et al [1997, 2003] established a mathematical model to predict the behaviors of frosting on a cold flat surface, by simultaneously considering airflow rate and a frost layer, and the behaviors of frost layer growth along airflow direction. All those studies were conducted to investigate frosting properties under different conditions based on a flat surface [Lüer and Beer, 2000; Mago and Sherif, 2003]. Besides, a number of assumptions related to heat and mass transfer [Negrelli and Hermes, 2015; Liang and Wu, 2022] were also made when modelling. These studies have laid an important foundation for the subsequent developments of frosting mitigation methods and defrosting control theories.

On the other hand, some models were developed based on a standalone complete heat exchanger to investigate the frosting characteristics of heat exchangers used in ASHP units.

These studies mainly concentrated on frost distribution characteristics [Seker et al., 2004], and their effects on the operating performances of a heat exchanger, including frost thickness, heating performance [Kondepudi and O'Neal, 1993] and effects on both the airside and refrigerant side. Besides, the impacts of different operating and design parameters, including the configuration of FTHXs, ambient air conditions, and evaporating temperature, on the frosting process on a standalone heat exchanger were also extensively investigated. For example, Cui et al [2011] developed a CFD model to predict frost behaviors in the initial frosting period on a FTHX, and the influence of surface structure under different ambient conditions was investigated. da Silva et al [2011] established a first principles simulation model to predict the frosting process and its influence on the thermal-hydraulic performance of a finned tube evaporator. The modelling results indicated that progressive frost clogging was the main cause of cooling capacity reduction under frosting conditions. Gao and Gong [2011] numerically investigated the airside dynamic behaviors of a heat exchanger under frosting conditions, where the effects of water vapor diffusion and uneven fin temperature distribution were considered. The frost at fin base was found to be thicker than that at the fin tip due to a lower tube surface temperature at the fin base. Hoffenbecker et al [2005] established a hot gas defrosting model based on an industrial air-cooling evaporator, to predict the time required for completely melting frost. Hwang and Cho [2014] investigated local frost thicknesses, blockage ratio, and local and total heat transfer rates of a finned tube heat exchanger under standard and severe frosting conditions, using a mathematical model. Study results indicated that the maximum frost thicknesses immediately downstream of each U-bend were thicker than those immediately upstream of each U-bend. Besides, Nielsen et al [2009] studied the dynamic performance of a counter flow air-air heat exchanger under condensation and frosting conditions based on a dynamic model. OSKARSSON et al [1990] mathematically investigated the frosting characteristics of an evaporator with dry, wet, and frosted finned surfaces.

It is noted that most of those modelling studies were carried out based on a non-evaporative refrigerant, such as ethylene glycol, so as to reveal the frosting mechanism on a simplified geometry for modelling accuracy and efficiency, and the impacts of a frosting process on the operating performances of heat exchangers.

2.4.2 Modelling studies for a complete ASHP unit

Modelling studies on the operating performances based on a complete ASHP unit are also found in the existing literature. However, most of those modelling studies are concentrated on investigating the cooling performances of ASHP units during cooling seasons, and those on the operating characteristics based on a complete ASHP unit under frosting conditions are relatively fewer. For example, to investigate the cooling performances of a direct expansion (DX) variable air volume (VAV) air conditioning (A/C) system, Chen and Deng [2006] developed a representative complete dynamic mathematical model for the DX-VAV A/C system, which considered the dynamic behaviours of both the DX refrigeration plant and the VAV air distribution subsystem simultaneously. Shah et al [2003] developed a dynamic model for simulating the operating characteristics of single and multi-Evaporator subcritical vapor compression systems, and a Linear Quadratic Regulator (LQR) control strategy was developed for disturbance rejection of a dual evaporator vapor compression cycle. Deng [2000] developed a dynamic mathematical model for a direct expansion water-cooled air-conditioning plant, which included a compressor, a thermostatic expansion valve, a water-cooled condenser and a direct expansion evaporator.

On the other hand, a number of models for simulating the operating characteristics of ASHP units under frosting conditions were developed based on those models for simulating cooling performances [Gupta et al., 2007]. For example, Su et al [2017] mathematically studied a novel no-frost ASHP unit combined with liquid desiccant dehumidification and compression-assisted regeneration. The model included a complete ASHP system sub-model and two additional sub-model, namely, a dehumidifier sub-mode and a refrigerator sub-mode. Based on the developed model, frosting suppression characteristics of the ASHP unit under various operating parameters and climatic conditions were investigated. Wang et al [2017] mathematically investigated the operating characteristics of a novel ASHP unit having a dedicated dehumidification and thermal energy storage system under frosting conditions. Correlations for frost-free working duration and the COP of the unit with ambient air temperature and relative humidity were obtained for optimising the operating parameters and heating performances of the novel ASHP unit.

Usually, a mathematical model for a complete ASHP unit under frosting conditions consists of three groups of sub-models [Yao et al., 2004; Chen and Deng, 2006], for refrigerant side, air side and a frost layer, and are reviewed as follows:

2.4.2.1 Sub-models for the refrigerant side

The refrigerant side of an ASHP unit is operated based on vapor compression refrigeration cycle, and consists of four key components, i.e., a compressor, one or more condensers in case of a multi-condenser ASHP unit, an expansion valve and finally one or more evaporators. Therefore, modelling for the refrigerant side of an ASHP unit is usually based on the module for each of these components. By linking the modules for these key cycle components and the

connecting piping, a sub-model for the refrigeration side of an ASHP unit may therefore be derived, and expressed by a set of ordinary differential equations and algebraic correlations. In this Section, modelling for these key components on the refrigerant side of an ASHP unit is separately reviewed as follows.

- *Compressor modelling*

  A compressor is the core component of an ASHP unit, which provides the driving force for moving refrigerant in the refrigeration cycle. There are different types of compressors, whose mathematical models are actually different due to different operating characteristics and performances. Chen and Deng [2006] established a model for a DX ASHP unit by using a variable-speed rotary compressor. In Deng's [2000] modelling study, a semi-hermetic reciprocating compressor was used for a water-cooled air-conditioning plant. Dutta et al [2001] experimentally and theoretically investigated the influence of liquid refrigerant injection on the performance of a refrigerant scroll compressor, and an analytical model of a scroll compressor cylinder with liquid refrigerant injection was developed. Generally, the compression process inside a compressor can be regarded as a poly-tropic and steady-state process [Rasmussen et al., 2002], whose mathematical module can be described by using the traditional thermodynamic approach. It assumes that a poly-tropic compression process could represent what takes place from suction to discharge in a compressor [Jiang et al., 2006].

  On the other hand, the operating characteristics of a compressor may also be described by using an empirical correlation based on the actual performance data with the aid of

curve fitting or regression analysis. For modelling an ASHP unit, this method in many cases can provide reasonably accurate operating performances for its compressor, based on a set of in-situ tests or performance data from compressor manufacturers. For example, the model of a variable speed rotary compressor developed by Chen and Deng [2006] was based on curve fitting the compressor's related performance data. This approach was suitable for both single-speed compressors and variable-speed compressors.

- *Heat exchanger modelling*

The heat exchanger of an ASHP unit includes a condenser and an evaporator. The modelling for these heat exchangers in ASHP units use similar approach. A large number of studies on heat exchanger modelling have been carried out using lumped-parameter modelling approach [Chi and Didion, 1982; Vargas and Parise, 1995] distributed-parameter modelling approach [Wang and Touber, 1991; Jia et al., 1995] and partial-lumped parameter modelling approach [Domanski, 1991; Deng, 2000; Yao et al., 2004]. When using lumped-parameter modelling approach, an evaporator was divided into two zones, i.e., two-phase, and superheated zone and a condenser three zones, i.e., two-phase, superheated and sub-cooling zone. Besides, Graph Theory modelling approaches were also useful for describing the detailed structures of an evaporator. For this method, the number of refrigerant tube and refrigerant flow direction within a single tube needed to be accounted first, which was necessary for creating a directed graph, to enable building an adjacent matrix [Liu et al., 2004] using the concepts of directed graph and graph-based search algorithms in Graph Theory. Liu et al [2004] developed a general steady-state distributed-parameter model for a FTHX.

With the help of the developed model, it was possible to analyse the operational performances of an evaporator having complex refrigerant circuits.

- *Expansion valve modelling*

An expansion valve is normally installed between evaporator and condenser to control the refrigerant mass flow and balance the system pressure. Conventionally, a steady-state model is usually used to describe the characteristics of an expansion valve due to its small thermal inertia. Refrigerant expansion is generally treated as an isenthalpic process so that an expansion valve can be modelled via an isenthalpic orifice equation [MacArthur and Grald, 1987]. One representative model for an electronic expansion valve (EEV) was developed by Damasceno et al [1990], based on the specifications given by EEVs' manufacturers and the empirical fittings for one set of distributor nozzle and tube size. Although the throttling mechanism in an EEV is identical to that of a short orifice valve, the flow coefficient is much more complex for an EEV than an orifice because the opening area of the EEV is dynamically adjusted. The characteristics of EEVs are usually obtained experimentally for different refrigerants. Park et al [2007] developed an empirical correlation for predicting the mass flow rate passing through an EEV by modifying a single-phase orifice equation with the consideration of EEV's geometry parameters and operating conditions. Li [2013a] modified the Bernoulli equation for a short orifice to develop a mass flow coefficient correlation for an EEV by introducing an expansion factor. EEV opening and the degree of sub-cooling were the two key parameters used to develop the coefficient correlation. Experimental analysis showed that the mass flow coefficient correlation could be used to well describe the refrigerant flow behaviour through the EEV with negligible errors.

- *Refrigerant pipework modelling*

  The fluid resistance of connecting refrigerant pipes is an important element when modelling refrigerant pipework. In some studies, the pressure loss in a single evaporator air conditioning (SEAC) system was usually ignored, but considered for a dual-evaporator A/C or multi-evaporator A/C system, because the connecting pipework in a multi-evaporator A/C system is actually more complex, thus the fluid resistance cannot be simply ignored. Pan et al [2012] reported a numerical study of the effects of refrigerant pipeline length differences on the operating performances of a dual-evaporator A/C system. Similar to that by Lu et al [2009], refrigerant pipelines were divided into single-phase and two-phase types according to the refrigerant state and the two types were separately analysed using fluid network theory. The famous Darcy-Weisbach Equation was applied to calculating pressure losses. For a two-phase pipeline, pressure drops were evaluated not only based on friction losses similar to that in single-phase pipelines, but also the kinetic energy change caused by refrigerant phase change. Other refrigerant pipeline models assumed that the liquid line and suction line were adiabatic, while the significant heat loss between the hot gas line and surroundings may be modelled using the effectiveness-NTU method [Cheung and Braun, 2014].

2.4.2.2 Sub-models for the frost layer

Frosting is a complex heat and mass transfer process. The condensing and freezing process of water vapor from humid air usually occurs with heat release and transfer. Therefore, most modelling studies on frosting on an evaporator are normally based on the principle of mass and

energy conservation. For mass conversation, it was believed that the mass of water vapor condensed from humid air determined the total mass of the deposited frost, and the loss of water vapor in the air was separated into two parts during frosting: one for the amount of condensed water vapor contributing to the increase in frost thickness, and the other to the increase in frost density [Yun et al., 2002; Yao et al., 2004]. For both parts, a set of equations, including one for the water vapor diffusion inside a frost layer, the ideal gas state equation for water vapor on frost surface [Eckert and Drake, 1987] and the Clapeyron–Clausius Equation for partial pressure of water vapor [Yao et al., 2004], etc., were adopted to describe the mass transfer for the frost layer, based on the mass conservation. On the other hand, the total energy during a frosting process consisted of the sensible heat transferred from air and the latent heat of solidification released by water vapor as it diffused into the frost layer and solidified [da Silva et al., 2011; Brèque and Nemer, 2016]. To calculate the heat flux of a frost layer, some empirical correlations, such as the thermal conductivity for the frost layer [Ye and Lee, 2013], would be used to establish energy conservation equations combined with the energy transfer process on the air side.

In many modelling studies, frost growth is usually assumed as a quasi-steady state and one-dimension problem. To facilitate a modelling process, a great number of empirical correlations on frost density [HAYASHI et al., 1977; Hadid, 2011], frost surface temperature, frost effective thermal conductivity and convective heat transfer coefficient [Lee et al., 1994; Negrelli and Hermes, 2015] have been established and used in frost growth models. However, when different empirical correlations for those parameters are used, the simulation results may be significantly different from each other [Brèque and Nemer, 2016]. Therefore, selecting proper correlations for different modelling parameters is important for improving the simulation performances of a frost growth model.

2.4.2.3 Sub-models for the air side

On the air side of an ASHP unit, the major components usually include a supply air fan and a DX heat exchanger, and their models are reviewed as follows:

Indoor and outdoor fans in ASHP units move air by forced convection through an evaporator or a condenser to achieve heat transfer. The pressure-volume flow characteristics of a fan can be represented in many different ways. In general, they are described by a set of constant-speed curves for pressure rise versus volume flow rate. For a variable speed air fan, its characteristics at different speeds are obtained by using the performance data from manufacturers or the fan performance law (fan pressure rises being proportional to the square of the change in fan speed). In order to get a better approximation with the experimental performance data, Mei and Levermore [2002] used a ten-neuron sigmoid artificial neural network (ANN) model to represent the characteristics of a variable speed fan. Besides, for an outdoor air fan under frosting conditions, frost growth will cause an increase in pressure loss in real-time, and thus, the correlations for air pressure drop of an outdoor coil under frosting conditions normally consider the impact of frost thickness and have been developed based on the performances of the outdoor coil at a non-frosting condition [Turaga et al., 1988].

2.4.2.4 Solving models of ASHP units

For solving a component-based model for an ASHP unit, there are two main methods: (1) simultaneous solving method and (2) sequential solving method.

For the former, all model equations, often of non-linear nature, and initial and boundary conditions, are solved simultaneously using the Euler Method or the Newton-Raphson Method, or the Runge-Kutta Method. Commercial software packages have been developed to help solve these non-linear equations [Klein and Alvarado, 2002]. Very often it can be difficult to find out the cause if divergence occurs when solving model equations, and thus calculation stability is not easily ensured. On the other hand, when applying this solving method to a developed system model whose structure is normally fixed, additional component sub-model cannot be easily inserted into the system model, and thus the flexibility of system simulation might be compromised [Winkler et al., 2008]. Therefore, for DX A/C system simulation, this solving method has not been popular.

The latter can be more conveniently used since component models are established first and treated as "black-box" objects. Only the knowledge of how these component sub-models are connected is required when using this method to solve a complete model. A set of initial values for model inputs are assumed. If the convergence criterion is not satisfied, the assumed initial values would be updated and then the iteration has to be repeated. Winkler et al [2008] studied the influence of setting initial values for the inputs to an A/C system model on computational speed. Component sub-models were run several times prior to solving the system model and it was shown that better initial values can help reduce the required computational time. The sequential solving method has clear physical meaning in solving a system model and is easy to debug to ensure calculation stability [Ding, 2007].

2.5 Defrosting methods

When the accumulated frost on the outdoor coil surface has caused severe deterioration of the heating performances of ASHPs, inevitably defrosting operation is required to be initiated to melt the frost layer to return the system to normal heating operation. The heat source for defrosting operation can come from the heat from a heated indoor environment or circulating hot water and hence indoor thermal comfort level can be lowered. Wang et al [2011, 2013a] revealed two mal-defrosting phenomena based on years of field tests: no defrosting initiation after excessive frost built-up and defrosting initiation without any frost formed on outdoor coil surface. Therefore, defrosting on demand was important for improving the defrosting efficiency and the stable operation of ASHP units. In general, an on-demand defrosting operation usually required a reasonable defrosting initiation strategy and an effective defrosting method. Existing studies on various defrosting initiation strategies and defrosting methods are reviewed, as follows:

2.5.1 Defrosting initiation strategies

A precondition of developing a reasonable defrosting initiation strategy is to accurately detect the actual growth of frost layer. Currently, based on different approaches of frost thickness measurements, the existing defrosting initiation strategies for ASHP units may be divided into two types [Xiao et al., 2009; Wang et al., 2011], as follows:

(1) 'Indirect measuring' strategy. By measuring one or more operating parameters of an ASHP unit during frosting operation, the extent of frosting may be estimated and a decision to initiate defrosting made. As an example, the widely used Time-Temperature (T-T) strategy initiates defrosting based on both outdoor coil surface temperature and a preset operating duration. However, T-T initiation strategy is unable to take into account the variations in ambient air

temperature and humidity, and therefore its accuracy in initiating defrosting cannot be guaranteed. As a further development to the T-T initiation strategy, Zhu et al [2015b] developed a novel Temperature-Humidity-Time (T-H-T) initiation strategy based on a frosting map [Zhu et al., 2015a], which was considered to be more favourable and suitable for the application to ASHPs. Hewitt and Huang [2008] tested and compared three indirect defrosting methods: (A) Temperature difference control, (B) Time-based defrost control and (C) Discharge temperature control, to find the accurate trigger point of defrosting initiation that gives the best performance of ASHP.

(2) 'Direct measuring' strategy. The thickness of the frost layer on an outdoor coil surface is measured directly, and if a preset value of frost layer thickness is reached, defrosting will be initiated. Over the years, various 'direct measuring' strategies, such as measuring frost thickness using laser [Storey and Jacobi, 1999; Qu et al., 2006], and a micrometer [Lee and Ro, 2001; Fossa and Tanda, 2002], and microscopic imaging observations [Cheng and Shiu, 2002; Kwon et al., 2006; Wang et al., 2004], etc., have been developed. However, there are a number of constraints when using these methods, such as the available installation space and high initial cost, making their application to actual installations difficult. Hence, Wang et al [2013b] and Xiao et al [2010] developed a tube-encircled photoelectric sensor (TEPS) to directly measure the thickness of a frost layer for defrosting initiation, and a TEPS-based defrosting initiation strategy has been developed and validated in different climate regions of China [Ge et al., 2016; Bai et al., 2018]. It was suggested that the use of the TEPS-based defrosting initiation strategy can effectively avoid mal-defrosting for ASHPs used in different ambient conditions, with a lower initial cost and higher defrosting performance.

2.5.2 Defrosting methods

Many defrosting methods have been developed to achieve defrosting effectively for ASHP units. Those methods include reverse cycle defrosting (RCD) method, hot gas bypass defrosting (HGBD) method, and mechanical vibration defrosting method [Wu and Webb, 2001], etc.

Currently, the most widely used defrosting method for ASHPs is RCD [Chen and Guo, 2009; Ding et al., 2004; Huang et al., 2004]. For this method, a four-way valve is used in the refrigerant circuit to reverse refrigerant flow direction when defrosting is initiated, and then refrigerant at high temperature and pressure flows into the outdoor coil to melt frost. However, a sudden pressure shooting and falling in the compressor suction and discharge lines during switching the four-way valve may cause mechanical shocks to the compressor and the refrigerant lines, leading to an undesired decline in indoor air temperature [O'Neal et al., 1991]. To avoid the cold feeling caused by a defrosting operation, Qu et al [2010] developed a thermal energy storage (TES) device to provide the energy source for defrosting, so as to improve indoor thermal comfort.

On the other hand, HGBD method has also been investigated. Huang et al [2009a] compared the dynamic characteristics of the HGBD method with the RCD method, and found that defrosting duration when using HGBD method was much longer than using RCD, but the thermal comfort level when using HGBD method was better than that using the RCD method, due to lower refrigerant noise, smaller indoor temperature fluctuation, and no cold air blowing. Choi et al [2011] and Kim et al [2015b] developed a Dual Hot-gas Bypass Defrosting (DHBD)

method by adding paths at compressor outlet and accumulator inlet in order to improve defrosting performances.

2.5.3 Drainage of melted frost following a defrosting operation

When defrosting is finished, due to different wettability of cold surfaces, certain water film or droplets can be left on the fin surfaces of an outdoor coil. The residual water on a cold surface can accelerate a re-frosting process when an ASHP unit returns to normal heating operation. As a result, the normal heating duration would be lowered. At a severer situation, a block of thick and solid ice will cover the bottom rows of the heat exchanger after multiple frosting-defrosting operations, causing serious deterioration of heating performance and frequent mal-defrosting operation of ASHP units [Song et al., 2016c]. To alleviate the negative impacts of residual water on frosting - defrosting performance of ASHPs, several methods have been developed.

Firstly, super hydrophobic and hydrophobic coatings have been widely used to FTHXs, where water droplets may have a bigger contact angle with the cold surfaces, compared to super hydrophilic and hydrophilic coatings. Therefore, a good drainage performance for fins can be expected. Li et al [2022] experimentally investigated the effect of hydrophilic and superhydrophobic coatings on frosting and defrosting performances, and the results demonstrated that the drainage performance for an outdoor coil having super-hydrophobic fins was better than that having hydrophilic fins, with a shorter defrosting duration, because the melted frost had smaller adhesive force on superhydrophobic fins, and melted frost may also carry some frost blocks that was separated from coil surface in the form of frost-water mixture. Similar conclusions were also obtained by [Liu et al., 2007b; Wang et al., 2015].

The second method is to shorten the drainage path in an outdoor coil heat exchangers. For example, Song et al [2016] experimentally compared the drainage performance of a finned tube heat exchanger by adjusting its installation position from vertical to horizontal. The results indicated that the drainage performance of the finned tube heat exchanger can be significantly improved when it was horizontally installed with a shorter drainage path. There are also some other methods adopted to reduce the residual water film or droplets following a defrosting operation, such as extending drying period or starting the outdoor air fan to accelerate the evaporation of residual water before leaving the defrosting operation.

2.6 Intelligent control optimization for HVAC systems

Control optimization for HVAC systems is important to achieve energy saving and low-carbon operation. The classical optimal control theory [Ross, 2015] is an important branch of modern control theory. For a traditional control optimization method, it is common to first establish a mathematical model for a controlled system, which consists of system variables, operational constraints and objective functions, based on the required optimization objective. Then the established model will be analysed and appropriate optimization methods selected. Finally, the mathematical model will be solved based on the selected optimization method, and the convergence, versatility, simplicity, calculation efficiency and error for the optimization algorithm evaluated. This is an ideal process called offline optimization to the mathematical model.

However, actual operational conditions are usually changed in real-time for the most controlled systems. Hence, a precise dynamic mathematical model for a controlled system is hard to be

established. On the other hand, controlled objects are becoming increasingly complicated as technology advances. For more complicated systems, their control performances are no longer simply expressed by a single indicator. Therefore, with the advancements of computer technology, an efficient and yet simple method, called intelligent optimization, has been developed and gradually applied to the control optimization for HVAC systems, e.g., an Artificial Neural Network method used in the optimization of supply airflow rate and temperature for variable air volume terminal units [Kim and Cho, 2022] and a variable refrigerant flow (VRF) cooling system [Chung et al., 2017], as well as the Generalized Regression Neural Network (GRNN) method [Wang et al., 2019] used for the control optimization of ASHP defrosting operation. GRNN, as a deep neural network, has been widely used in many application fields for achieving optimal control [Polat and Yıldırım, 2008; Hu et al., 2021]. Using nonlinear regression of statistics, it can approximate the hidden mapping relationship based on the sample data and converge to the optimised regression surface where the samples are more concentrated [Liu et al., 2023]. Besides, GRNN has a fast-learning speed, a good nonlinear mapping performance and prediction effect with a small number of sample cases [Lu et al., 2022]. As for the application of GRNN modelling to the studies of frosting and defrosting for ASHPs, Li et al [2020] and Wang et al [2019] developed an optimal defrosting initiation method based on the optimal results by using GRNN modelling. In their studies, a database was firstly established and a GRNN model trained and tested using the database. According to an output heating capacity loss coefficient, an optimal empirical formula for developing defrosting initiation method was developed. Many other similar studies may also be found in the existing literature. Therefore, GRNN, as an effective tool for predicting and control optimization, can be used as a tool for control optimization for ASHP units.

Besides, Genetic Algorithm (GA) [Zhang et al., 2023] and Fuzzy optimization control [Taleizadeh et al., 2013] are also widely used in the control optimization for HVAC systems. The former is a structural optimization method with a good potential, and has excellent advantages in solving complex optimization problems such as nonlinear structure optimization, dynamic structure optimization, shape optimization, topology optimization, etc. The latter is a control system based on fuzzy logic, a mathematical system that analyses analogy input values in terms of logical variables that take on continuous values between 0 and 1, in contrast to classical or digital logic, which operates on discrete values of either 1 or 0 (true or false, respectively) [Pedrycz, 1993]. Therefore, it is necessary to select an appropriate optimization method based on the desired optimization objectives for better control performances.

2.7 Conclusions

A number of existing studies have concentrated on solving the frosting problem for ASHP units by looking into frosting mechanism, and developing effective frosting mitigation and efficient defrosting methods, so as to improve the heating performances of ASHPs under frosting conditions. During a frosting-defrosting operating cycle, frosting characteristics, such as frost distribution, frost density and thickness over outdoor coil surface in ASHP units would significantly affect the frosting and defrosting operating performances of ASHP units and ultimately the level of indoor thermal comfort. Therefore, achieving frost suppression or even frosting is necessary for the efficient operation of ASHP units under frosting conditions. However, as mentioned in Section 2.3.1, uneven frosting along airflow direction has been widely observed in outdoor coils having a traditional single-fan configuration in ASHP units, which limits the efficient use of outdoor coil surface and lowers operating efficiency.

In the existing literature, inadequate attention has been paid to the phenomenon of uneven frosting along the airflow direction, and only a few limited methods have been experimentally tried to alleviate this phenomenon. However, these methods cannot be used to completely mitigate uneven frosting between the windward and leeward sides of an outdoor coil because of its traditional single-fan configuration with a fixed air flow direction. On the other hand, there have been extensive studies on the modelling of ASHP units, and these available models for ASHP units can be used for numerically investigating even / uneven frosting characteristics of ASHP units under frosting conditions, with particular reference to uneven frosting along airflow direction, for improved operating performances of ASHP units.

The literature review presented in this Chapter has identified that, to completely mitigate uneven frosting along the airflow direction, modifying the configuration of a traditional single fan outdoor coil with a fixed air flow direction in an ASHP unit is an effective approach. Therefore, experimentally and numerically studying even frosting characteristics and heating performances as well as developing an optimised control strategy of the ASHP unit having updated modified outdoor coil are the targets of the research project presented in this Thesis.

Chapter 3

Proposition

3.1 Background

The literature review presented in Chapter 2 has identified that uneven frosting along the airflow direction is always inevitable for ASHP units having a traditional single-fan outdoor coil with a fixed airflow direction, when operating under frosting conditions. Besides, it is also noted that uneven frosting along the airflow direction has not received sufficient attention so far, with only a very few number of methods reported in the existing literature to mitigate this uneven problem. However, all these methods were based on traditional ASHP units having a single-fan outdoor coil, and thus cannot be used to fundamentally achieve even frosting between the windward side and leeward side.

Therefore, to achieve even frosting along the airflow direction on the outdoor coil of an ASHP unit for a higher heating performance, a more stable frosting-defrosting operating and a higher level of indoor thermal comfort under frosting conditions, it becomes highly necessary to revise the configuration of a traditional single-fan outdoor coil with a fixed airflow direction used in existing ASHP units. Therefore, a novel outdoor coil that can alternately reverse the airflow direction has been proposed and a complete experimental ASHP unit having an experimental novel outdoor coil also established, so as to facilitate the experimental and numerical investigations of even frosting characteristics and heating performances of the experimental ASHP unit under frosting conditions.

3.2 Project title

This Thesis focuses on the following four issues related to even frosting along the airflow direction of an ASHP unit:

1) proposing a novel dual-fan outdoor coil (DFOC) that has two identical fans which are respectively placed on both the up- and down-stream of a FTHX to alternately reverse the airflow direction passing through the FTHX or the outdoor coil.

2) establishing an experimental ASHP unit having the novel DFOC (ASHP / DFOC) and an experimental ASHP / DFOC setup including the experimental ASHP / DFOC unit and an environmental chamber to experimentally study the even frosting characteristics and heating performances of the experimental ASHP / DFOC unit.

3) building up and experimentally validating a complete dynamic mathematical model for the experimental ASHP / DFOC unit and carrying out a modelling study using the validated model for obtaining the operating characteristics at other non-experimental conditions.

4) developing an optimal control strategy for the experimental ASHP unit with a novel dual-fan outdoor coil for evener frosting along airflow direction based on GRNN modelling.

The research project reported in this Thesis is therefore entitled “Achieving even frosting on the outdoor coil along the airflow direction in a space heating air source heat pump for improved energy efficiency and occupant thermal comfort”.

3.3 Aims and objectives

The research project has the following objectives:

1) To propose and develop a novel DFOC that can alternately reverse the airflow direction based on a pre-set value of time interval for alternate operation (t_{TIAO}) to achieve even frosting along the airflow direction on an outdoor coil;

2) To build an experimental ASHP / DFOC unit and an experimental ASHP / DFOC setup including the experimental ASHP / DFOC unit and an environmental chamber to experimentally study its even frosting characteristics and heating performances, under different dual-fan operating modes;

3) To develop a complete dynamic mathematical model and to experimentally validate the model, and to further investigate the even frosting characteristics and heating performances of the experimental ASHP / DFOC unit using the validated mathematical model;

4) To develop an optimal control strategy for the experimental ASHP / DFOC unit based on GRNN modelling so that the experimental ASHP / DFOC unit can be used at different

operating ambient air conditions to achieve evener frosting and higher heating performances.

3.4 Research methodologies

In this research project, both experimental and mathematical modelling approaches will be adopted. Firstly, an experimental novel DFOC having two identical fans, and an experimental ASHP unit having the DFOC (ASHP / DFOC) will be developed. The two fans, Fan A and Fan B, may operate alternately to reverse airflow direction based on a pre-set value of t_{TIAO}. An experimental ASHP / DFOC setup including the experimental ASHP / DFOC unit and an environmental chamber where there were two rooms, one for a simulated indoor heated space and the other for a simulated outdoor environment, will also be set up. The experimental ASHP / DFOC setup will be fully instrumented and all of its key operating parameters can be real-time measured and recorded via a comprehensive computerised monitoring system.

Secondly, with the availability of the experimental ASHP / DFOC setup and the computerised monitoring system, an experimental study to investigate the even frosting characteristics of the experimental ASHP / DFOC unit at different dual-fan operating modes will be carried out.

Thirdly, a dynamic mathematical model for the experimental ASHP / DFOC unit will be developed, by updating a sub-model for a traditional single-fan outdoor coil to establish a sub-model for the novel DFOC, and taking reference to the previously developed models for a complete ASHP unit. The model will be physically based and consist of sub-models for its

refrigerant side, frost layer and airside. The developed model will be experimentally validated using the data collected from the experimental ASHP / DFOC setup;

Finally, an optimal control strategy will be developed based on GRNN modelling to enable the experimental ASHP / DFOC unit to be operated efficiently at different operating ambient conditions, so as to achieve evener frosting along the airflow direction with higher heating performances. A database consisting of the experimental data from a series of study cases will be established and a new performance-based index for evaluating even frosting along airflow direction for the experimental ASHP / DFOC unit will be put forward for developing a GRNN model. The optimal control strategy will be developed based on the optimisation results of the developed GRNN model. The controllability tests for the developed optimal control strategy will be carried out using the experimental ASHP / DFOC setup, so as to evaluate its control effect by analysing the operating performances of the experimental ASHP / DFOC unit operated with different outdoor-fan control modes and at different simulated ambient conditions.

Chapter 4

An experimental ASHP / DFOC setup

4.1 Introduction

A novel experimental DFOC having two identical fans has been proposed and an experimental ASHP having a DFOC unit built. An experimental ASHP / DFOC setup that included the experimental ASHP / DFOC unit and an environmental chamber, was purposely established in the Multi-Function Chamber Laboratory in the Department of Building Environment and Energy Engineering, The Hong Kong Polytechnic University, to facilitate carrying out the research work proposed in Chapter 3, i.e., experimentally investigating the even frosting characteristics of the experimental ASHP / DFOC unit at different dual-fan operating modes, developing and validating a dynamic mathematical model, and finally developing an optimal control strategy for the experimental ASHP / DFOC unit at different ambient conditions.

In this Chapter, the experimental ASHP / DFOC setup is introduced in great detail. The detailed configurations of the proposed experimental DFOC are firstly reported. This is followed by reporting the details of the experimental ASHP / DFOC setup, covering both the experimental ASHP / DFOC unit and the environmental chamber. Finally, a computerized instrumentation and data acquisition system used real time measure and collect the operating parameters, such as temperature, humidity and pressure, etc, are introduced.

4.2 Detailed configurations of an experimental DFOC

In the proposed novel DFOC, there were two identical fans, positioned on both sides of a FTHX. The two fans can be controlled to operate alternately, so as to reverse alternately the direction

of airflow passing through the FTHX according to a pre-set pattern. In this way, windward and leeward sides became interchangeable to achieve a more balanced frosting on both sides.

An experimental novel DFOC, whose schematics are shown in Fig. 4.5, was built-up. A three-row FTHX with 7 sub-circuits was used. Two identical fans, Fan A and Fan B, were positioned on both sides of the FTHX. The fans and FTHX were housed inside a metal shell measuring at 1600 mm (L) × 720 mm (H) × 900 mm (W). Furthermore, four identical air dampers, i.e., dampers A1, A2, B1 and B2, were placed on the metal shell, as shown in Fig. 4.5 a). Dampers A1, A2, and Fan A were operated together, and so were dampers B1, B2 and Fan B. When Fan A was operated, dampers A1 and A2 were fully open, but Fan B was shut down and dampers B1 and B2 fully closed, and vice versa.

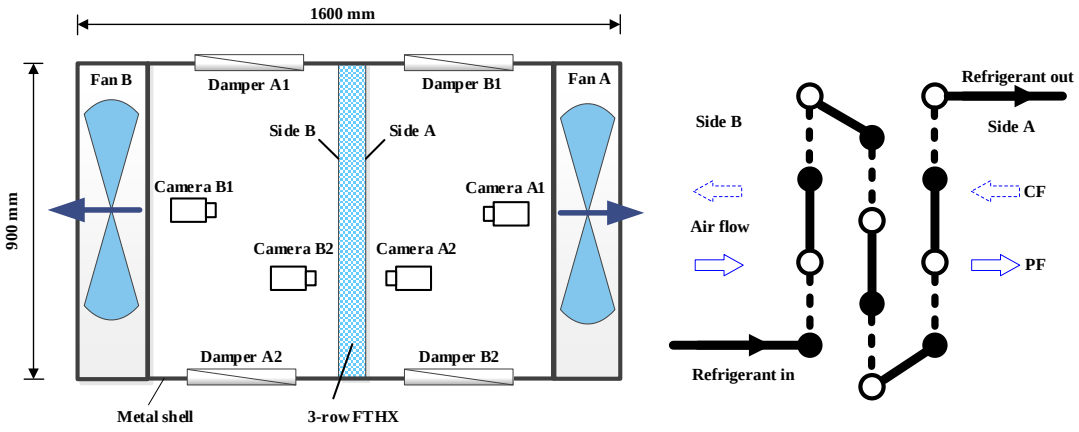

a) b)

Fig. 4.5 Schematics of the experimental novel DFOC and refrigerant-air flow directions in the 3-row FTHX

Furthermore, as seen from Fig. 4.5 b), during heating or frosting operation of the novel experimental DFOC, refrigerant flow direction in the FTHX was fixed from side B to side A.

When Fan A was operated, the airflow direction was also from side B to side A, which was regarded as a parallel flow (PF) operation mode. However, when Fan B was in operation, the airflow direction was from side A to side B, which was regarded as a counterflow (CF) operation mode. The CF mode has been widely adopted for a higher heat transfer efficiency.

In addition, a visualization system, where there were altogether four cameras installed inside the metal shell, was established. As seen in Fig. 4.5 a), Cameras A1 and B1 were used to capture the frosting states of the entire surface area of, and Camera A2 and B2 those of selected local surface areas on, both sides of the FTHX.

4.3 Descriptions of the experimental ASHP / DFOC setup

To enable the required experimental work, an experimental ASHP setup was established. The setup was made of an experimental ASHP / DFOC unit, and an existing environmental chamber, which are separately described as follows.

4.3.1 The experimental ASHP / DFOC unit

The experimental ASHP / DFOC unit was purposely made and its schematic diagram is shown in Fig. 4.6. As seen, the experimental unit mainly consisted of a variable speed rolling rotor compressor, a four-way valve, the novel DFOC described in Section 4.2, an indoor coil, and an electronic expansion valve (EEV). Although the range of variable frequency for the compressor was 20 Hz - 80 Hz, only a fixed input frequency of 70 Hz was used. The nominal output heating capacity of the experimental ASHP / DFOC unit was 8.5 kW, at the nominal space heating ambient condition of 7 ℃ / 6 ℃ (air dry-bulb /wet-bulb temperature). R410A

was used as refrigerant. The detailed specifications of components in the experimental ASHP / DFOC unit are listed in Table 4.1.

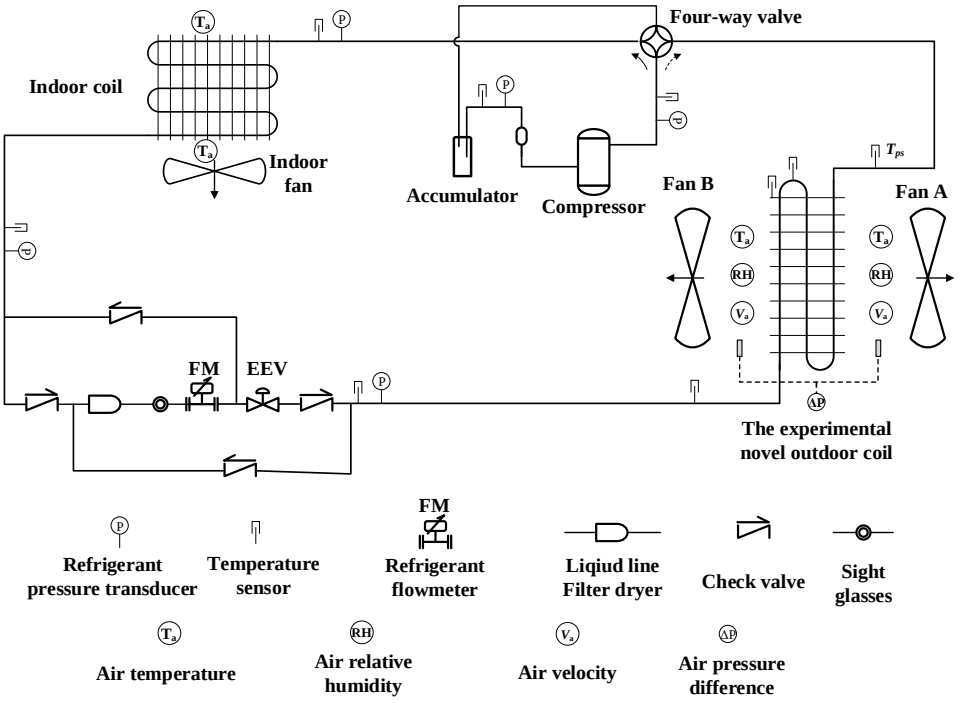

Fig. 4.6 Schematic diagram and instrumentations for the experimental ASHP / DFOC unit

Table 4.1 Specifications of the compressor and experimental novel DFOC

Components	*Parameters*	*Values / Details*
Compressor	Number	1
	Compressor type	Rolling rotor
	Adjustable frequency (Hz)	20 - 80
	Rated output heating capacity (kW)	8.5
	Refrigerant	R410A
Novel dual-fan outdoor coil	Dimensions (mm)	650 (L) × 700 (H) × 60 (W)
	Fin type	Wavy
	Fin thickness (mm)	0.1
	Fin pitch (mm)	2
	Tube external diameter (mm)	9.52
	Tube inner diameter (mm)	8.12
	Tube pitch (mm)	25
	Number of tube row	3
	Number of tube circuit	7
	Number of outdoor fan	2
	Fan speed	constant speed
	Rated input power (W) to each fan	180
	Number of damper	4
	Power input (W) to each damper	10
	Dimensions (mm) of each damper	400(L)×450(H)

4.3.2 The environmental chamber

As shown in Fig. 4.7, the existing environmental chamber consisted of two rooms, Room A and Room B. The former was used as a simulated outdoor space, and the latter as a simulated

heated indoor space. The size of each room was 3.7m (L) × 3.7m (W) × 3.3m (H). The experimental ASHP / DFOC unit was placed inside the experimental chamber, with its compressor and novel DFOC inside outdoor space or Room A, and the rest inside indoor space or Room B. In Room A, in addition to the experimental novel outdoor coil of the experimental ASHP unit, there were also a separate booster air cooling unit and a sensible and latent load generation unit (LGU). With these, the air temperature and humidity in the simulated outdoor space may be controlled to satisfy different experimental ambient conditions required in this research project. The minimum air dry-bulb temperature (T_a) in the simulated outdoor space could actually reach as low as -3 °C, and air relative humidity (RH) be controlled at between 30 % and 95 % (±3 %).

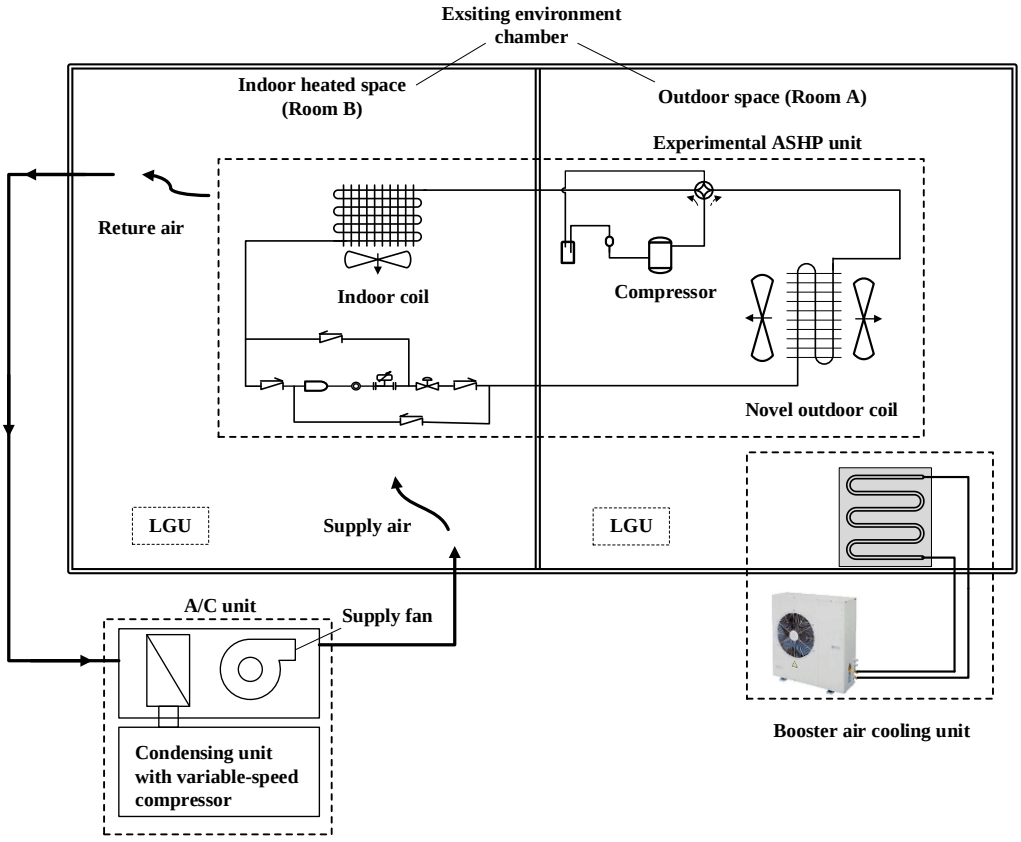

Fig. 4.7 The schematic diagram of the experimental ASHP system

4.4 Computerized instrumentation and data acquisition system

Various high-precision sensors and transducers to measure the key operating parameters of the experimental setup, such as temperatures, pressures and flow rates of air and refrigerant, etc., and all measured data, were computerized for real-time monitoring and recording.

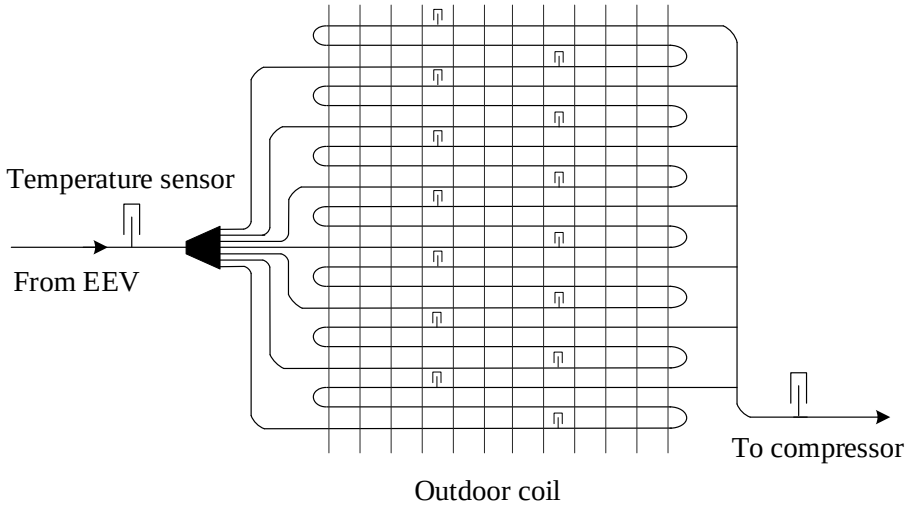

Fig. 4.8 The schematics of the installation positions for the outdoor coil surface temperature sensors

On the refrigerant side of the experimental ASHP / DFOC unit, a refrigerant mass flow meter was installed between the indoor coil and the EEV to measure the refrigerant mass flow rate. Both temperature sensors and refrigerant pressure sensors were installed at the inlet to, and the outlet from the compressor, the EEV, the indoor coil and the DFOC to measure the refrigerant temperatures and pressures at these locations.

On the air side of the experimental ASHP / DFOC unit, air temperature, air velocity and air relative humidity sensors were installed on both the windward and leeward sides of both the indoor coil and the DFOC. An air pressure difference sensor was also installed on the air side of the DFOC to measure the air pressure difference across it. In addition, in order to measure

the surface temperature of the 3-row FTHX in the DFOC, a total of fourteen temperature sensors were installed at different positions of each of the seven outdoor coil circuits, as illustrated in Fig. 4.8. The average value of the readings from the sixteen temperature sensors was taken as the averaged outdoor coil surface temperature.

Table 4.2 Detailed technical specifications of the sensors/transducers used in the experimental ASHP / DFOC setup

Sensors/Devices	*Uncertainty*	*Full scale*
Temperature sensor (PT1000)	Class A	-50 - 200 ℃
Humidity sensor	± 3.0 %	0 - 100 %
Air velocity sensor	± 0.02 %	0 - 5 m/s
Air pressure difference sensor	± 0.1 Pa	-125 -125 Pa
High-pressure transducers (Refrigerant)	± 0.4 %	0 - 40 bar
Low-pressure sensor transducers (Refrigerant)	± 0.4 %	0 - 25 bar
Refrigerant mass flowmeter	± 0.5 %	0 - 70 g/s
Power meter	± 1.0 %	/
Electronic scale	± 1 g	0 - 30 kg
CCD camera	/	100×micro magnification; Panoramic

Furthermore, power meters were also installed in the experimental setup to monitor and record electrical energy consumption of compressor and outdoor air fan. Data sampling interval for

all operating parameters in the experimental setup was 1 s. The details of all the sensors and transducers used in the experimental setup are given in Table 4.2.

4.5 Summary

An experimental ASHP / DFOC setup was specially established for carrying out the required experimental work of the research project reported in this Thesis. It consisted of the experimental ASHP / DFOC unit, the environmental chamber and the built-in computerized data monitoring and acquisition system.

The operation of the novel DFOC in the experimental ASHP / DFOC unit could be controlled manually or by program according to different experimental requirements. All operating parameters of the experimental setup can be measured, monitored and recorded real time by the installed high-precision sensors and transducers. The installation of the visualization system on the experimental ASHP / DFOC unit enabled the real-time observation of the outdoor coil surface status.

The availability of the established experimental ASHP / DFOC setup was expected to provide an essential basis in carrying out the experimental work in the research project reported in this Thesis, such as experimentally investigating even frosting characteristics and heating performances of the experimental ASHP / DFOC unit under different fan operating modes, validating a dynamic mathematical model for the experimental ASHP / DFOC unit and evaluating a novel control strategy to be developed for even frosting operation of the novel experimental ASHP / DFOC unit.

The photo images showing the experimental setup are given in Appendix.

Chapter 5

An experimental investigation on the even-frosting characteristics and heating performances of the experimental ASHP / DFOC unit

5.1 Introduction

The availability of the experimental ASHP / DFOC setup described in Chapter 4 enabled the carrying out the research project proposed in Chapter 3. In this thesis, different parts of the research project, including an experimental study, a mathematical modelling study and the development of a novel control strategy for the experimental ASHP / DFOC unit to achieve even frosting along the airflow direction, will be respectively presented in Chapters 5 to 7. In this Chapter, the feasibility and operating stability of using the novel DFOC to achieve even frosting along air flow direction were experimentally studied using the experimental ASHP / DFOC unit via 7 experimental cases under standard frosting operating ambient conditions.

The schematics of the developed novel DFOC, the experimental ASHP / DFOC unit and the experimental ASHP / DFOC setup are shown in Fig. 4.1, Fig. 4.2 and Fig. 4.3, respectively, in Chapter 4. In this Chapter, the experimental groups and cases are firstly specified. This is followed by reporting the experimental results and related discussion. Finally, conclusions are given.

5.2 Experimental cases and data reduction

5.2.1 Experimental groups and cases

In order to study the operating performances of the experimental ASHP / DFOC unit including its ability to achieve even frosting, two different experimental groups, consisting of a total of 7 experimental cases with different experimental purposes, were designed. Cases 1 - 4 were in Group 1 and Cases 5 - 7 in Group 2. All experimental cases were carried out at the same ambient condition of T_a at 2 ± 0.3 °C and RH at 85 ± 5 % in the simulated outdoor space, or Room A, respectively, and the same pre-set heating temperature at 20 °C in the simulated indoor heated space, or Room B. The two experimental groups are detailed in Table 5.1 and described separately as follows.

5.2.1.1 Operating modes and the control of the dual-fan operation

In this Chapter, three operating modes for fans and dampers in both groups during experiments were used, as follows:

PF mode: only Fan A was operated and dampers A1 and A2 fully opened, but Fan B was shut down with dampers B1 and B2 fully closed. This mode was used in Case 1 and Case 5.

CF mode: only Fan B was operated and dampers B1 and B2 fully opened, but Fan A was shut down and dampers A1 and A2 fully closed. This mode was used in Case 2 and Case 6, Furthermore, as this mode resembled the operating mode for a traditional single-fan outdoor coil, therefore, the experimental results obtained at this CF mode were used as a basis for

comparison.

Alternate operating mode: fans and dampers were alternately operated between CF mode and PF mode till defrosting was initiated, according to a pre-set time interval for alternate operation (t_{TIAO}). For example, in Case 3, with a t_{TIAO} of 15 mins for Fan A and Fan B, each fan took turns to operate for 15 mins till defrosting was initiated. During the alternate operation of the two fans, their matching dampers were either fully open or fully closed, according to Table 5.1. This mode was used in Cases 3, 4 and 7.

5.2.1.2 Purpose of cases in different groups

All experimental cases in Groups 1 and 2 were designed for different purposes. For Group 1, Cases 1 - 4 were all for a single frosting-defrosting operation cycle, aiming at verifying the feasibility of achieving evener frosting by using the novel DFOC. On the other hand, based on the experimental results from Group 1, Cases 5 - 7 in Group 2, which were all for multiple frosting-defrosting operation cycles lasting for 8 hours, were to validate the operating stability of the novel DFOC and to evaluate its ability in achieving even frosting during long-term operation. In addition, as shown in Table 5.1, the same operating mode was employed in Cases 1 and 5 and in Case 2 and 6, respectively, except test duration. In Case 4, t_{TIAO} was set at 10 mins for both fans, but in Case 7, unequal t_{TIAO} values were used, 6 mins for Fan A and 8 mins for Fan B, respectively, to evaluate even frosting performances when using unequal values of t_{TIAO}.

In addition, defrosting initiation strategy in Cases 1 - 7 was based on a fixed refrigerant tube

surface temperature (T_{ts}) at the exit from the FTHX. When T_{ts} reached -20 °C, defrosting was initiated, and reverse cycle defrosting method was used.

Table 5.1 Details of experimental groups and cases

Group	*Case*	*Fan status*		*Operating duration of each fan*		*Damper status*				*Single (S)/Multiple(M) frosting-defrosting cycles*
		A	**B**	**A**	**B**	**A1**	**A2**	**B1**	**B2**	
1	1	OP	SD	One complete frosting-defrosting cycle	None	FO	FO	FC	FC	*S*
	2	SD	OP	None	One complete frosting-defrosting cycle	FC	FC	FO	FO	
	3	Alternately OP	Alternately OP	15 mins in each alternation	15 mins in each alternation	When Fan A was operated, A1 and A2 were FO, B1 and B2 FC; When Fan B was operated, B1 and B2 were FO, A1 and A2 FC;				
	4	Alternately OP	Alternately OP	10 mins in each alternation	10 mins in each alternation	When Fan A was operated, A1 and A2 were FO, B1 and B2 FC; When Fan B was operated, B1 and B2 were FO, A1 and A2 FC;				
2	5	OP	SD	Complete multiple frosting-defrosting cycles	None	FO	FO	FC	FC	*M*
	6	SD	OP	None	Complete multiple frosting-defrosting cycles	FC	FC	FO	FO	
	7	Alternately OP	Alternately OP	6 mins in each alternation	8 mins in each alternation	When Fan A was operated, A1 and A2 were FO, B1 and B2 FC; When Fan B was operated, B1 and B2 were FO, A1 and A2 FC;				

OP: Operated SD: Shut down FO: Fully open FC: Fully closed

5.2.2 Data reduction

A number of performances indicators were used to evaluate the operating performances of the experimental ASHP / DFOC unit for both single and multiple frosting-defrosting operation cycles in the seven experimental cases.

Firstly, the relative evenness degree of frost layer, ε, was defined to directly evaluate the frosting evenness level on both sides of the FTHX, as follows:

$$\varepsilon = \frac{\left|\delta_{fA} - \delta_{fB}\right|}{1/2(\delta_{fA} + \delta_{fB})} \times 100\% \tag{5.1}$$

Where δ_{fA} and δ_{fB} are the averaged values of frost thickness on sides A and B of a FTHX at the same time point, respectively.

The closer to 0 the ε value, the evener the frosting on both sides.

In a single frosting-defrosting operation cycle, the heating energy loss due to frosting, ΔE_f (kJ), during a frosting operation [Bai et al., 2018], was also defined as follows:

$$\Delta E_f = \int_{t_0}^{t_f} (q_{NF} - q_t)\,\mathrm{d}t \tag{5.2}$$

Where t_0 and t_f are the starting time point and ending time point of a frosting operation prior to defrosting initiation, q_{NF} the instantaneous heating output capacity under a non-frosting condition, q_t the actual instantaneous output heating capacity at a certain time point, and can be evaluated by:

$$q_t = m_r(h_{rd} - h_{rs}) \tag{5.3}$$

Where m_r is the refrigerant mass rate (kg/s), h_{rd} and h_{rs} the refrigerant enthalpy (kJ/kg) at compressor discharge and suction, respectively.

Secondly, an output heating capacity loss efficient due to frosting, κ_f, during a frosting operation, was used to indicate the rate of reduction in output heating capacity loss per unit time, %/min, as follows:

$$\kappa_f = \frac{\Delta E_f}{60(t_f - t_0)\int_{t_0}^{t_f} q_{NF}\mathrm{d}t} \tag{5.4}$$

For multiple frosting-defrosting operation cycles, an averaged output heating capacity loss coefficient due to frosting, $\bar{\kappa}_f$, was:

$$\bar{\kappa}_f = \frac{1}{n}\sum_{i=1}^{n}\kappa_{fi} \tag{5.5}$$

Where κ_{fi} is the output heating efficiency loss efficient in the i^{th} frosting-defrosting operation cycle and n the total number of frosting-defrosting operation cycles.

Thirdly, the averaged output heating capacity, $\bar{q}$, in a complete single frosting-defrosting operation cycle, was defined as:

$$\bar{q} = \frac{\int_{t_0}^{t_{end}} q_t\mathrm{d}t}{t_{end} - t_0} \tag{5.6}$$

$$t_{end} = t_f + t_{def} \tag{5.7}$$

Where t_{def} is the duration of the defrosting operation, s, and t_{end} the end time point in single frosting-defrosting operation cycle.

For multiple frosting-defrosting operation cycles:

$$t_{end} = \sum_{i=1}^{n} (t_f + t_{def})_i \tag{5.8}$$

When Equation (5.8) was used, $\bar{q}$ in Equation (5.6) would be the averaged output heating capacity in multiple frosting-defrosting operation cycles, accordingly.

Finally, the coefficient of performance at any time point of t, COP_t, was defined to evaluate the overall energy performances of the experimental ASHP unit:

$$COP_t = \frac{q_t}{W_t} \tag{5.9}$$

Where W is the instantaneous power input to the experimental ASHP unit at a time point t.

The averaged coefficient of performance, $\overline{COP}$, for a single or multiple frosting-defrosting operation cycles was:

$$\overline{COP} = \frac{\int_{t_0}^{t_{end}} q_t \mathrm{d}t}{\int_{t_0}^{t_{end}} W_t \mathrm{d}t} \tag{5.10}$$

When using Equation (5.10), using Equation (5.7) for a single frosting-defrosting operation

cycle, and Equation (5.8) for multiple frosting-defrosting operation cycles.

5.3 Experimental results and discussions

5.3.1 Results from Group 1

In this Section, the experimental results from the four cases in Group 1 are reported in Fig. 5.1, and results of Case 2 using the traditional single fan outdoor coil were selected as the basis for comparison in this section. Fig. 5.1 a) shows the refrigerant tube surface temperature, T_{ts}, in all cases of Group 1. As seen, T_{ts} values for Cases 1 - 4 all declined during frosting operation. However, as the operating modes were different, the frosting operating duration prior to defrosting initiation, t_f, was different from case to case. t_f was 2668s (44.5 mins) for Case 1, 3235s (53.9 mins) for Case 2, 3960s (66.6 mins) for Case 3 and 4360s (72.5 mins) for Case 4, respectively. Compared to the result in Case 2, the frosting operation durations in Cases 3 and 4 were increased by 23.6 % and 34.5 %, respectively. These experimental results clearly demonstrated that frosting operation durations when using the novel DFOC in Case 3 and Case 4 were remarkably lengthened as compared to those in Case 2. Furthermore, the experimental results from Case 3 and Case 4 suggested that the use of a smaller t_{TIAO} value can lead to a longer frosting duration, from 66.6 mins in Case 3 at a t_{TIAO} value of 15 mins to 72.5 mins in Case 4 at a t_{TIAO} value of 10 mins.

Fig. 5.1 b) shows the variations in q_t values and Fig. 5.1 c) COP_t values in the four cases. As seen, the values of both q_t and COP_t in the four cases were all decreased to a similar level prior to defrosting initiation. The averaged output heating capacity, $\bar{q}$, was 5.71 kW in Case 1, 6.22

kW in Case 2, 6.54 kW in Case 3 and 6.81 kW in Case 4 respectively, and the averaged *COP* values, $\overline{COP}$ s, in Cases 1 - 4 were 2.86, 2.94, 3.13 and 3.25, respectively. Hence, when compared to the results in Case 2, $\bar{q}$ and $\overline{COP}$ values were increased by 5.5 % and 6.7 % in Case 3, and by 9.5 % and 10.5 % in Case 4, respectively.

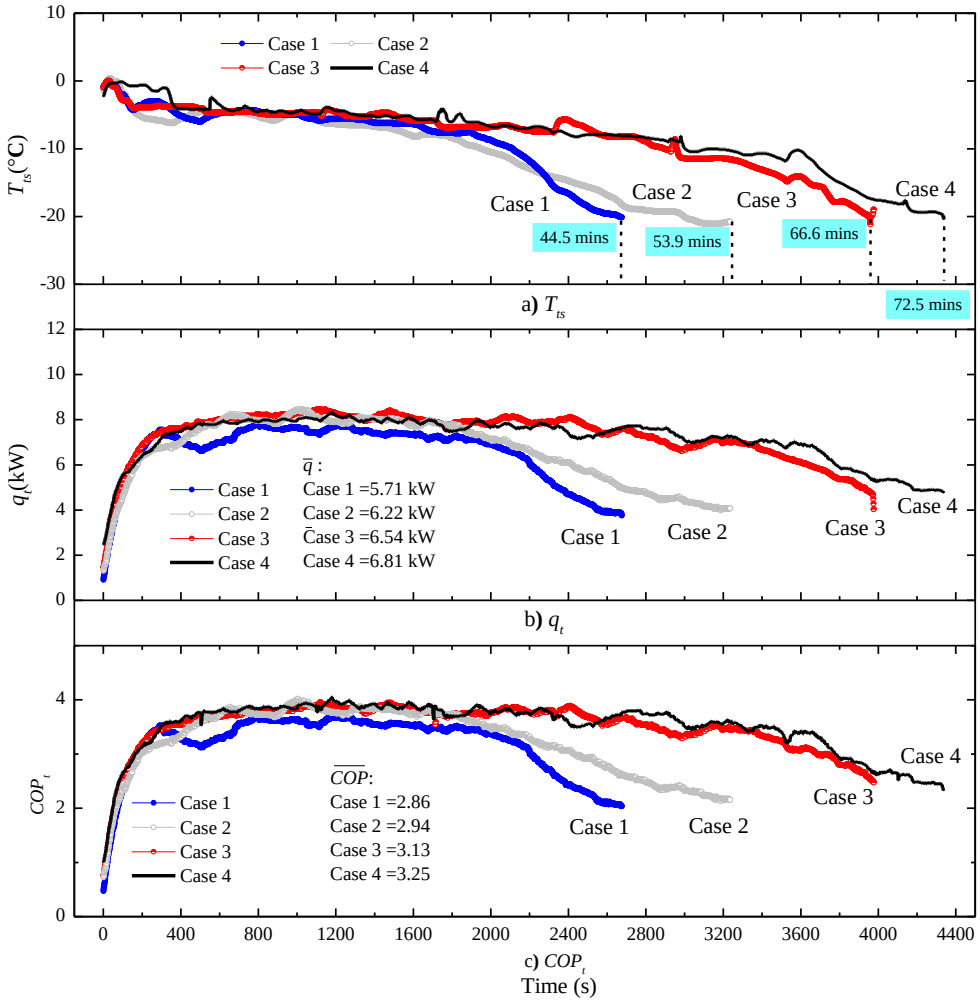

Fig. 5.1 The experimental results for the four cases in Group 1

Fig. 5.2 presents the weighted melted frost mass, M_{dfw}, and defrosting duration, t_{def}, in the four cases. As seen, M_{dfw} was 2.13 kg in Case 1, 2.28 kg in Case 2, 3.64 kg in Case 3 and 3.70 kg in Case 4, respectively. M_{dfw} in Case 3 was 159 % and in Case 4 162% of that in Case 2. This demonstrated that more frost would deposit on the FTHX in Cases 3 - 4, because when frosting

on both windward and leeward sides was more balanced, frost would be accumulated on both sides, as compared to that frost would only deposit on the windward side when traditional single fan outdoor coils were used. Besides, values for t_{def} in Cases 1 - 4 were at 158 s,164 s, 179 s and 183 s, respectively.

Fig. 5.3 shows the photo images of local view of frosting on both the windward and leeward sides of the FTHX in Cases 1 - 4. As seen, at the same time point, frost deposited on the windward side was always much more than that on the leeward side in Case 1 and 2 prior to defrosting operation. However, similar levels of frosting on both sides in Cases 3 and 4, where the novel DFOC was used, were observed prior to defrosting. This further indicated that using the novel DFOC can achieve evener frosting on both sides of the FTHX, as compared to using the single-fan coil in Cases 1 and 2.

The evaluated values of frost thickness based on the photo images shown in Fig. 5.3 are listed in Table 5.2. As seen, the relative evenness degree of frost thickness, ε, was changed from 87.2 % to 116 % in Case 1, from 115.2% to 80.9 % in Case 2, from 42.8 % to 5.4 % in Case 3 and from 40 % to 4.3 % in Case 4. The ε values in Cases 3 and 4 were significantly smaller than those in Cases 1 and 2, demonstrating that using the novel DFOC can significantly improve the frosting evenness on both sides of the experimental FTHX, as compared to using the single fan coils. Besides, with the t_{TIAO} value reduced from 15 mins in Case 3 to 10 mins in Case 4, ε was further decreased, suggesting that frosting evenness on both sides was improved further.

The experimental results in Group 1 suggested that using the novel DFOC to achieve evener frosting can remarkably prolong the heating/frosting duration and improve the heating

performances in terms of averaged output heating capacity and *COP*, and enabled frost to be more evenly deposited on the both sides of the FTHX as a result of alternate reversed airflow direction, when compared to using the traditional single-fan outdoor coil. Therefore, the novel dual-dan outdoor coil can help achieve the evener frosting on the FTHX with better operating performances and longer heating duration, compared to the traditional single-fan coil.

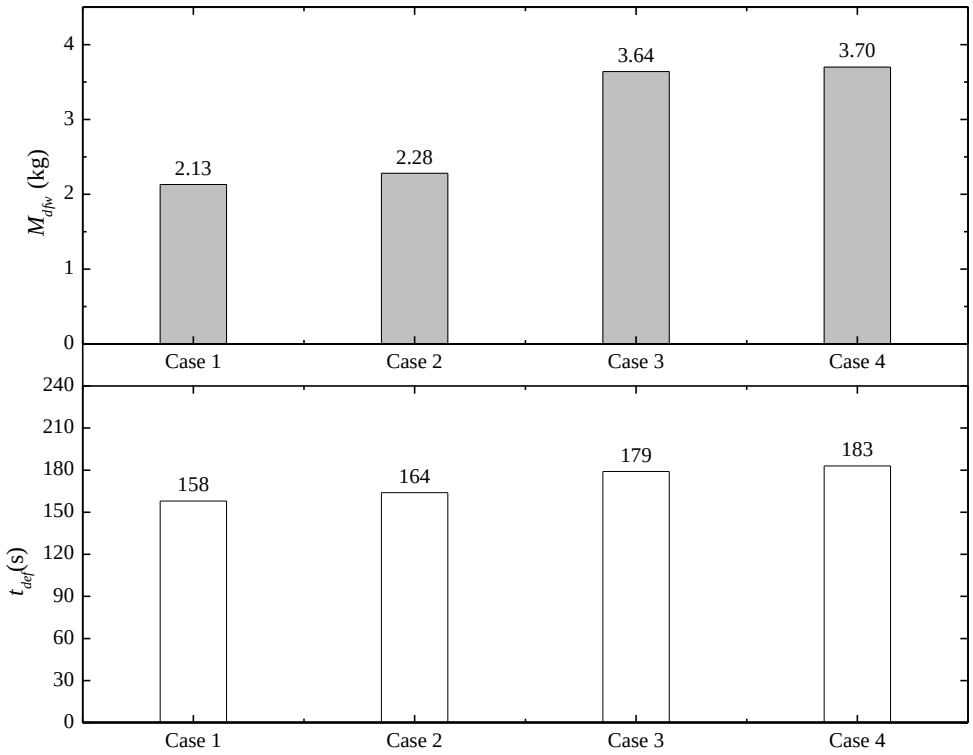

Fig. 5.2 Melted frost mass, M_{dfw}, and defrosting duration, t_{def}, in the four experimental cases in Group 1

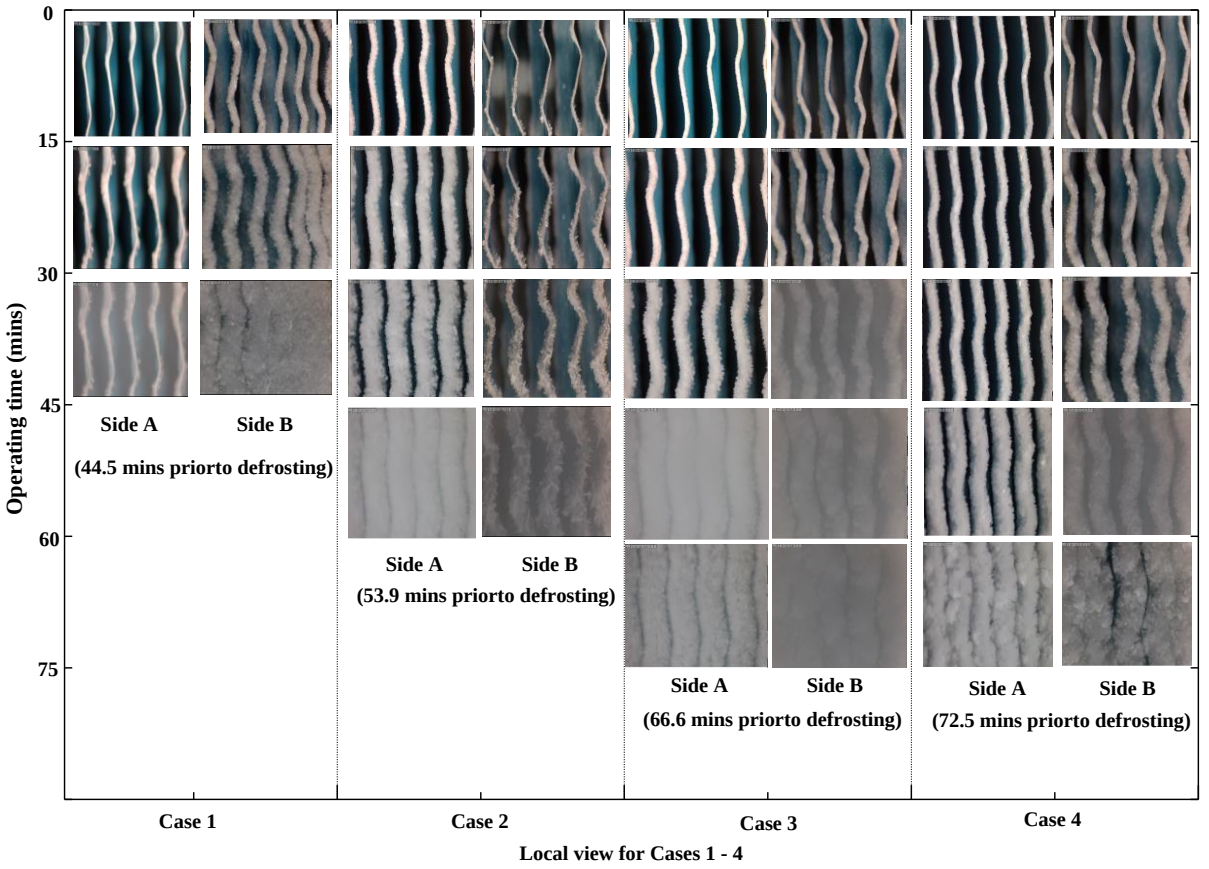

Fig. 5.3 Frosting photo images of local view for Cases 1- 4 in Group 1

Table 5.2 Averaged values of frost thickness on both sides of a FTHX in Cases 1 - 4 in Group 1

Operating time (mins)	Averaged values of frost thickness in different cases (mm)											
	Case 1			Case 2			Case 3			Case 4		
	δ_{fA}	δ_{fB}	ε (%)	δ_{fA}	δ_{fB}	ε (%)	δ_{fA}	δ_{fB}	ε (%)	δ_{fA}	δ_{fB}	ε (%)
15	0.11	0.28	87.2	0.26	0.07	115.2	0.17	0.11	42.8	0.15	0.10	40
30	0.24	0.64	90.9	0.55	0.17	105.6	0.35	0.24	37.3	0.28	0.20	33.3
45	0.25*	0.94*	116	0.81	0.34	81.7	0.51	0.39	26.7	0.46	0.36	24.4
60				0.92*	0.39*	80.9	0.82	0.66	21.6	0.75	0.61	20.6
75							0.95*	0.90*	5.4	0.95*	0.92*	4.3

*Thickness values prior to defrosting initiation

5.3.2 Results from Group 2

The experimental results in Cases 5 - 7 of Group 2 are shown in Figs. 5.4 - 5.7, and results in Case 6 were used as a basis for comparison. Fig. 5.4 shows the values of T_{ts}, in the three cases. As seen, within the experimental duration of 8 hours, there were totally ten and nine frosting-defrosting cycles in Case 5 (PF mode) and Case 6 (CF mode), respectively, but only six frosting-defrosting cycles in Case 7, where the novel DFOC was used. The number of defrosting operation was decreased by 33.3 % in Case 7, as compared to the result in Case 6. These demonstrated that the use of the novel DFOC can help remarkably reduce the defrosting frequency of the experimental ASHP unit, to achieve a longer and more stable heating/frosting operation duration, as a result of evener frosting on both sides of the FTHX.

Fig. 5.5 shows the measured output heating capacity, q_t, and Fig. 5.6 COP_t values in the three experimental cases. As seen, similar decreasing trends in q_t and COP_t during each frosting-defrosting cycle in each case prior to defrosting were demonstrated. $\overline{q}$ in Cases 5 - 7 was 5.74 kW, 6.15 kW and 6.74 kW, respectively, and $\overline{COP}$ was 2.76 in Case 5, 2.89 in Case 6 and 3.21 in Case 7, respectively. $\overline{q}$ was increased by 9.6 %, and $\overline{COP}$s by 11.1% in Case 7, when compared to those in Case 6. Therefore, once again, it can be seen the use of the novel DFOC can result in an improved heating operating performance of the experimental ASHP unit, in terms of *COP* and output heating capacity as compared to the use of traditional single-fan outdoor coils.

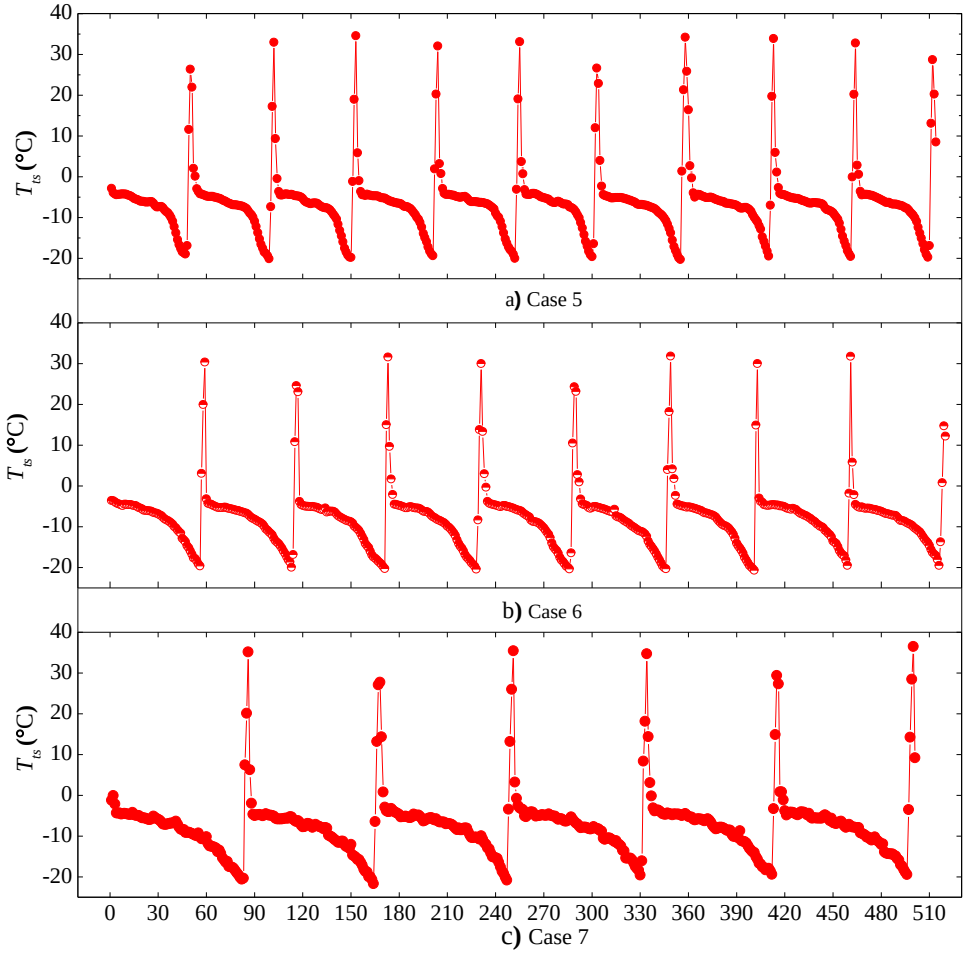

Fig. 5.4 The measured refrigerant tube surface temperature, T_{ts}, in Cases 5 - 7

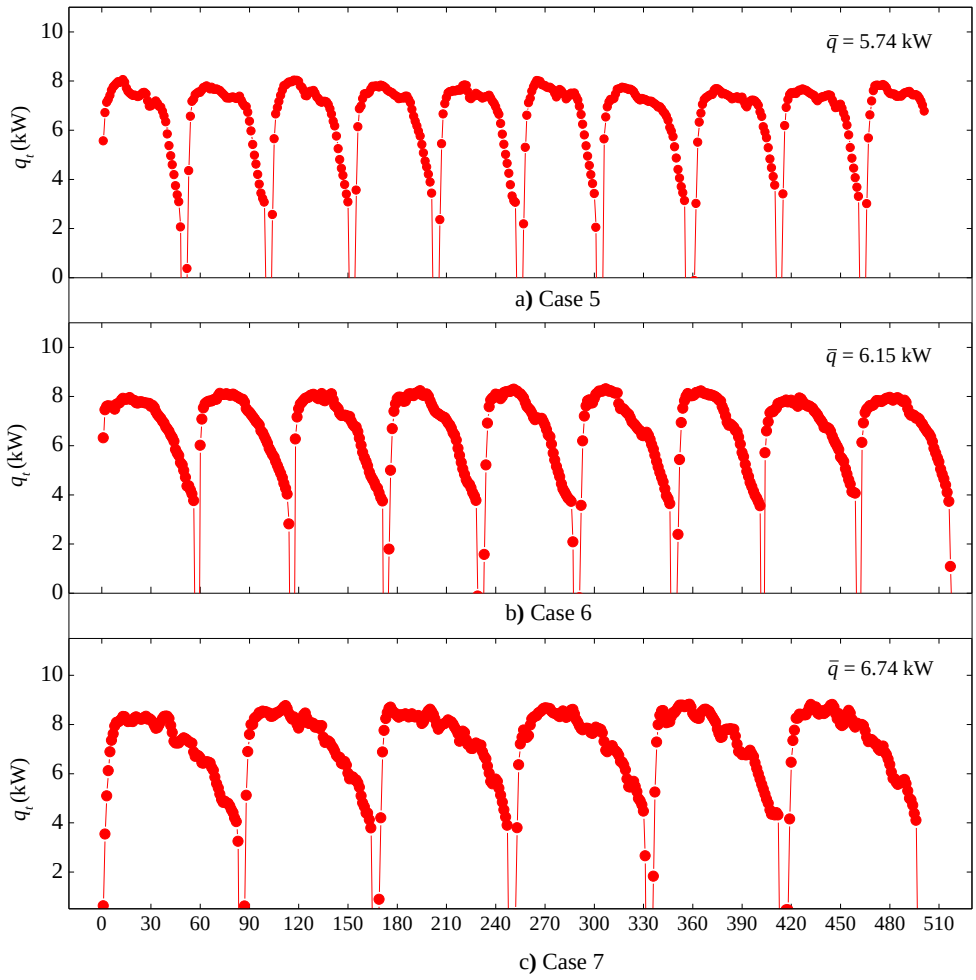

Fig. 5.5 The measured output heating capacity, q_t, and its averages of the experimental ASHP unit in Cases 5 - 7

Fig. 5.7 shows the values of t_f, and t_{def}, and M_{dfw} in each frosting-defrosting cycle in Cases 5 - 7. As shown in Fig. 5.7 a), t_f values in each frosting-defrosting cycle in the same case were similar, but significantly different in different cases. The averaged t_f was 46.2 mins in Case 5, 54.3 mins in Case 6 and 79.5 in Case 7. The averaged t_f value was remarkably increased by 46.4 % in Case 7 when compared to that in Case 6. However, the averaged value of t_{def} in Cases 5, 6 and 7 was 160.7s, 161.2 s and 182s, respectively, reflecting more frost was deposited on both sides of the FTHX surface. Therefore, a longer duration was required to melt frost on the FTHXs surface in Case 7.

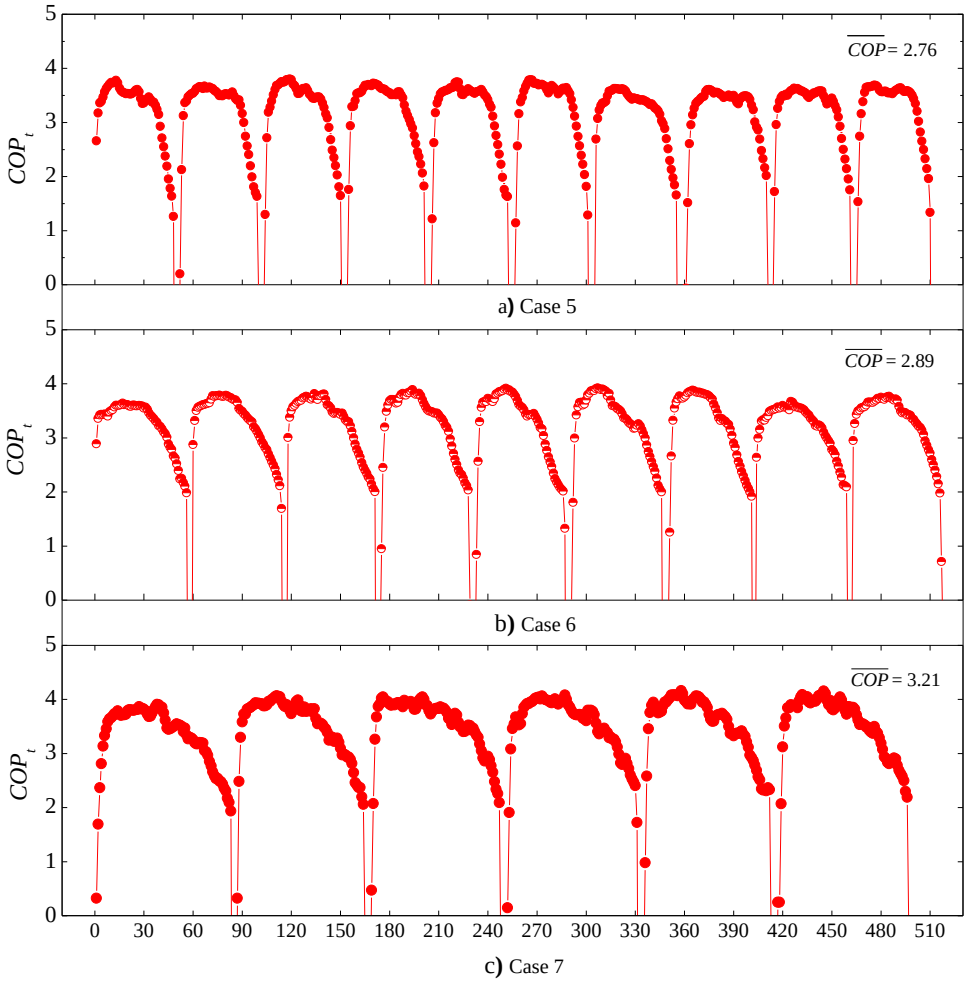

Fig. 5.6 The measured COP_t and its averages of the experimental ASHP unit in Cases 5 - 7

On the other hand, as seen from Fig. 5.7 c), M_{dfw} values in each of the frosting-defrosting cycles in Case 5 were similar to that in Case 6, and the averaged M_{dfw} value in all frosting-defrosting cycles was 2.1 kg in Case 5 and 2.3 kg in Case 6, respectively. However, the averaged value of M_{dfw} in Case 7 was 3.6 kg in all the six frosting-defrosting cycles, which was 157 % of that in Case 6. This further reflected that more frost was deposited on both sides of the FTHX surface due to evener frosting, when the novel DFOC was used.

The experimental results from Group 2 further demonstrated that at a longer experimental operating duration, the use of the novel DFOC could operate steadily and also help achieve

evener frosting on both sides of the FTHX, leading to a longer frosting operating duration, higher operating efficiency and output heating capacity.

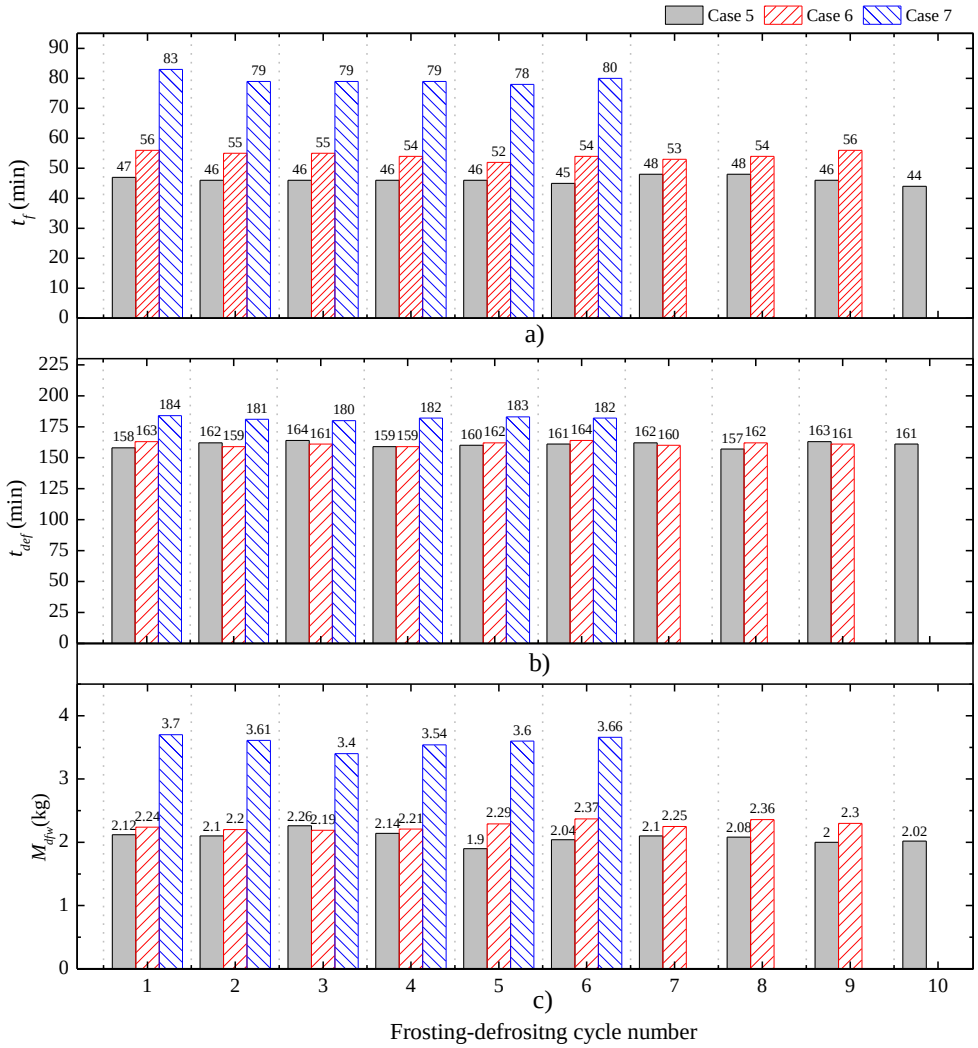

Fig. 5.7 The measured t_f, t_{def} and M_{dfw} in each of the frosting-defrosting cycles in Cases 5 - 7

5.3.3 Discussions

In experimental Cases 3 and 4 of Group 1 and Case 7 of Group 2, different values of t_{TIAO} were used. In this section, the impacts of using different values of t_{TIAO} on the operating performances of the experimental ASHP unit having the dual-fan outdoor coil are further discussed.

The characteristics of even frosting using different values of t_{TIAO} may be indirectly reflected

by $\bar{\kappa}_f$, as shown in Fig. 5.8. As mentioned in earlier sections, the value of t_{TIAO} was 15 mins in Case 3 and 10 mins in Case 4, and 6 mins for Fan A and 8 mins for Fan B in Case 5. Therefore, when a smaller t_{TIAO} value was used, the averaged value of $\bar{\kappa}_f$ was reduced gradually from 0.73 %/min in Case 3, 0.68 %/min in Case 4, to 0.64 %/min in Case 7, a reduction by 8.2 % in Case 4 and 12.3% in Case 7 as compared to the results in Case 3. Correspondingly, heating/frosting operating duration was increased from 66.6 mins in Case 3 to 72.5 mins in Case 4 and further to 79.5 mins in Case 7, an increase by 8.9 % in Case 4 and 19.4 % in Case 7 as compared to the results in Case 3. Meanwhile, $\bar{q}$ was at 6.45 kW in Case 3, 6.81 kW in Case 4 and 6.74 kW in Case 7, and $\overline{COP}$ was 3.13, 3.25 and 3.21 in Cases 3, 4 and 5, respectively. $\bar{q}$ was increased by 5.6 % in Case 4 and 4.5 % in Case 7, and $\overline{COP}$ by 3.8 % in Case 4 and 2.6 % in Case 7, as compared to those in Case 3.

Moreover, considering the frosting rate difference on sides A and B, as demonstrated by the results from Cases 1 and 2 shown in Table 5.2, unequal t_{TIAO} values for Fan A and Fan B used in Case 7 were actually more preferred. Therefore, properly selecting values of t_{TIAO} for Fan A and Fan B can help further prolong a heating duration and improve heating performance of the experimental ASHP unit.

Therefore, the smaller the t_{TIAO} value, the higher heating capacity and longer heating/frosting duration would result in, and the use of unequal values of t_{TIAO} for two fans could lead to better results. However, using smaller t_{TIAO} values for Fan A and Fan B may lead to frequent switching of the operation of the two fans, thus reducing their service life and leading potentially to the unstable operation of the experimental ASHP unit. Therefore, it became necessary to carry out further studies to identify the most appropriate value of t_{TIAO} for efficient yet stable operation of the experimental ASHP unit.

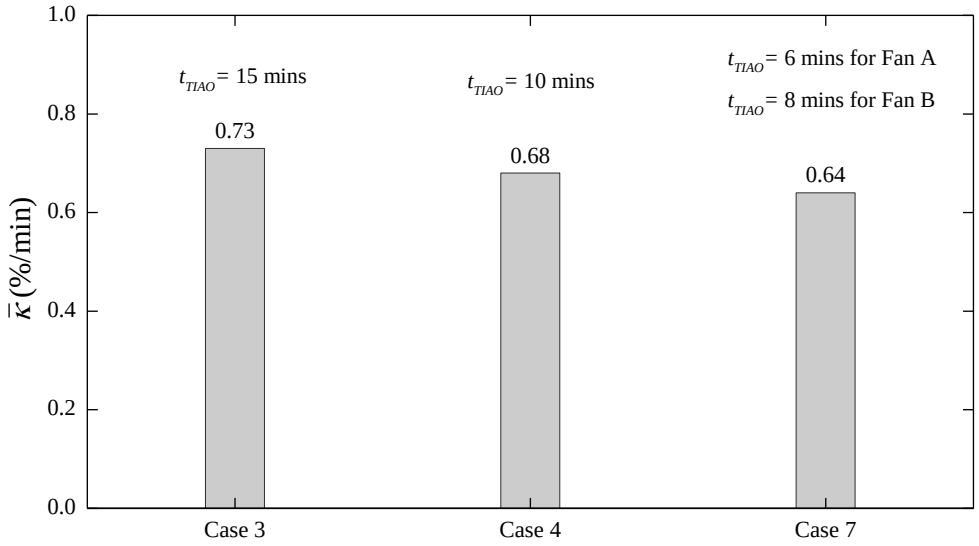

Fig. 5.8 Heating capacity loss coefficient, $\overline{\kappa}_f$, in Cases 3, 4 and 7

5.4 Conclusions

In this Chapter, in order to achieve evener frosting on both sides of FTHXs used in an outdoor coil and thus improve the operating performances of ASHP units, an experimental ASHP / DFOC unit was experimentally studied. Two experimental groups having a total of 7 cases were designed to investigate the feasibility and operating stability in achieving evener frosting on FTHXs. The conclusions for this Chapter are as follows:

(1) The experimental results from Group 1 demonstrated that the use of the novel DFOC can achieve even frosting on both sides rather than a single side of a FTHX by alternately reversing air flow direction, leading to a longer heating duration and higher operating performances compared to the use of a traditional single fan outdoor coil. Furthermore, when the values of t_{TIAO} for two fans were set at 15 mins and 10 mins, respectively, the heating/frosting duration was increased by 23.6 % and 34.5 %, $\overline{q}$ by 5.5 % and 9.5 %, and $\overline{COP}$ by 6.7 % and 10.5 %, respectively, when compared to those using the traditional single-fan outdoor coil.

(2) The experimental results from Group 2 suggested that using the novel DFOC can lead to a

longer and more stable heating duration, better heating performance and less defrosting frequency, as compared to using the traditional single-fan outdoor coil. When using the novel dual-fan outdoor coil, defrosting frequency was reduced by 33.3 %, the averaged heating/frosting duration was increased by 46.4 %, $\bar{q}$ and $\overline{COP}$ by 9.6 % and 11.1 %, respectively, when compared to those using the traditional single fan outdoor coil.

(3) The comparison results when using different t_{TIAO} values demonstrated that, the smaller the t_{TIAO} values, the evener the frosting on the FTHXs, and smaller the $\bar{\kappa}_f$ values, and thus the better the heating performances of the experimental ASHP / DFOC unit. When the value of t_{TIAO} at 15 mins for two fans was changed to t_{TIAO} at10 mins for both fans, and to 6 mins for Fan A and 8 mins for Fan B, heating/frosting operation duration was increased by 8.9 % and 19.4%, $\bar{q}$ by 5.6 % and 4.5 %, and $\overline{COP}$ by 3.8% and 2.6 %, $\bar{\kappa}_f$ reduced by 8.3 % and 12.6 %, respectively, when using the experimental results at 15 mins t_{TIAO} value as the basis for comparison.

Therefore, the experimental results reported in this Chapter have proved that the use of the novel DFOC can help achieve evener frosting on the both sides of the FTHX, leading to the longer heating/frosting operation duration, higher heating efficiency and lower defrosting frequency, compared to the use of a traditional single fan outdoor coil. However, to fully understand the operating characteristics of the experimental ASHP / DFOC unit at other non-experimental configuration and operating conditions, and to control the operation of experimental ASHP / DFOC unit for the desired even frosting along air flow direction, it became necessary to further develop a dynamic mathematical model for the experimental ASHP /DFOC unit and an optimal control strategy for achieving evener frosting along the airflow direction at higher heating performances. These will be reported respectively in Chapters 6 and 7.

Chapter 6

Development of a dynamic mathematical model for investigating the even frosting characteristics of an ASHP / DFOC unit

6.1 Introduction

An experimental study on the even frosting characteristics of the experimental ASHP / DFOC unit was successfully carried out and the study results are presented in Chapter 5. It was demonstrated that the use of the experimental ASHP / DFOC unit was able to help achieve even frosting along the airflow direction of the FTHX with higher heating performances. However, both the experimental ASHP unit and the DFOC had a fixed configuration, with a fixed total rated output heating capacity or heat transfer surface area, fixed rated air flow rates for both fans, and the related experiments were carried out at a limited number of experimental conditions. Therefore, it was considered highly necessary to further develop a comprehensive physics-based dynamic mathematical model that can be used to numerically study the operating performances of an ASHP / DFOC unit, where the configurations of an ASHP / DFOC unit and the operating ambient conditions may be varied.

Therefore, a dynamic mathematical model for the experimental ASHP / DFOC unit used in the experimental study presented in Chapter 5 has been developed and is reported in this Chapter. Firstly, the establishment of a dynamic mathematical model is presented and a new sub-model for the experimental DFOC described in great detail. Then, the experimental validation for the dynamic model using the experimental data presented in Chapter 5 is reported. This is followed by presenting a follow-up modelling study using the validated model. There were three study groups for the different values of t_{TIAO} for the two fans, different fin pitches used in a DFOC

and different operating ambient conditions in the modelling study. Finally, conclusions are given.

6.2 Model development and validation for the experimental ASHP / DFOC unit

6.2.1 Model development for the experimental ASHP / DFOC unit

Fig. 6.1 shows schematically the conceptual model for the complete experimental ASHP / DFOC unit. As seen, the model was made of sub-models for these key components of the ASHP unit, corresponding to those shown in Fig. 4.2 in Chapter 4. Except for the sub-model for the novel DFOC, which was specially developed for this research project, all other sub-models were made available by referring to existing ones for these components in a direct-expansion air conditioning system.

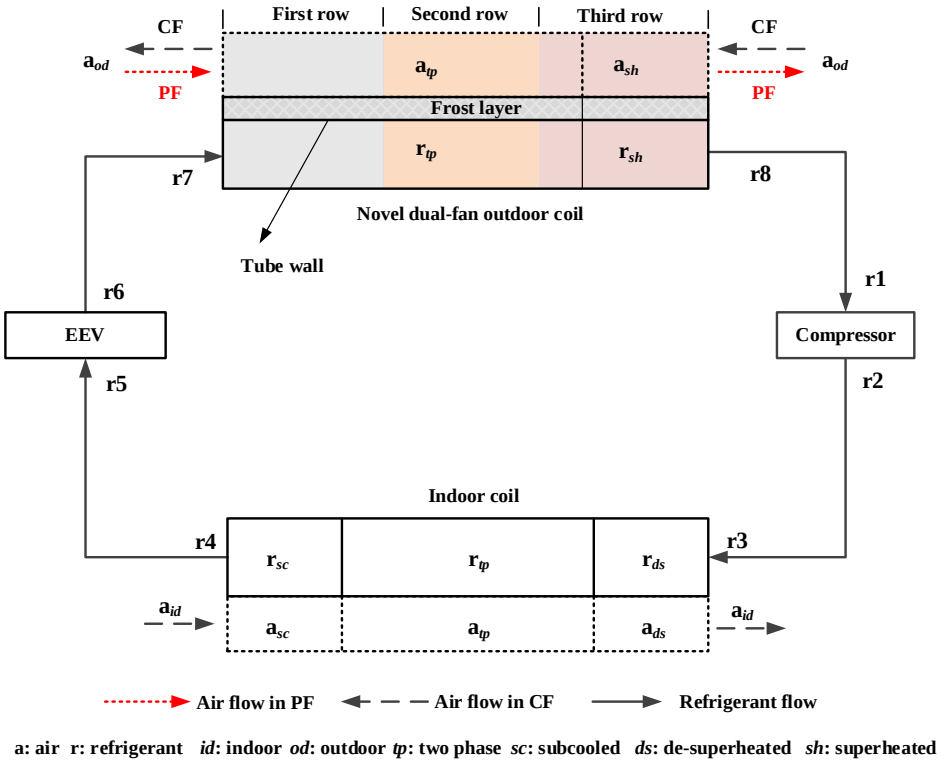

Fig. 6.1 The conceptual model of the complete experimental ASHP / DFOC unit

6.2.1.1 Sub-model of the experimental DFOC

The sub-model of the DFOC was made of two modules: a frosting module, and a FTHX module which had three parts including refrigerant side, pipe wall and air side. For the frosting module, Zhang et al [2022] has developed a detailed dynamic frosting model based on a single row FTHX, and the main equations used are reproduced in Table 6.1. To solve the equations for frost growth in the sub-model, the segment-by-segment method was employed along the direction of frost growth. Equations (6.1) - (6.3) and (6.11) in Table 6.1 were discretized by using the finite difference method, and they were then solved together with all other remaining equations in Table 6.1.

Table 6.1 Main equations for frost formation used in the frosting model developed by Zhang et al [2022]

Physical process	Equations	No.	Explanations	References
Heat and mass transfer equations inside a frost layer	$\dot{m}_w(x) = D_{eff}(x)\rho_a(x)\frac{dw_f(x)}{dx}$	(6.1)	Local water vapor mass flux inside the frost layer	[Brèque and Nemer, 2016]
	$\frac{d\dot{m}_f(x)}{dx} = C\rho_a(x)[w_f(x) - w_{sat}(x)]$	(6.2)	Amount of water vapor absorbed in each control volume of the frost layer	
	$\dot{q}(x) = k_f(x)\frac{dT_f(x)}{dx}$	(6.3)	Local heat flux inside the frost layer	[Lee et al., 1997]
	$\frac{d\dot{q}(x)}{dx} = -l_{sv}C\rho_a(x)[w_f(x) - w_{sat}(x)]$	(6.4)	Energy balance in each control volume of the frost layer	
Heat and mass transfer equations on a frost surface	$\dot{q}_{sens,fs} = h_{eff}[\overline{T}_a - \overline{T}_{fs}]\ \ \dot{q}_{lat,fs} = l_{sv}\dot{m}_{\delta,f}$	(6.5, 6)	Sensible and latent heat flux at frost surface	
	$\dot{m}_{fs} = h_{m,eff}\rho a(\overline{w}_a - w_{fs})$	(6.7)	Water vapor mass flux at frost surface	
	$\dot{m}_{\rho,f} = D_{eff}\rho_a\left.\frac{dw_f}{dx}\right\|_{fs}$	(6.8)	Water vapor mass flux used for increasing frost density	
	$\dot{m}_{\delta,f} = m_{f,a} - m_{\rho,f}$	(6.9)	Water vapor mass flux used for increasing frost thickness	
	$\delta_f\big\|_{t+\Delta t} = \delta_f\big\|_t + \frac{\dot{m}_{\delta,f}\big\|_t}{\rho_f\big\|_{t,x\to fs}}$	(6.10)	Frost thickness at each time interval	
	$\dot{q}_{tot,fs} = k_{eff}\left.\frac{dT_f}{dx}\right\|_{fs} = \dot{q}_{sen,fs} + \dot{q}_{lat,fs}$	(6.11)	Total heat flux at frost surface	
Heat and mass transfer equations in the air stream	$Q_{sens,a} = c_{p,a}m_a(T_{a,in} - T_{a,out}) = \dot{q}_{sens,fs}A_{fs}$	(6.12)	Air side sensible heat transfer rate	
	$m_{f,a} = m_a(w_{a,in} - w_{a,out}) = \dot{m}_f A_{fs}$	(6.13)	Air side mass transfer rate	
	$Q_{tot,a} = Q_{sens,a} + l_{sv}m_{f,a}$	(6.14)	Total heat transfer rate on air side	

* x in Equations (6.1) – (6.4) represents the arbitrary thickness of frost layer perpendicular to a cold surface.

Furthermore, to model the three-row FTHX used in DFOC, a frosting model developed by Yao et al [2004] may be used as a basis, by modifying its fixed air flow direction and certain geometry parameters, such as fin type and fin pitch. Therefore, the above-mentioned two frosting models were referenced but updated according to the actual configuration of the novel experimental DFOC. Besides, since wave fins were actually used in the three-row FTHX of the DFOC, to obtain accurate convective heat transfer coefficients under different operating conditions, Colburn factor, *j*, used in the above-mentioned models was correspondingly updated as follows [Wang et al., 2002]:

Under dry condition, at Reynolds number, Re_{Dc}, ≥1000, j_{dry} was evaluated by

$$j_{dry} = 0.0646 Re_{Dc}^{j_1} \left(\frac{D_c}{D_h}\right)^{j_2} \left(\frac{F_s}{P_t}\right)^{-0.103} \left(\frac{P_l}{D_c}\right)^{0.432} \times (\tan\theta)^{-0.692} N^{-0.737} \tag{6.15}$$

Where j_1 and j_2 are

$$j_1 = -0.0545 - 0.0538\tan\theta - 0.302 N^{-0.24} \times \left(\frac{F_s}{P_l}\right)^{-1.3} \times \left(\frac{P_l}{P_t}\right)^{0.379} \left(\frac{P_l}{D_h}\right)^{-1.35} (\tan\theta)^{-0.256} \tag{6.16}$$

$$j_2 = -1.29 \left(\frac{P_l}{P_t}\right)^{1.77 - 9.43\tan\theta} \left(\frac{D_c}{D_h}\right)^{0.229 - 1.43\tan\theta} \times N^{-0.166 - 1.08\tan\theta} \left(\frac{F_s}{P_t}\right)^{-0.174\ln(0.5N)} \tag{6.17}$$

$$F_s = F_p - \delta_{fin} \tag{6.18}$$

It should be noted that the dimension parameters of the FTHX, such as fin pitch, F_p, fin space, F_s, tube outer diameter, D_c and transverse tube spacing, P_t, etc, used in Equations (6.16) - (6.18) under frosting conditions should consider local frost thickness. For example, the value of fin space at a time point, *t*, or $F_s\big|_t$, under frosting conditions was evaluated by

$$F_s\big|_t = F_p - \delta_{fin} - 2\,\delta_f\big|_t \tag{6.19}$$

Where $\delta_f\big|_t$ is the local frost thickness at *t* time point, δ_{fin}, fin thickness.

6.2.1.2 Dynamic model for the experimental ASHP / DFOC unit

To develop the complete dynamic model for the experimental ASHP / DFOC unit shown in Fig. 4.2 in Chapter 4, in addition to the sub-model for the DFOC described in Section 6.2.1.1, sub-models for other key components including the compressor, condenser or indoor unit and EEV should also be established. In the existing literatures, Pan et al [2012] and Chen and Deng [2006] developed and experimentally validated models for direct expansion air cooling systems, whose compressor, condenser and EEV were similar to those in the experimental ASHP unit. Therefore, the sub-models of compressor, condenser and EEV in references [Pan et al., 2012] and [Chen and Deng, 2006] were adopted, with necessary updates according to the actual specifications of these components in the experimental ASHP unit. Consequently, together with the sub-model for the DFOC, the complete dynamic model for the experimental ASHP unit having the novel DFOC has been established, with a total of more than 90 equations.

As seen from Fig. 6.1, all the sub-models were systematically integrated by the refrigerant flow on the refrigerant side and the outputs from one sub-model were the inputs to the next one connected downstream. For example, the outputs from the sub-model for EEV, including the refrigerant mass, flow rate, pressure and temperature, were used as the inputs to the sub-model of DFOC. Besides, the equations for the thermal properties of the refrigerant used in the experimental ASHP unit, R410A, were obtained from Refprop [Lemmon et al., 2013] and the State Equations for humid air from ASHRAE Handbook [2010].

In addition, the output heating capacity, *Q*, and the coefficient of performance, COP, of the experimental ASHP unit, based on Fig. 6.1, were as follows:

$$Q = m_r(h_{r4} - h_{r3}) \tag{6.20}$$

where m_r is the refrigerant mass flow rate, h_{r3} and h_{r4} refrigerant enthalpy at the inlet to, and the outlet from, the indoor coil, evaluated based on the refrigerant temperatures and refrigerant pressures at indoor coil's inlet and outlet.

$$COP = \frac{Q}{W} \tag{6.21}$$

where W is the total power input to both the compressor and outdoor air fan of the experimental ASHP unit.

6.2.1.3 Numerical scheme for solving the developed model

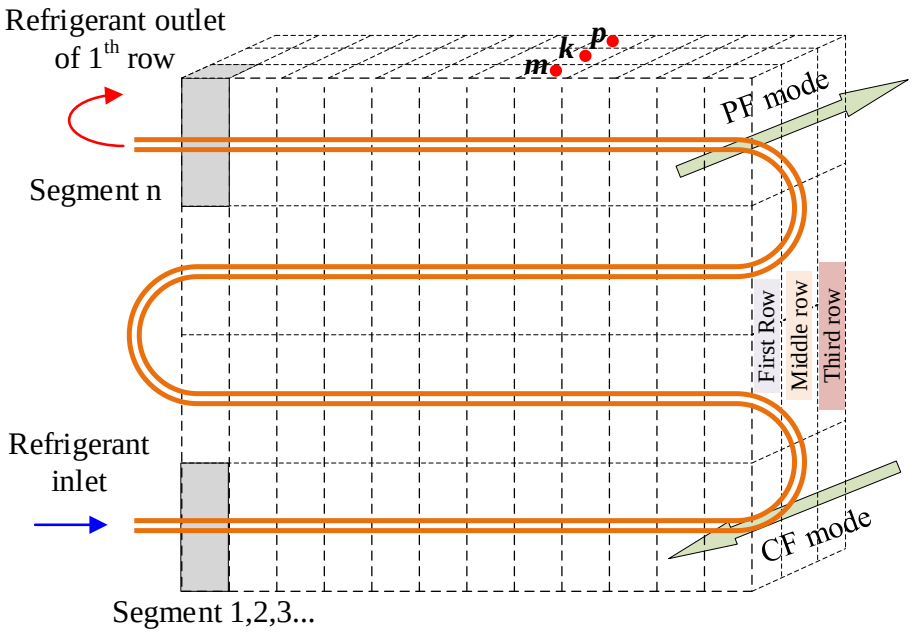

Fig. 6.2 Schematics of the segments of the 3-row FTHX in the experimental DFOC

The overall numerical scheme for solving the developed dynamic model for the complete ASHP unit having the novel DFOC was similar to that in Reference [Chen et al., 2018], except the calculating process for the sub-model for the DFOC. Fig. 6.2 shows the schematics of the segments of the 3-row FTHX in the experimental DFOC. As seen, the 3-row FTHX in the experimental DFOC was divided into many identical segments along the refrigerant flow

direction for each row. When solving the dynamic model, at any time point, segment by segment method on both air side and refrigerant side was employed. On the air side, along the airflow direction, the outlet air parameters, including the air temperature, moisture content and velocity, from the segment on the front row were the inputs to the segment on the next row. For example, as shown in Fig. 6.2, in PF mode, the outputs from the segment *m* in the first row were the inputs to the segment *k* in the middle row. However, in CF mode, the outputs from the segment *k* in the middle row were the inputs to the segment *m* in the first row. For a frost layer, the frosting module was discretised and solved using the same solving method as that in Reference [Zhang et al., 2022]. On the refrigerant side, along the refrigerant flow direction, the outputs from an upstream segment were the inputs to a downstream segment, from starting segment of the first row to the last segment of the third row.

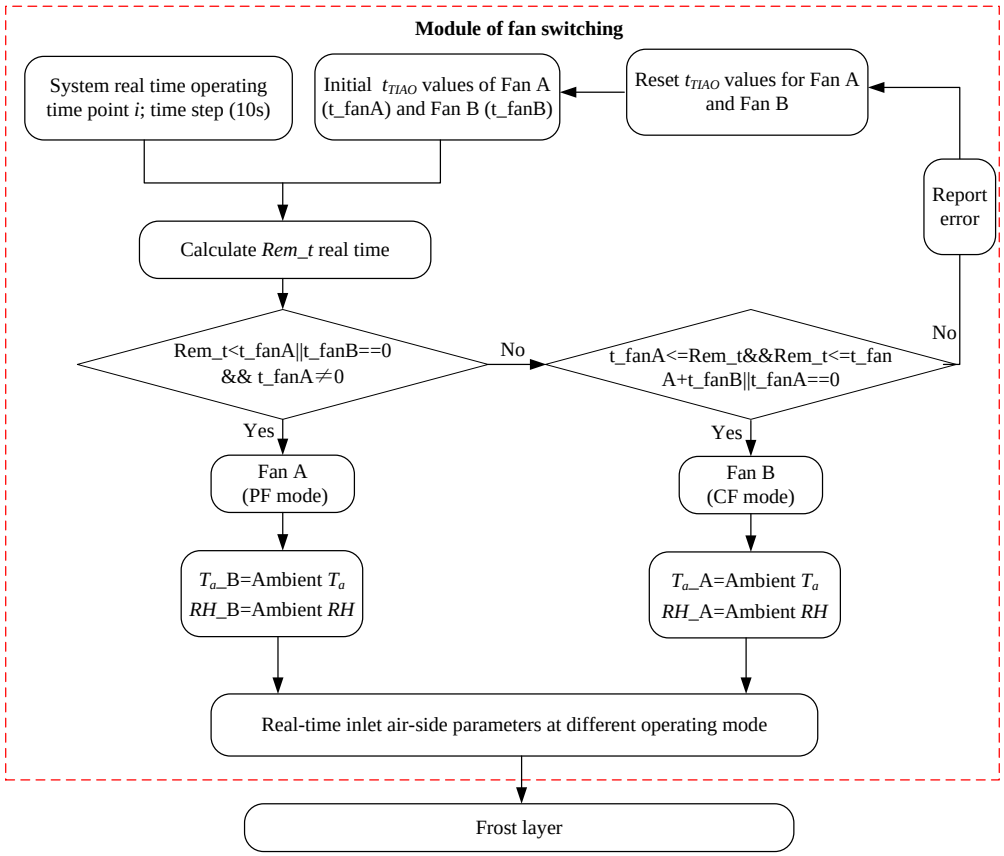

Fig. 6.3 Flowchart of fan switching scheme in solving the novel DFOC sub-model

On the other hand, the alternate operation of Fan A and Fan B resulted in a regular switching process for the input air parameters to the air side of the sub-model for the DFOC shown in Fig. 6.2. The flowchart of fan switching scheme in solving the novel DFOC sub-model is shown in Fig. 6.3. As seen, when t_{TIAO} values of Fan A and Fan B were set, as the operating time went by, the operating states of Fan A and Fan B were controlled by a periodical function *Rem_t*(*i*) at an operating time point, *i*, then the ambient air conditions were used as the input parameters to the windward side of the 3-row FTHX according to the specified operating fan. For example, when Fan A was in operation, side B of the FTHX was on the windward side, then ambient air temperature and humidity were the inputs to the segment on side B at the PF mode. This alternate switching process of entering ambient air parameters to the segments on either Side A or Side B would not be stopped until a defrosting operation was initiated.

Finally, in the current modelling study, a quasi-steady-state process was assumed. Therefore, all parameters on the air side, frost side and refrigerant side in the simulation were started when the experimental ASHP unit reached a relatively stable operating state, i.e., indoor supply air temperature at 20 ˚C ± 0.5 ˚C. In addition, an initial frost thickness at 0.0025 mm was also assumed according to earlier experimental observations in Chapter 5 and references [Kim and Lee, 2013; Zhang et al., 2022]. Besides, by referring to the defrosting initiation strategy used in the previously reported experimental study in Chapter 5, in the follow-up modelling study, a fixed refrigerant tube surface temperature of -20 °C at the exit from the FTHX was used to determine the duration of a frosting operation.

Moreover, to better compare the simulation results with the experimental ones, the measurement uncertainty for experimental parameters is detailed in Table 6.2.

Table 6.2 Detailed measurement uncertainty for experimental parameters

Category	*Parameters*	*Uncertainty* [Bai et al., 2018; Bound et al., 2001]
Directly measured	Temperature sensor (PT1000)	± 0.1 %
	Air velocity sensor	± 2 %
	Air pressure difference sensor	± 1 %
	Refrigerant mass flowmeter	± 0.5 %
	Power meter	± 1.0 %
	Frost thickness	± 4.1 %
Indirectly measured	Output heating capacity	± 2.86 % (averaged)
	COP	± 2.93 % (averaged)

6.2.2 Model validation

The developed dynamic model of the experimental ASHP unit having the novel DFOC was validated using the experimental data from the previous experimental study in Chapter 5. The experimental conditions are listed in Table 6.3. As seen, the two fans in the DFOC were alternately put into use, with the same t_{TIAO} values of 10 minutes. The simulated variations of the key operating parameters, including the averaged frost thickness, frost mass, averaged output heating capacity and COP of the experimental ASHP unit using the developed dynamic model, were compared to the experimental results for the same parameters, for the purpose of model validation.

Table 6.3 Experimental conditions for model validation

Fan A states	**Fan B states**	**Frosting operation duration**	**Experimental ambient condition**
Alternately operated (10 mins in each alternation)	Alternately operated (10 mins in each alternation)	72.5 mins	Air temperature: 2 °C Humidity ratio: 0.00374 kg/kg Initial air velocity: 2.8 m/s

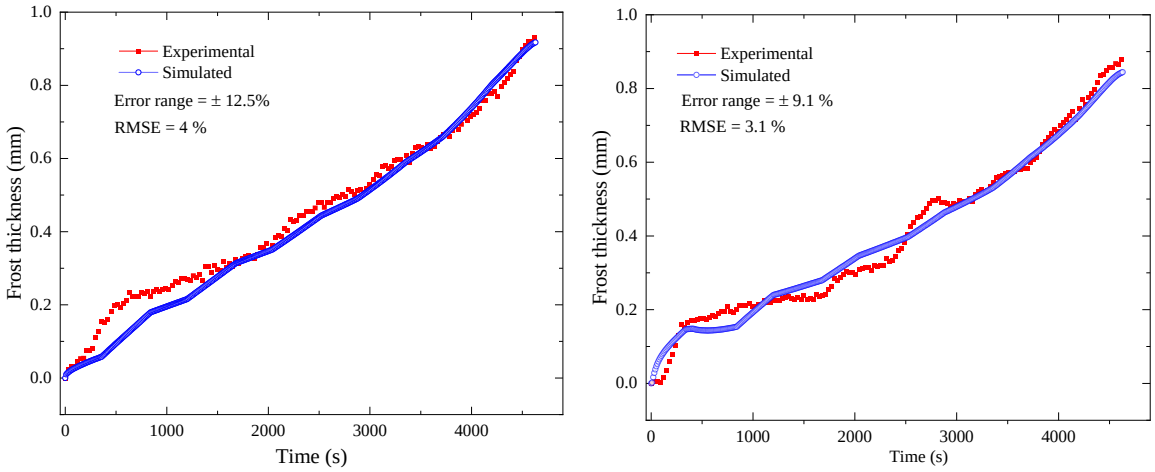

a) Side A b) Side B

Fig. 6.4 Comparisons of simulated and experimental variations in frost thickness on side A and side B of the FTHX in the novel DFOC

Figs 6.4 - 6.5 show the experimental validation results for the dynamic model of the experimental ASHP unit having the novel DFOC. Firstly in Fig. 6.4, the experimental and simulated variations in frost thickness deposited on sides A and B of the FTHX in the DFOC are compared. As seen in Fig. 6.4 a) and Fig. 6.4 b), the total frosting operating duration was 72.5 mins (4350 s) when -20 ˚C tube surface temperature arrived, and the simulated variations in frost thickness deposited on both side A and side B agreed well with the corresponding experimental variations, with the averaged relative error for frost thickness on side A at 12.5 %

and side B at 9.1 %, respectively. The Root Mean Square Error (RMSE) values between the experimental and predicted deposited frost thickness on Side A and Side B were at 4 % and 3.1 %, respectively.

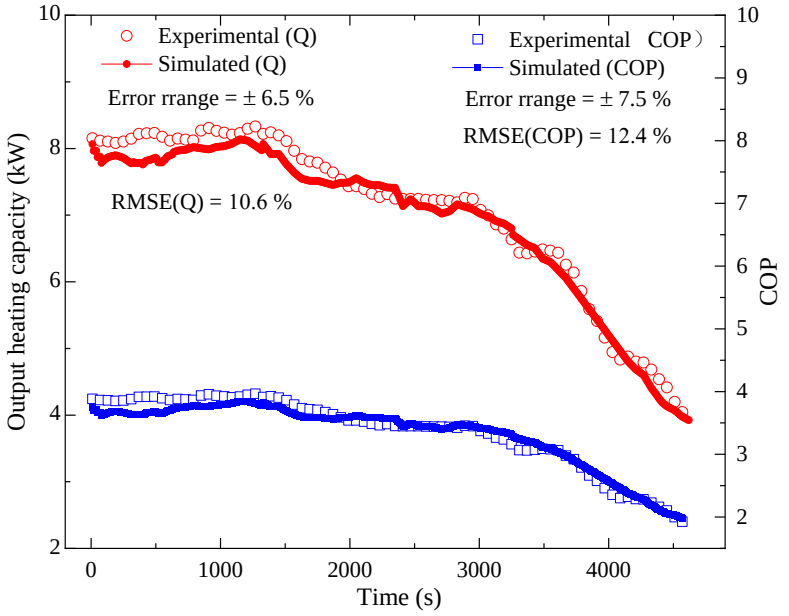

Fig. 6.5 Comparisons of simulated and experimental variations in the output heating capacity and COP of the experimental ASHP / DFOC unit

Secondly, the comparisons between the simulated and experimental variations in the output heating capacity and COP of the experimental ASHP unit within the frosting duration of 72.5 mins are shown in Fig. 6.5. As seen, the simulated variations in the output heating capacity and COP also agreed well with the experimental result, with an averaged error at ± 6.5% for the output heating capacity and ± 7.5% for COP, respectively. Then the maximum errors involved for model validation were however within ± 9.3 % for the output heating capacity and ± 10.3 % for COP, respectively. The RMSE value for the output heating capacity was 10.6% and that for COP 12.4 %, respectively. Thirdly, the simulated and experimental total frost mass accumulated during the frosting operating duration were also compared. The simulated and experimental total mass of frost deposited on the 3-row FTHX, during the frosting operating

duration of 72.5 minutes, was at 3708.5 g and 3600 g, respectively, with a percentage error of 3 %.

The above comparison results shown in Figs 6.4 - 6.5 demonstrated that the developed dynamic model of the experimental ASHP unit having a novel DFOC can be used to predict its key operating parameters with an acceptable accuracy. Therefore, the model was considered experimentally validated and can be used to further study the dynamic frosting characteristics of an ASHP unit having a novel DFOC at other configurations and ambient operating conditions than those used in the previous experimental study.

6.3 Modelling study using the validated dynamic model

The validated dynamic model was used to investigate the frosting characteristics and operating performances of an ASHP unit having a DFOC at, a) different fan operating modes, b) different values of fin pitch for the FTHX in its DFOC, and c) different ambient conditions. Therefore, the modelling study including three simulation groups corresponding to a) to c) was carried out and the modelling study results are presented in this Section. Details of the three simulation groups are given in Table 6.4.

As seen in Table 6.4, in Group A, the study objective was to investigate the operating performances and frosting characteristics of an ASHP unit having the novel DFOC at different values of t_{TIAO} for Fans A and B, through five study cases. In this Group, Case 4, which was the same previous experimental study, was selected as the base for comparison and the values of t_{TIAO} for Fan B was fixed at 8 mins in all the five cases, so as to identify an optimized combination of t_{TIAO} values for both Fan A and Fan B under a fixed operating ambient condition.

For Group B, its aim was to examine the operating characteristics of an ASHP unit when using different values of fin pitch of the FTHX in its DFOC. There were two study cases in this group,

Case 6 and Case 7. Case 6 was exactly same as Case 4 in Group A, and was included in this Group to provide a base for comparison. The operating performances and frosting characteristics of a FTHX with a fin pitch of 2.6 mm were simulated in Case 7, and the results were compared to Case 6 (or Case 4) where fin pitch was at 2 mm. The only difference in Case 6 and Case 7 was that different fin pitches were used. Therefore, the impacts of using different fin pitches in a FTHX on frosting performances of an ASHP / DFOC unit may be numerically evaluated.

Table 6.4 Detailed information of simulation cases in Groups A - C

Group No.	**Study Case**	**Fan A operation duration (Alternately operated)**	**Fan B operation duration (Alternately operated)**	**Fin pitch (mm)**	**Operating ambient condition (Windward side)**	**Simulated frosting duration (min)**
A	1	12 mins	8 mins	2	T_a: 2 °C RH: 84% Initial V_a: 2.8 m/s	73.5
	2	10 mins	8 mins			75
	3	8 mins	8 mins			79.3
	4#	6 mins	8 mins			78.2
	5	4 mins	8 mins			70.5
B	6*	6 mins	8 mins	2		78.2
	7	6 mins	8 mins	2.6		80.2
C	8*	6 mins	8 mins	2	T_a: 2 °C RH: 84% Initial V_a: 2.8 m/s	78.2
	9	6 mins	8 mins		T_a: 4 °C RH: 60% Initial V_a: 2.8 m/s	124.5

Same as the experimental study *Same as Case 4

In Group C, the operating performances and frosting characteristics of an ASHP / DFOC unit at different operating ambient conditions were numerically investigated. There were also two cases in Group C, Case 8 and Case 9. Case 8 was once again exactly the same as Case 4 in

Group A, and was included as a base for comparison. In Case 9, a mild frosting ambient condition, where the ambient temperature and relative humidity was at 4 °C and 60%, respectively, as opposed to Case 8 at a severe frosting condition, was selected according to the frosting map developed by Zhu et al [2015a]. Therefore, based on the simulation results in Case 8 and Case 9, the influences of different ambient conditions on the frosting characteristics of an ASHP / DFOC unit may be evaluated.

In addition, in all study cases, the simulated frosting operating duration was according to the defrosting initiation strategy described in Section 6.2.1.3, so that different frosting operating durations were resulted in, shown in the last column in Table 6.4. Besides, the same return air temperature for the indoor coil in all cases of 20 ˚C was set.

6.3.1 Modelling study results in Group A

The modelling study results in study Group A are presented in Figs 6.6 - 6.8. Firstly, the simulated variations in frost thickness deposited on side A and side B in Cases 1 - 5 are compared in Fig. 6.6. For the simulated frost thickness deposited on side A as shown in Fig. 6.6 a), as t_{TIAO} for Fan A was decreased, frosting rate on side A was increased, from Case 1 to Case 5, with the largest growth rate in frost thickness in Case 5 and the smallest in Case 1. Furthermore, the simulated frost thickness variations on side B in Cases 1 - 5 are shown in Fig. 6.6 b). As seen, when the frost thickness on side A in Case 5 reached the maximum value of 0.93 mm at the shortest frosting duration of 70.5 minutes, the frost thickness on side B was only at 0.68 mm, with a difference of 0.25 mm. In addition, in Case 1, where the frost thickness on side B reached the largest value, the smallest on side A was observed at the end of the frosting duration. Hence, the simulation results shown in Fig. 6.6 demonstrated that when t_{TIAO} for Fan B was at a fixed value, a larger or a smaller t_{TIAO} value for Fan A than that of Fan B was not reasonable because it may lead to a significant difference in frost thickness between

the two sides. In other words, it would be highly desirable to set the t_{TIAO} values for both fans as close to each other as possible.

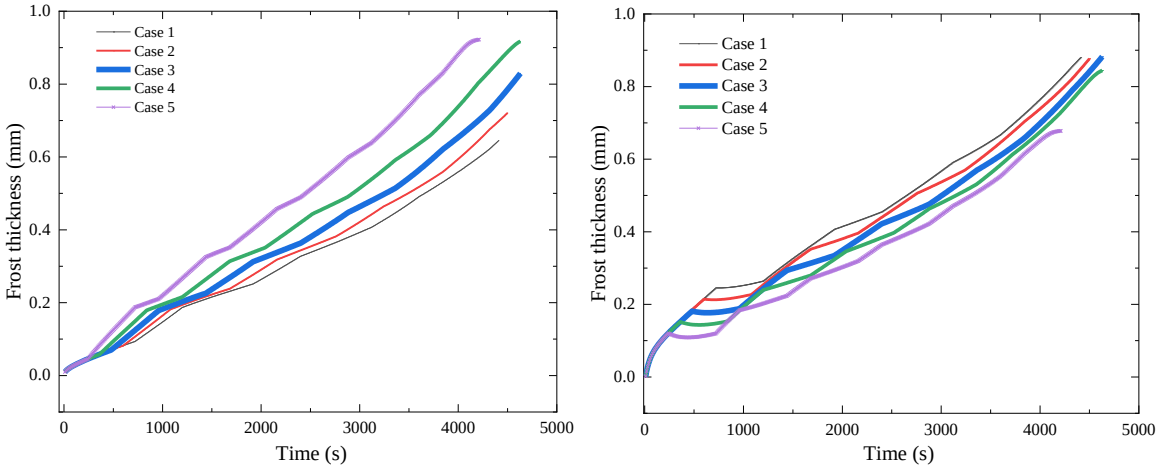

a) Side A b) Side B

Fig. 6.6 Simulated variations in the deposited frost thickness on side A and side B in Cases 1 - 5

To facilitate further comparison, the differences in simulated frost thickness between side A and side B at all time points for the five cases shown in Fig. 6.6 were calculated and are compared in Fig. 6.7. As seen, in each case, a similar variations pattern for the differences in the frost thickness may be observed. For example, in all study cases, before the first switching operation of the two fans, the difference was increased rapidly. Then, the difference was decreased gradually after the first switching operation, till the end of frosting duration. Furthermore, the differences in t_{TIAO} values for the two fans in Case 1 and Case 5 were remarkably greater than those in the other three cases, therefore, the simulated frost thickness differences in Case 1 and Case 5 were much greater than those in the other three cases. In addition, it was also interesting to note that the simulated variations in the differences in frosting thickness between the two sides in Case 3 and those in Case 4 intersected at the time point of 2880 seconds. Prior to this time point, the differences in frost thickness in Case 4 were

always smaller than those in Case 3. However, after this time point, the differences in Case 4 were always greater than those in Case 3. This demonstrated that during an entire frosting operation, using fixed values of t_{TIAO} for Fan A and B cannot at all time lead to a minimised difference in frost thickness between the two sides, but using varied values of t_{TIAO} of Fan A and B during a frosting operation may actually help achieve evener frosting on both sides. Hence, prior to 2880s, the operating mode in Case 4 should be adopted, but after 2880s, the operating mode in Case 3 may be used.

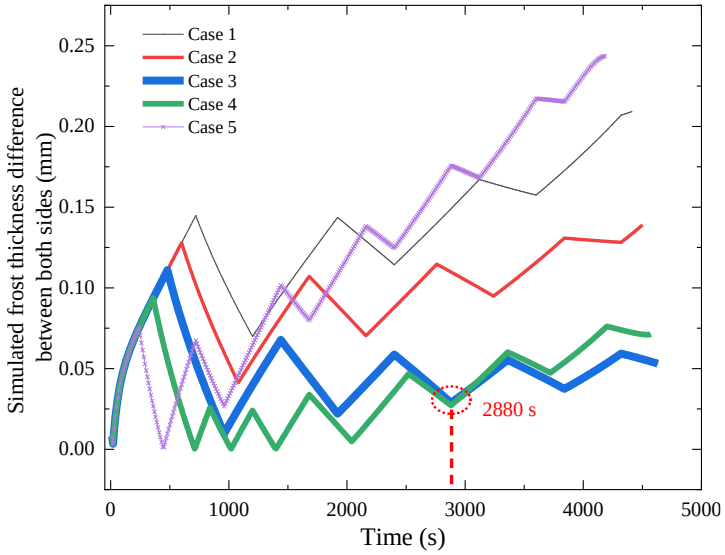

Fig. 6.7 Simulated variations in the difference of deposited frost thickness between the two sides in Cases 1 - 5

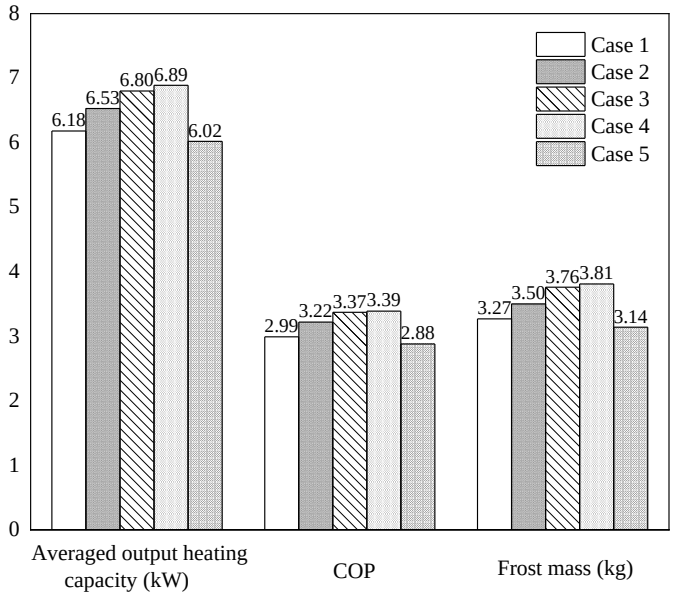

Fig. 6.8 Simulated averaged output heating capacity, averaged COP and the total frost mass deposited during their respective frosting durations in Cases 1 - 5

The simulated averaged output heating capacity, averaged COP, and the total frost mass deposited in Cases 1 - 5 during their respective frosting operation durations are shown in Fig. 6.8. As seen, as the value of t_{TIAO} for Fan A was gradually lowered, the averaged output heating capacity, averaged COP and the total frost mass deposited were all increased first from Case 1 to Case 4, but all declined from Case 4 to Case 5. The highest values in averaged output heating capacity, averaged COP, and total frost mass deposited, occurred all in Case 4, at 6.89 kW, 3.39 and 3.81 kg, respectively.

The simulated results from this study group suggested that using the same or similar values for t_{TIAO} for Fan A and B would help result in a higher output heating capacity, longer operating duration and evener frosting, and that using varied values for t_{TIAO} for the two fans may help achieve evener frosting on both sides of a FTHX, as a frosting operation went by.

6.3.2 Modelling study results in Group B

In this Section, the simulated operating performances and frosting characteristics of an ASHP / DFOC unit where the different fin pitches of 2 mm and 2.6 mm were used in the FTHX, including the difference of the frost thickness deposited on the FTHX, the averaged output heating capacity and COP during the frosting operation in Cases 6 - 7, are presented in Figs. 6.9 and 6.10, respectively.

As seen in Fig. 6.9, when the fin pith was increased from 2 mm in Case 6 to 2.6 mm in Case 7, the frosting operating duration was increased from 78.2 mins to 80.2 mins before defrosting initiation, but the difference in the deposited frost thickness between the two sides at the termination time point was increased from 0.15 mm to 0.22 mm, or 46.7%. This indicated that optimal t_{TIAO} values for the two fans in Case 6, may no longer be appropriate when the fin pitch was enlarged.

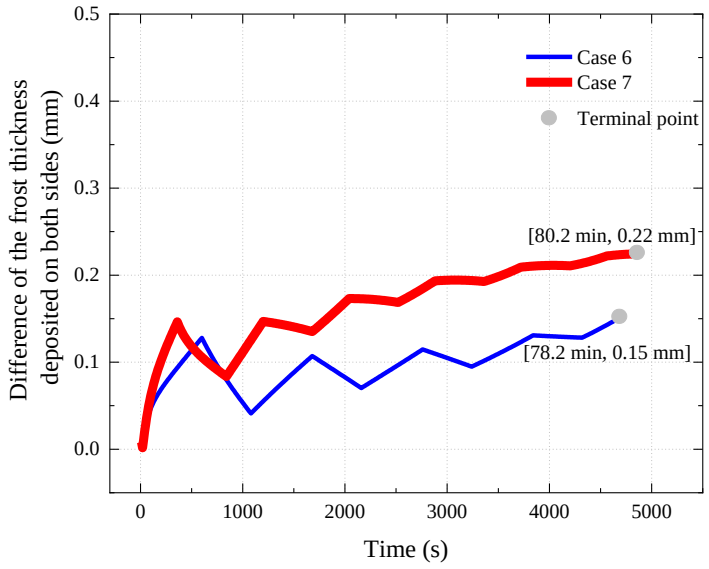

Fig. 6.9 Simulated variations in the difference of deposited frost thickness between the two sides in Cases 6 - 7

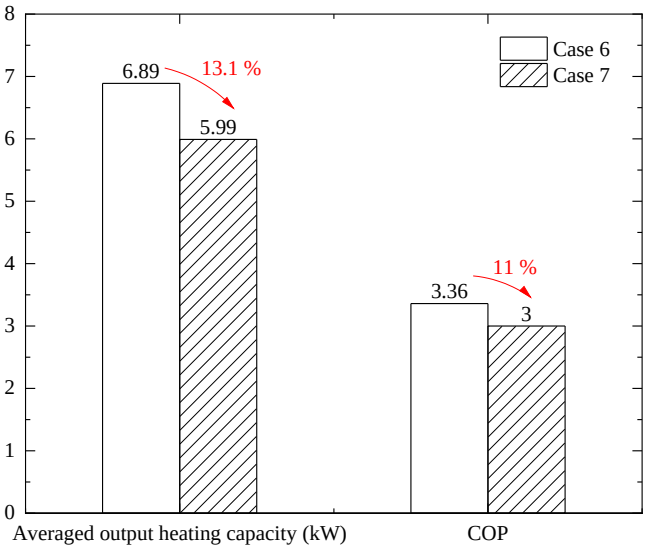

Fig. 6.10 Simulated averaged output heating capacity and COP in Cases 6 - 7

The simulated averaged output heating capacity and COP of an ASHP unit in Case 6 and Case 7 are shown in Fig. 6.10. As seen, for Case 6 and Case 7, the simulated averaged output heating capacity were at 6.89 kW and 5.99kW, and averaged COP at 3.36 and 3, respectively, during their respective frosting operation durations. These demonstrated that when the fin pitch was enlarged from 2 mm to 2.6 mm, the averaged output heating capacity and COP in Case 7 were decreased by 13.1% and 11%, respectively, as a result of reduced heat transfer area of the FTHX due to enlarged fin pitch.

6.3.3 Modelling study results in Group C

The simulated variations in the difference of deposited frost thickness on side A and side B in Case 8 and Case 9 during their respective frosting operating durations, are shown in Fig. 6.11.

As seen, the frosting operating duration in Case 8, was 78.2 mins, and that in Case 9 was 124.5 mins, an increase of 59.2 %. However, the difference in the deposited frost thickness at the termination time point in Case 9 was only 0.06 mm, much smaller than 0.22 mm in Case 8, with a percentage difference of 27.3% (reduced by 72.7 %). This demonstrated that when the

ambient air temperature and relative humidity were changed from 2 ˚C and 84 % (severe frosting) to 4 ˚C and 60 % (mild frosting), frosting operating duration can be significantly lengthened, and the frosting evenness improved further by keeping the same t_{TIAO} values for the two fans.

The simulated averaged output heating capacity and averaged COP in Cases 8 - 9 during their respective frosting operating durations are shown in Fig. 6.12. As seen, the averaged heating capacity was at 6.89 kW and 7.3 kW, and COP at 3.36 and 3.48, in Case 8 and Case 9, respectively. The averaged output heating capacity and COP in Case 9 were improved by 6 % and 3.6 %, respectively, compared to those in Case 8.

The simulation results in this group suggested that when an ASHP / DFOC unit was operated at a mild frosting zone, its frosting operating duration can be lengthened remarkably and a smaller t_{TIAO} value may help achieve evener frosting on both sides of the DFOC.

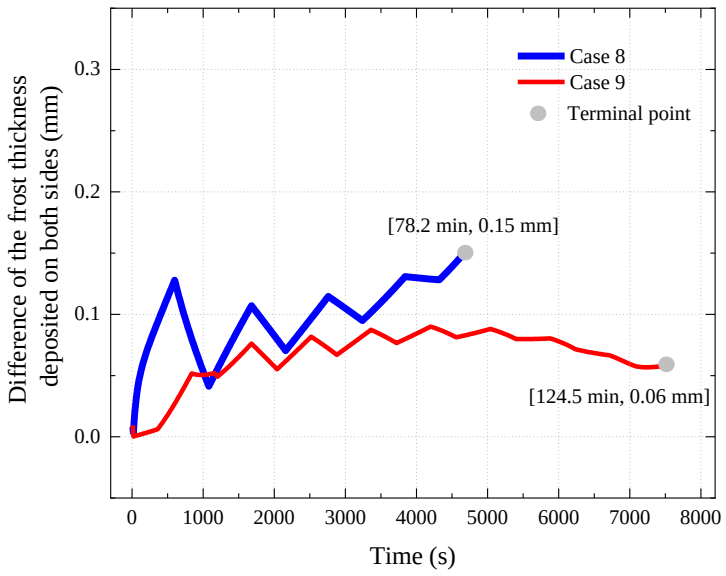

Fig. 6.11 Simulated variations in the difference in the deposited frost thickness between the two sides in Cases 8 - 9

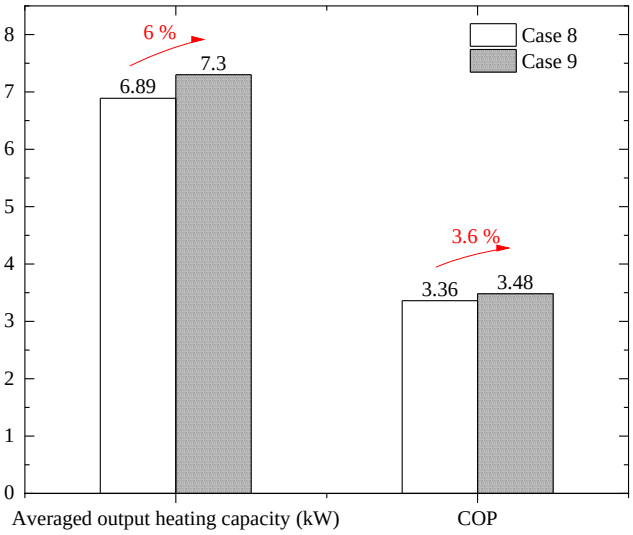

Fig. 6.12 Simulated averaged output heating capacity and COP in Cases 8 - 9

6.3.4 Discussions

In Sections 6.3.2 and 6.3.3, the comparisons of frosting characteristics of an ASHP / DFOC unit with different fin pitches, and at different ambient conditions are presented. However, it was inadequate to conclude that the values of t_{TIAO} used in Case 4 (or Case 6 and Case 8), was suitable for Case 7 and Case 9. Therefore, the impacts of different fin pitches and different ambient conditions on the values of t_{TIAO} for achieving evener frosting and higher operating performances of the ASHP / DFOC units deserved further discussion. Hence, four additional study cases were designated to evaluate the impact of different fin pitches and different ambient conditions on the values of t_{TIAO} for the novel DFOC, i.e., study cases 10 - 13, as detailed in Table 6.5.

Table 6.5 Detailed information of simulation cases for further discussions

Study case	**Fan A operation duration (Alternately operated)**	**Fan B operation duration (Alternately operated)**	**Fin pitch (mm)**	**Operating ambient condition (Windward side)**	**Simulated frosting duration (min)**
7	6 mins	8 mins	2.6	T_a: 2 °C RH: 84 % Initial V_a: 2.8 m/s	80.2
10	0 min	62 mins			62
11	6 mins	10 mins			85
9	6 mins	8 mins	2	T_a: 4 °C RH: 60 % Initial V_a: 2.8 m/s	124.5
12	0 min	90.5 mins			90.5
13	15 mins	15 mins			134

As seen in Table 6.5, the only difference among Case 7, Case 10 and Case 11 was the values of t_{TIAO}, with all other conditions being the same. For Case 10, only Fan B was operated during its entire frosting duration, which was a traditional single fan operating mode. For Case 11, the value of t_{TIAO} was set at 6 mins for Fan A and 10 mins for Fan B. Similarly, the only difference among Case 9, Case 12 and Case 13 was also the value of t_{TIAO}. In Case 12, only Fan B was operated for its entire frosting duration. In Case 13, the t_{TIAO} value was set at 15 mins for both fans. In the four additional cases of 10 - 13, the simulated frosting operating duration was also according to the defrosting initiation strategy described in Section 6.2.1.3.

The comparisons between the simulation results in Case 7, Cases 10 - 11, and those in Case 9, Cases 12 - 13, are shown in Figs. 6.13 – 6.16, respectively. As seen, for Fig. 6.13, the simulated frosting duration was only at 62.2 mins in Case 10, where only single fan, or Fan B, was operated during the entire frosting operating duration, but 80.2 mins in Case 10 and 85.2 mins in Case 11. The difference in the deposited frost thickness at the termination of frosting operation was 0.65 mm in Case 10, 0.22 mm in Case 7 and 0.05 mm in Case 11, respectively. As compared to those in Case 7, the frosting operating duration in Case 11 was lengthened by

6.23 %, and the difference in the deposited frost thickness decreased by 77.3 %. In other words, when the value of t_{TIAO} was changed from 6 mins for Fan A and 8 mins for Fan B in Case 7, to 6 mins for Fan A and 10 mins for Fan B in Case 11, the frosting operating duration was further increased, but the difference in frosting thickness between the two sides of the FTHX actually reduced. This was because increasing fin pitch can alleviate uneven frosting to some extent along the air flow direction [Zhang et al., 2018]. Thus, this positive impact led to an increase in the operating duration for Fan B to obtain evener frosting and a longer heating operating duration.

The simulated averaged output heating capacity and COP of an ASHP unit in Case 7, Cases 10 - 11 during their respective frosting operating durations are shown in Fig. 6.14. As seen, the highest values in averaged output heating capacity and COP, at 6.11 kW and 3.1, respectively, were in Case 11, compared to at 5.99 kW and 3 in Case 9. The averaged output heating capacity and COP in Case 11 were improved by 2 % and 3.3 %, respectively, as compared to those in Case 7, and by 11.1 % and 12.7 %, respectively, as compared to Case 10, where the traditional single fan operating mode was used.

The simulation results shown in Figs 6.13 - 6.14 demonstrated that when fin pitch was increased, an optimal value of t_{TIAO} at a small fin pitch in Case 7 may no longer be appropriate, and a longer t_{TIAO} value for Fan B should be used for a larger fin pitch, for achieving evener frosting and higher operating performances.

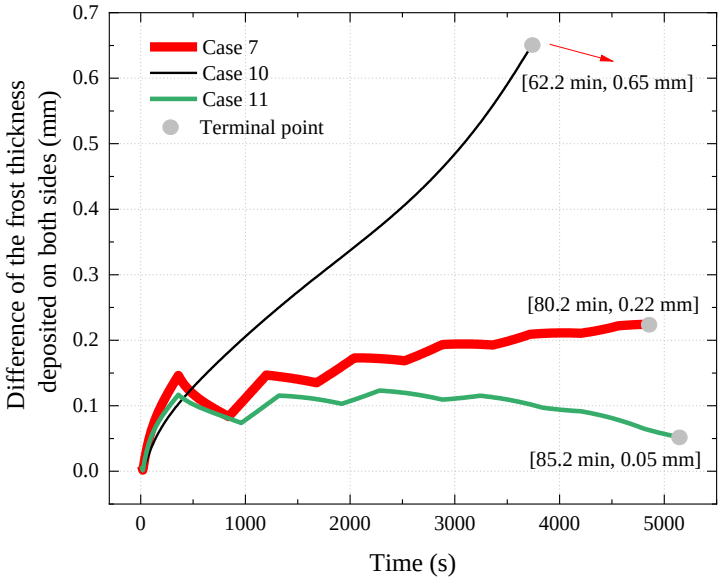

Fig. 6.13 Simulated variations in the difference in the deposited frost thickness between the two sides of the FTHX in Case 7, Cases 10 - 11

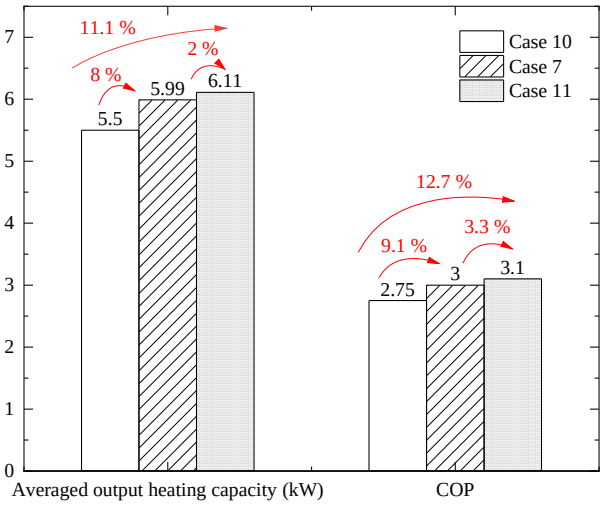

Fig. 6.14 Simulated averaged output heating capacity and COP in Case 7, Cases 10 - 11

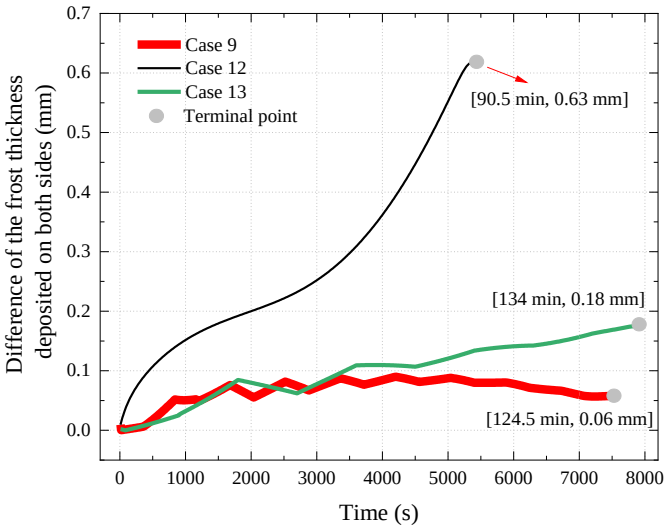

Fig. 6.15 Simulated variations in the difference in the deposited frost thickness between the two sides of the FTHX in Case 9, Cases 12 - 13

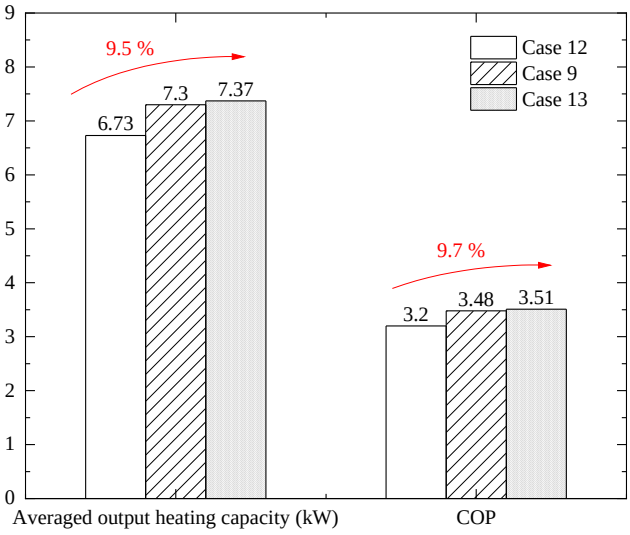

Fig. 6.16 Simulated averaged output heating capacity and COP in Case 9, Cases 12 - 13

On the other hand, the simulated variations in the difference in the deposited frost thickness between the two sides of the FTHX in Case 9, Cases 12 - 13 are shown in Fig. 6.15. As seen, in Case 9, where the value of t_{TIAO} was at 6 mins for Fan A and 8 mins for Fan B, a smaller difference in the deposited frost thickness at 0.06 mm than that at 0.18 mm in Case 13 with the value of t_{TIAO} at 15 mins for both fans, was resulted in. There were only 8 switching operations

for the two fans in the DFOC, at a longer frosting operating duration of 134 mins in Case 13, as compared to 18 switching operations in Case 9, at a shorter frosting operating duration of 124.5 mins. This was because at a mild frosting condition, the saturation water vapour pressure was relatively low and frosting rate also slow, and the deposited frost thickness between Side A and Side B in Case 9 and Case 13 were similar. Therefore, frequent switching operations can adversely accelerate the deterioration in air flow during switching, as a result, speed up the decline of tube surface temperature and the frost growth in Case 9. Hence, different ambient condition required a proper value of t_{TIAO} for the two fans. Besides, the frosting operating duration in Case 13 was lengthened by 48.1 %, as compared to that in Case 12 where only Fan B was operated during entire frosting duration. Therefore, when the values of t_{TIAO} at 6 mins for Fan A and 8 mins for Fan B in Case 9, were changed to 15 mins for both fans in Case 13, outdoor fan switching frequency was decreased by 55.6 % at a mild frosting ambient condition.

Furthermore, the simulated averaged output heating capacity and COP in Case 9, Cases 12 - 13 during their respective frosting operating durations are shown in Fig. 6.16. As seen, when the values of t_{TIAO} were changed from 6 mins for Fan A and 8 mins for Fan B in Case 9, to 15 mins for both fans in Case 13, the averaged output heating capacity and COP in Case 9 and Case 13 were similar, at 7.3 kW and 7.37 kW, and 3.48 and 3.51 for COP, respectively. Besides, the averaged output heating capacity and COP in Case 13 were improved by 9.5 % and 9.7 %, respectively, as compared to Case 12, where the traditional single fan operating mode was used.

The simulation results shown in Figs 6.15 - 6.16 suggested that when the ambient operating condition was at a mild frosting zone, setting a greater and similar values of t_{TIAO} for the two fans impacted less on the operating performances of the ASHP unit having the novel DFOC, to avoid frequent switching for the two fans.

In addition, it is worth noting that, according to the simulation results reported above and the experimental results reported in Chapter 5, the use of the novel DFOC in ASHPs can help significantly lengthen heating operation duration, reduce defrosting frequency and energy consumption with a higher averaged output heating capacity and COP under the experimental and the simulated ambient frosting conditions. Therefore, a higher seasonal COP over an entire heating season can be expected, since the use of the novel DFOC in ASHP units with different dual-fan operating modes prolonged the frosting operation duration due to evener frosting along air flow direction. On the other hand, when it came to defrosting, although the total frost on coil surface was increased, the defrosting was not proportionally increased, for an evenly frosted outdoor coil. However, the actual heating performances for ASHP units having the novel DFOC may also be subject to certain other limitations such as ambient conditions and the associated control strategies for both fans. Nonetheless, using the novel DFOC in ASHPs can help reduce the energy use for building heating in the long run, and therefore, further related studies should be continued to improve the configuration and operation of a DFOC.

6.4 Conclusions

In this Chapter, a dynamic mathematical model for an ASHP / DFOC unit was developed by referring / updating the existing sub-models and experimentally validated using the experimental data presented in Chapter 5. Using the developed dynamic model, a follow-up modelling study with three study groups for different operating modes of the two fans, different fin pitches in the FTHX and different ambient conditions, was carried out and the simulation results are presented and discussed. The following conclusions may be drawn:

1) The first-of-its-kind dynamic mathematical model reported in this paper can be used to, with an adequate accuracy, simulate the frosting characteristics and heating performances of an ASHP / DFOC unit. The simulated variations of the key operating

parameters, such as frost thickness, output heating capacity and COP, all agreed well with the previously reported experimental data, with the maximum percentage error of 12.5 % and maximum RMSE values of 12.4 %, respectively.

2) Different values of t_{TIAO} for Fan A and Fan B may significantly impact the frosting characteristics and the operating performances of ASHP / DFOC unit. Using the same or similar values of t_{TIAO} for Fan A and B would help achieve a higher output heating capacity, longer frosting operating duration and evener frosting. Besides, as the frosting operation went by, using variable values for t_{TIAO} for the two fans may help further achieve evener frosting on both sides;

3) When the fin pitch was increased from 2 mm to 2.6 mm, with 6 mins operating duration for Fan A and 8 mins for Fan B, the averaged output heating capacity and COP were decreased by 13.1 % and 11 %, respectively, and the difference in the deposited frost thickness before defrosting initiation was increased by 33.3 %, but with a longer frosting operating duration. Besides, larger fin pitches in combination of a greater value of t_{TIAO} for Fan B may lead to evener frosting and higher operating performances, and the averaged output heating capacity and COP can be increased by up to 11.1 % and 12.7 %, respectively, as compared to those at the traditional single fan operating mode.

4) For an ASHP / DFOC unit, when operated at a mild frosting climate zone, frosting operating duration can be increased remarkably, and using a smaller t_{TIAO} value may help achieve evener frosting on both sides, as compared to those operated at a severe frosting climate zone. Besides, in a mild frosting climate zone, by setting a greater and similar value of t_{TIAO} for both fans, the number of switching operations of the two fans

can be reduced by 55.6 %, the frosting operating duration lengthened by 48.1%, and the averaged output heating capacity and COP improved by 9.5 % and 9.7 %, respectively, when compared to those at the traditional single fan operating mode.

The dynamic model developed in this Chapter has been proved adequately accurate for the experimental the ASHP / DFOC unit, and thus could be used to investigate the even frosting characteristics of the ASHP / DFOC unit at various ambient conditions / with different configurations of FTHXs.

For an ASHP / DFOC unit to be successfully operated for achieving the desired characteristics of even frosting along air flow direction, the development of a control strategy for its optimum operation became necessary. This will be reported in Chapter 7.

Chapter 7

Development of an optimal control strategy for ASHP / DFOC units for evener frosting along airflow direction based on GRNN modelling

7.1 Introduction

To alleviate uneven frosting along airflow direction, an experimental study on the even frosting characteristics in an experimental ASHP / DFOC unit having an experimental novel DFOC (ASHP / DFOC unit) has been carried out and is reported in Chapter 5. The experimental study results demonstrated that the experimental ASHP / DFOC unit can achieve evener frosting along airflow direction, with a longer frosting duration and a better heating performance than those having a traditional single fan outdoor coil. Furthermore, to more comprehensively investigate even frosting performances of the experimental ASHP / DFOC unit at various non-experimental operating and frosting ambient conditions, and with different unit configurations, a dynamic mathematical model of the experimental ASHP / DFOC unit was also developed and experimentally validated, as presented in Chapter 6. However, there was still a lack of a suitable control strategy to enable the optimum operation of an ASHP / DFOC unit to achieve the desired even frosting performances. Therefore, developing a control strategy for the optimal operation of the novel DFOC has become highly necessary.

In this Chapter, the development of a GRNN-model based optimal control strategy applied to the experimental ASHP / DFOC unit for achieving even frosting along airflow direction is reported. Firstly, to establish a database that was required for developing a GRNN model, case studies were carried out using both the experimental ASHP / DFOC unit described in Chapter 4 and the validated mathematical model presented in Chapter 6. Based on the database, the impacts of different dual-fan operating modes on the even frosting performances of the

experimental ASHP / DFOC unit at different operating ambient air conditions were analyzed; Secondly, a new COP-related performance index to comprehensively evaluate the operating performances in multiple frosting - defrosting operation cycles of the experimental ASHP / DFOC unit was proposed. Thirdly, a GRNN model that can be used to predict frosting - defrosting duration and evaluate the new COP-related performance index was developed and validated based on the established database, and an objective dataset which consisted of optimal dual-fan operating modes at different ambient air conditions was obtained using the validated GRNN model. Fourthly, an optimal control strategy for the experimental ASHP / DFOC unit was developed based on the objective dataset, and validated via three experimental cases. Finally, conclusions are given.

7.2 Establishing a database for developing GRNN and a new COP-related performance index

To establish a database for developing the GRNN model, and develop a new COP-related performance index to evaluate the operating performance of an ASHP / DFOC unit in its multiple frosting - defrosting operation cycles, a series of case studies using an experimental ASHP / DFOC unit described in Chapter 4 and the validated mathematical model reported in Chapter 6 were carried out.

7.2.1 Establishment of database and results analysis

7.2.1.1 Study groups for establishing the database

In the previous related studies reported in Chapters 5 and 6, both experimental and numerical results have demonstrated that the operating performances of the experimental ASHP / DFOC unit under frosting conditions were strongly affected by the following four parameters: t_A and t_B values, ambient air temperature, T_a, and relative humidity, RH. Therefore, based on these

parameters, four groups of study cases using the experimental ASHP / DFOC unit described in Chapter 4 and the validated mathematical model presented in Chapter 6 were designated based on different ambient air temperatures of 0, 2, 4 and 6 ˚C. In each group, study cases with different t_A and t_B values, and at different ambient air *RH*, were organized, as shown in Table 7.1.

As shown in Table 7.1, in each group, at a fixed T_a, there can be different numbers of combinations for t_A, t_B, and *RH*, and at each combination, operating performance data needed to be obtained using either the experimental ASHP / DFOC unit or the validated mathematic model to establish the database. Therefore, there were totally 48 combinations in study Group 1, 52 in study Group 2, 44 in study Group 3 and 42 in Study Group 4. For all the four groups, there were a total of 186 combinations when establishing the database. To provide more reliable results, performance data at 90 % of the totally 186 combinations were obtained by using the experimental ASHP / DFOC unit, with the remaining 10 % using the validated mathematic model to speed up the process of establishing the database. As a result, the database contained a total of 186 sets of data at the 186 combinations.

Moreover, the minimum values for t_A and t_B at each combination were not smaller than 6 mins, to protect the novel experimental DFOC from frequent switching between the two fans. To improve the efficiency of establishing the database, ranges for t_A and t_B in each study group were all confirmed based on experimental results. Besides, the increment for both t_A and t_B was set at 3 mins in Group 3 and Group 4, at a higher T_a, and that in Group 1 and Group 2, t_A and t_B at 2 mins, at a lower T_a. Besides, a much greater difference between t_A and t_B settings for Fan A and Fan B at a fixed ambient air condition may lead to a poorer heating performance or a shorter frosting duration of the experimental ASHP / DFOC unit. This explained that in Table 7.1, the combinations with a very large difference in t_A and t_B values were not included.

In addition, at each combination, the operating duration for multiple frosting - defrosting cycles when using either the experimental ASHP / DFOC unit or the validated mathematical model was set at 10 hours, which corresponded to the normal heating duration of office buildings [Bai et al., 2018].

Table 7.1 Details of designated study groups

Study Group	**Ambient air condition**		**Fan operating mode**		**Number of combinations**
	T_a (˚C)	RH (%)	t_A (min)	t_B (min)	
1	0	70 80 90	6 8 10 12	6 8 10 12	48
2	2	70 80 85 90	6 8 10 12	6 8 10 12 14	52
3	4	70 80 90	6 9 12 15	6 9 12 15 18	44
4	6	70 80 90	9 12 15 18	9 12 15 18 21	42

7.2.1.2 Results analysis based on established database

An effective and reasonable performance index for accurately and completely reflecting the

operating performances of the experimental ASHP / DFOC unit at different ambient air conditions and dual-fan operating modes was essential when developing an optimal control strategy for the ASHP / DFOG unit. Therefore, the established database was analysed to evaluate the effectiveness of using the following three existing operational parameters, i.e., the average duration of a single frosting - defrosting cycle in multiple frosting - defrosting cycles, $t_{f\text{-}d}$, averaged COP, COP_{ave}, and defrosting frequency in multiple frosting - defrosting cycles, when examining the operating performances of the experimental ASHP / DFOC unit. The variation characteristics of the three parameters in the total of 186 data sets in the established database were all analysed and compared. It was observed that similar variation trends for the data sets in Groups 1 - 4 were demonstrated. Therefore, only the variation trends of some selected data sets in Group 2 and Group 3 are presented here as example. Besides, according to the previous related study results in Chapters 5 and 6, at the same ambient air condition, the longer the $t_{f\text{-}d}$ values, the evener frosting between the two sides of the outdoor coil, and vice versa. Therefore, $t_{f\text{-}d}$ was used to indirectly reflect the level of even frosting at the same ambient air condition.

Values of averaged $t_{f\text{-}d}$ at different dual-fan operating modes and different ambient air conditions in some selected data sets from Groups 2 and 3 are shown in Fig. 7.1. These included the selected data sets at 2 ˚C, and 70 % *RH* from Group 2 and that at 4 ˚C, and 70 % *RH* from Group 4, respectively. There were a few points to note here. Firstly, at the same ambient air condition, when t_A was fixed, there always existed a t_B value at which $t_{f\text{-}d}$ was the longest. For example, in Fig. 7.1 a) showing the selected data sets from Group 2, at a fixed t_A of 8 mins, when t_B was increased from 6 mins to 12 mins, the longest $t_{f\text{-}d}$ was at 114 mins at a t_B of 10 mins, or at the dual-fan operating mode of '8+10' (i.e., t_A = 8 mins, t_B = 10 mins). Similar situations for other fixed t_A values may also be observed, and the longest $t_{f\text{-}d}$ value was 119 mins at '6+10' mode, 108 mins at '10+12' mode and 97 mins at '12+12' mode, respectively.

For easy identification, all these longest $t_{f\text{-}d}$ values are marked with a red circle in Fig. 7.1 a). Secondly, when further comparing the four longest $t_{f\text{-}d}$ values under the same ambient air condition of 2 ˚C, the maximum $t_{f\text{-}d}$ of 119 mins occurred at '6+10' mode, for all the 17 data sets selected from Group 2 shown in Fig. 7.1 a). Similarly, in Fig. 7.1 b) showing the selected data sets from Group 4, at a fixed T_a of 4 ˚C and a fixed *RH* of 70 %, the longest $t_{f\text{-}d}$ among all the 16 data sets was 156 mins, at '12+12' mode. Variation trends similar to those presented in Fig. 7.1 can also be observed in other data sets at the same ambient air condition in the four groups of the developed database. Although the observations from Fig. 7.1 for the longest values for $t_{f\text{-}d}$ were based on the limited number of data sets in the developed database, they were actually indicative. Lastly, it can also be observed that at the same dual-fan operating mode and *RH* level, when increasing T_a from 2 ˚C to 4 ˚C, $t_{f\text{-}d}$ value can be also significantly prolonged, when comparing the results shown in Fig. 7.1 a) and Fig. 7.1 b). For example, at '6+6' mode for Groups 2 and 3, $t_{f\text{-}d}$ value was increased from 101 mins in Fig. 7.1 a) to 121 mins in Fig. 7.1 b), when T_a was increased from 2 ˚C to 4 ˚C.

On the other hand, $t_{f\text{-}d}$ for the experimental ASHP / DFOC unit with the same dual-fan operating mode but different ambient air conditions from selected data sets of Groups 2 - 4 are compared in Fig. 7.2. As seen, at the same dual-fan operating mode of '12+12', when T_a remained unchanged, a higher ambient *RH* would result in a lower $t_{f\text{-}d}$ value. For example, at a fixed T_a of 4 ˚C, increasing *RH* from 70 % to 90 %, would shorten $t_{f\text{-}d}$ from 156 mins to 70 mins. Similar variation trends can also be observed for the data sets for fixed T_a at 2 ˚C and 6 ˚C, respectively. Moreover, when comparing the $t_{f\text{-}d}$ values at a fixed *RH*, the longest $t_{f\text{-}d}$ at a fixed *RH* of 70 % at three different ambient air temperatures of 2 ˚C, 4 ˚C and 6 ˚C, was 156 mins, at a fixed *RH* of 80 % 97 mins, and at a fixed *RH* of 90 % 89 mins. Furthermore, when comparing the data sets selected from Group 4 and those from Group 3 shown in Fig. 7.2, at a fixed RH of 70% and a fixed dual-fan operating mode '12+12', a longer $t_{f\text{-}d}$ of 156 mins was achieved at an

ambient air temperature of 4˚C, as compared to 136 mins at an ambient air temperature of 6 ˚C where a longer $t_{f\text{-}d}$ was expected because of a higher ambient air temperature thus a slower frosting rate. Therefore, these analysis results implied that while ambient air temperature and relative humidity can significantly impact frosting - defrosting operation duration, the different dual-fan operating modes may also impact frosting - defrosting operation duration.

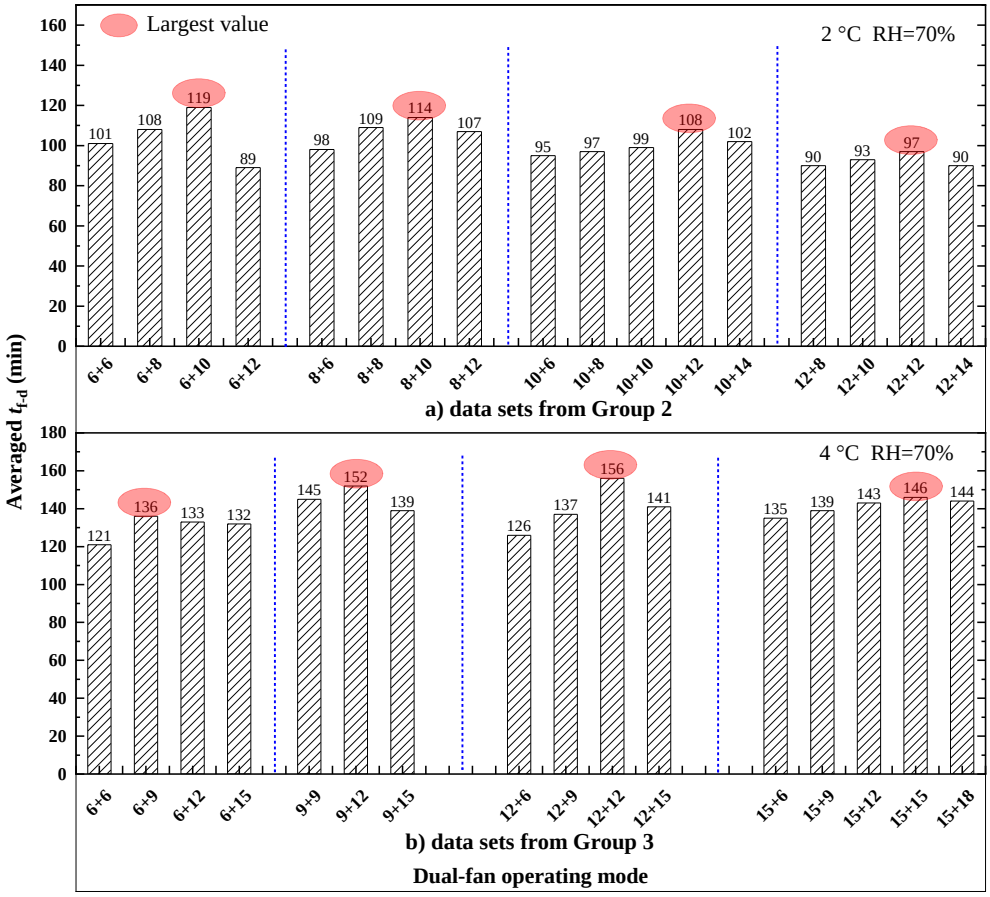

Fig. 7.1 The averaged $t_{f\text{-}d}$ values for the experimental ASHP / DFOC unit using different dual-fan operating modes at different ambient air conditions (selected data sets from Groups 2 and 3)

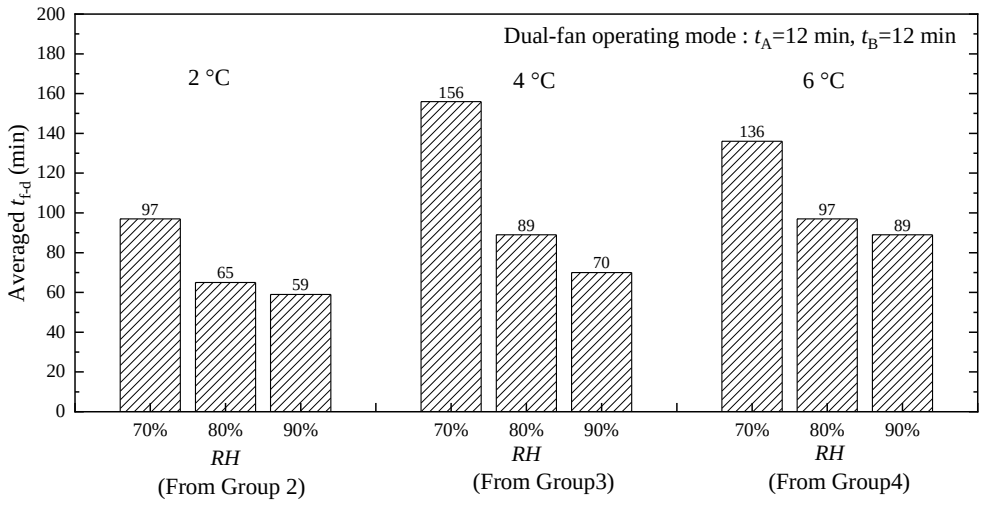

Fig. 7.2 Comparison of averaged t_{f-d} for the experimental ASHP / DFOC unit at the same dual-fan operating mode but different ambient air conditions (selected data sets from Groups 2, 3 and 4)

Furthermore, the COP_{ave} values for multiple frosting - defrosting cycles of the experimental ASHP / DFOC unit at different dual-fan operating modes and different ambient air conditions, for the same data sets selected from Groups 2 and 3 as shown in Fig. 7.1, are shown in Fig. 7.3. As seen, at the same ambient air condition, the differences in the COP_{ave} values at different dual-fan operating modes was relatively small. For example, in Fig. 7.3 a), at a fixed T_a of 2 ˚C and fixed *RH* of 70 %, the COP_{ave} values varied between 2.94 and 3.15 at all operating modes. In Fig. 7.3 b), at fixed T_a of 4 ˚C and fixed *RH* of 70 %, the COP_{ave} values varied between 3.2 and 3.39. It was also noted that at a dual-fan operating mode that led to the longest frosting - defrosting durations, its corresponding COP value may not necessarily be the highest. For example, in Fig. 7.3 a), at a fixed t_A of 6 mins, '6+8' dual fan operating mode can lead to the highest COP_{ave} of 3.1, with a t_{f-d} of 108 mins. However, the longest t_{f-d} of 119 mins was achieved at '6+8' mode but with a COP_{ave} of 3.08. Similar observations may also be found in Fig. 7.3 b). All these observations would suggest that an appropriate dual fan operating mode

may lead to the longest $t_{f\text{-}d}$ value, but not necessarily the highest COP value. However, a longer $t_{f\text{-}d}$ only implied a lower defrosting frequency and a better indoor thermal comfort during multi-cycle frosting and defrosting operation, but a higher COP value, on the other hand, represented a better heating efficiency of an ASHP / DFOC unit. Therefore, it would be difficult to directly use the averaged COP value currently used to judge which dual-fan operating mode was better at different ambient air conditions, and a new COP-related performance index for evaluating the overall operating performances for an ASHP / DFOC unit at different dual-fan operating modes became necessary.

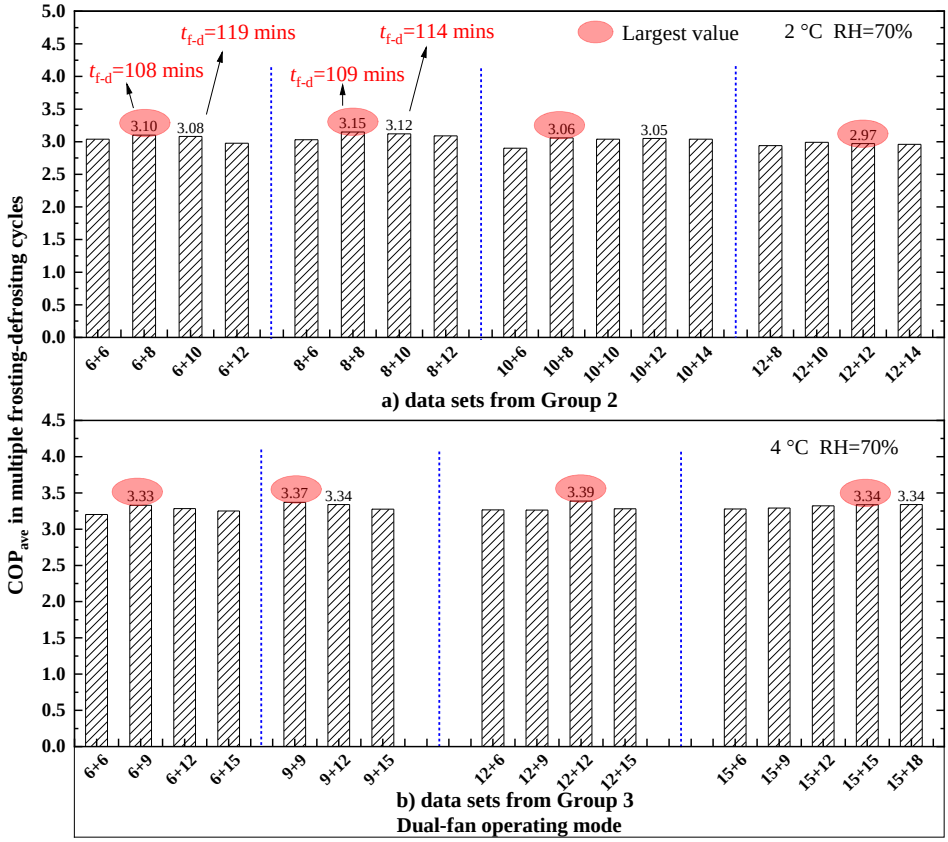

Fig. 7.3 COP_{ave} values during multiple frosting - defrosting cycles for the experimental ASHP / DFOC unit at different dual-fan operating modes and ambient air conditions (selected data sets from Groups 2 and 3)

Lastly, the defrosting frequency for the experimental ASHP / DFOC unit at different dual-fan operating modes and different ambient air conditions, for the same data sets selected from Groups 2 and 3 as shown in Fig. 7.1, are shown in Fig. 7.4. As seen, under a fixed ambient air condition, these operating modes that led to a longer frosting - defrosting operating duration would result in a lower defrosting frequency. For example, at a fixed T_a of 2 ˚C and a fixed *RH* of 70 %, the lowest defrosting frequency among the selected 17 data sets shown in Fig. 7.4 a) was 1 time every 2 hours at the longest $t_{f\text{-}d}$ value of 119 mins at the dual-fan operating mode of '6+10'. However, as understood, the defrosting frequency cannot be used to comprehensively reflect the operating energy efficiency for the experimental ASHP / DFOC unit.

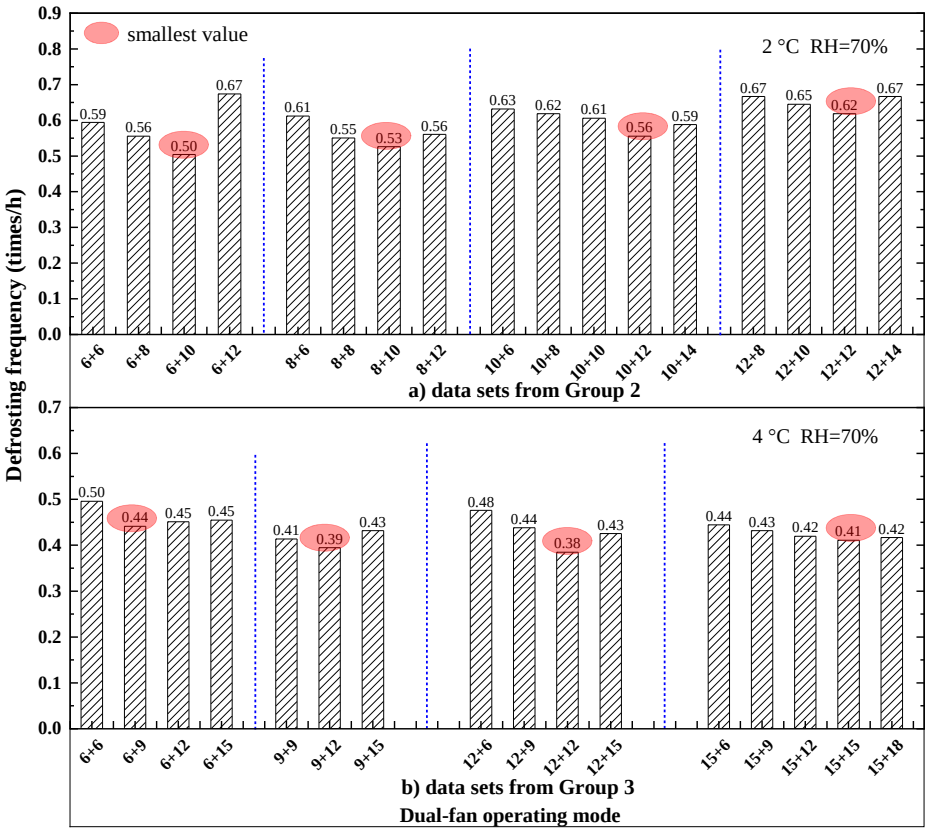

Fig. 7.4 Defrosting frequency of an experimental ASHP / DFOC unit for different dual-fan operating modes under different ambient air conditions for the data sets selected from Groups 2 and 3

The analysis results illustrated in Figs. 7.1 - 7.4 demonstrated that:

a) Ambient air temperature, relative humidity and the dual-fan operating mode can significantly impact the operating performance and heating efficiency of the experimental ASHP / DFOC unit;

b) At a fixed ambient air condition, among all dual-fan operating modes, there existed one mode at which frosting - defrosting duration was the longest;

c) Existing individual operating parameters such as $t_{f\text{-}d}$, COP_{ave} or defrosting frequency in the multiple frosting - defrosting cycles, cannot be used to effectively evaluate both the operating performance and heating efficiency for the experimental ASHP / DFOC unit, at different dual-fan operating modes but at the same ambient air conditions. Therefore, a new COP-related performance index for evaluating the overall operating performance of an ASHP / DFOC unit at different dual fan operating modes needed to be further developed.

7.2.2 Development of COP-related index for the experimental ASHP / DFOC unit

The analysis results in Section 7.2.1.2 proved that only an individual operational parameter was not able to comprehensively evaluate both the operating performances and heating efficiency of an experimental ASHP / DFOC unit by considering all three factors including $t_{f\text{-}d}$, defrosting frequency, and the COP_{ave} of ASHP units, etc. Therefore, a comprehensive COP-related performance index that can take all three factors into consideration was proposed here.

Fig. 7.5 shows the schematic of multiple frosting - defrosting operations of an ASHP unit, where q_i is the instantaneous output heating capacity of the ASHP unit, kW, t_{fn} and t_{defn} the

duration of frosting and defrosting operation in the nth cycle, s, respectively, t_i the current moment during the ASHP unit operation, s.

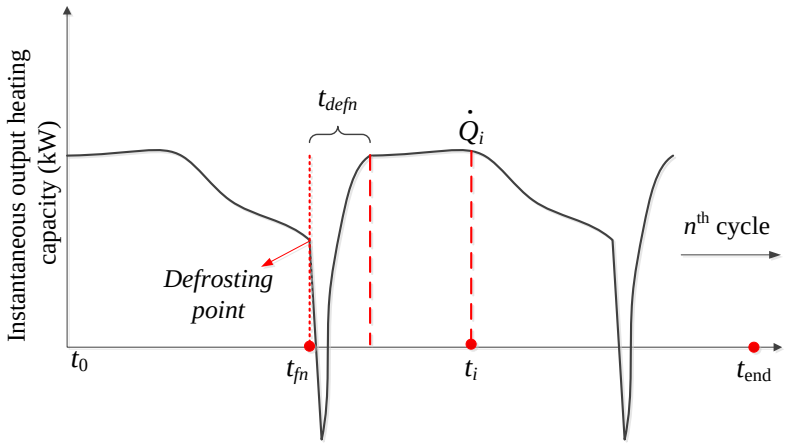

Fig. 7.5 Schematic of multiple frosting - defrosting operations for an ASHP unit

From Fig. 7.5, the COP_{ave} over the multiple frosting - defrosting cycles was evaluated as follows,

$$COP_{ave} = \frac{\int_{t_0}^{t_{end}} \dot{Q}_i(t)dt}{\int_{t_0}^{t_{end}} \dot{W}_{sys}(t)dt} \tag{7.1}$$

where t_{end} is the ending time point for the multiple frosting - defrosting cycles, $\dot{W}_{sys}$ the total instantaneous input power to the ASHP unit, kW.

Then, based on the analysis results presented in Section 7.2.1.2, a new COP-related performance index, the change rate of averaged COP (CRAC), CRAC, which was COP_{ave} divided by the averaged operating duration for the multiple frosting - defrosting cycles, min^{-1}, was defined as follows,

$$CRAC = \frac{COP_{\text{ave}}}{\frac{1}{n}\sum_{c=1}^{n}(t_f + t_{def})_n} \tag{7.2}$$

where n is the total number of the multiple frosting - defrosting cycles, which was also the same as the number of the defrosting operation in the multiple frosting - defrosting cycles, t_f the frosting duration, and the t_{def} the defrosting duration in a frosting-defrosting cycle.

According to Equation (7.2), CRAC was the time-averaged variation rate of COP_{ave}, which can comprehensively reflect the heating performances of the experimental ASHP / DFOC unit in multiple frosting - defrosting cycles. This was because CRAC indirectly reflected all negative and positive impacts resulted from the dual-fan operating modes and the variation in ambient air conditions, such as the additional power used for damper switching, the output heating capacity loss when reversing airflow direction, and defrosting frequency. Therefore, under different dual-fan operating modes but at the same ambient condition, the smaller the value of CRAC, the slower the COP_{ave} was deteriorated over the multiple frosting - defrosting cycles.

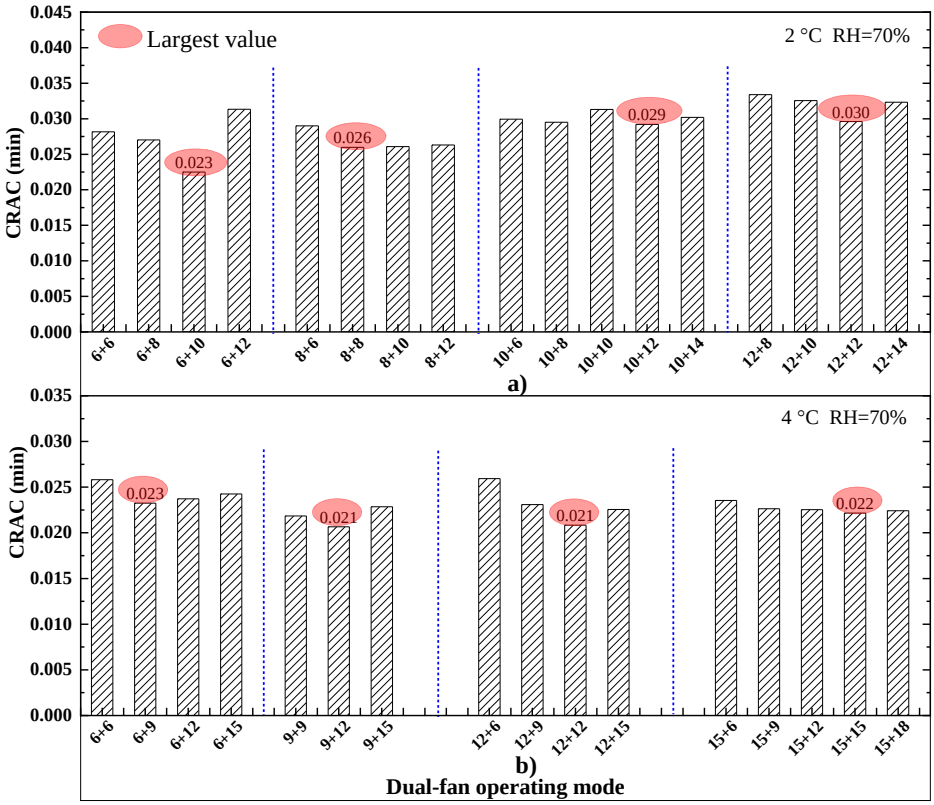

Fig. 7.6 Comparison of CRAC in different dual-fan operating modes and ambient air conditions of the experimental ASHP / DFOC unit based on data sets selected from Groups 2 - 3

To validate the usefulness of CRAC on comprehensively assessing the operating performances of the experimental ASHP / DFOC unit in multiple frosting - defrosting cycles, the values of CRAC at different dual-fan operating modes and ambient air conditions for the same data sets selected from Groups 2 and 3 as shown in Fig. 1, were evaluated, and are shown in Fig. 7.6. As seen, at the same ambient air condition, at a fixed t_A, there existed a t_B value at which the value of CRAC was the smallest among all the selected data sets. For example, in Fig. 7 a), at t_A of 6 mins when T_a was at 2 ˚C and RH at 70 %, the smallest CRAC of 0.023 min^{-1} was achieved when t_B was at 10 minutes, or at '6 + 10' mode. In Fig. 7.6, as a result, there were four smallest CRAC values corresponding to four different operating modes, i.e., 0.023 min^{-1} at '6+10' mode, 0.026 min^{-1} at '8+8' mode, 0.029 min^{-1} and 0.030 min^{-1} for mode '10+12' and

‘12+12’, as marked with a red circle in Fig. 7.6 a), respectively. Hence, the value of CRAC at ‘6+10’ mode was significantly lower than the other three smallest CRAC values, by between 13 % and 30.5 %. Thus, the use of mode ‘6+10’ can result in the lowest rate of reduction in COP_{ave} among the 17 selected data sets in Fig. 7.6 a). Similar variation trends may also be observed in Fig. 7.6 b). Therefore, CRAC can be used to better reflect the frosting - defrosting operating performances of the experimental ASHP / DFOC unit in multiple frosting - defrosting cycles that COP_{ave} itself.

The above analysis results demonstrated that CRAC was able to better reflect the comprehensive operating performances of the experimental ASHP / DFOC unit during multiple frosting - defrosting operating cycles. The smaller the CRAC, the better the frosting - defrosting operating performances of the experimental ASHP / DFOC unit. Therefore, with this newly defined COP-related performance index, i.e., CRAC, it was possible to determine the most suitable optimal dual-fan operating modes for the experimental ASHP / DFOC unit when operated under different ambient air conditions to achieve the best possible frosting - defrosting operating performances, using GRNN modelling approach, as reported in Section 7.3.

7.3 Development of a GRNN model for optimising the dual-fan operating mode of the experimental ASHP / DFOC unit based on CRAC

Based on the established database and the newly index CRAC defined in Section 7.2.2, a GRNN model was developed and validated, and the validated GRNN model was used to develop a GRNN-model based optimal control strategy for the experimental ASHP / DFOC unit.

7.3.1 GRNN model development, training and validation

7.3.1.1 Development of a GRNN model

The schematics of net structure for the GRNN model is shown in Fig. 7.7. As seen, the GRNN model consisted of 4 layers: an input layer, a pattern layer, a summation layer and an output layer. The input layer was made of different distributed neurons, which can directly pass the input parameters to the pattern layer. The Gaussian function was used as the transfer function. In the summation layer, there were two different kinds of neurons, one to sum up the outputs from all the neurons in the pattern layer and the other the weighted outputs from all the neurons in the pattern layer. Finally, the output layer output the objective parameters [Gokhale et al., 2022; Hu et al., 2021; Savadkoohi et al., 2023]. According to the analysis results detailed in Section 7.2.1, there were four main parameters, i.e., T_a, RH, t_A and t_B, that determined the operating performances of the ASHP / DFOC unit, at fixed compressor and fan speeds. Therefore, in this study, these four were designated as the input parameters to the GRNN model, and CRAC and $t_{f\text{-}d}$, the output parameters from the GRNN model.

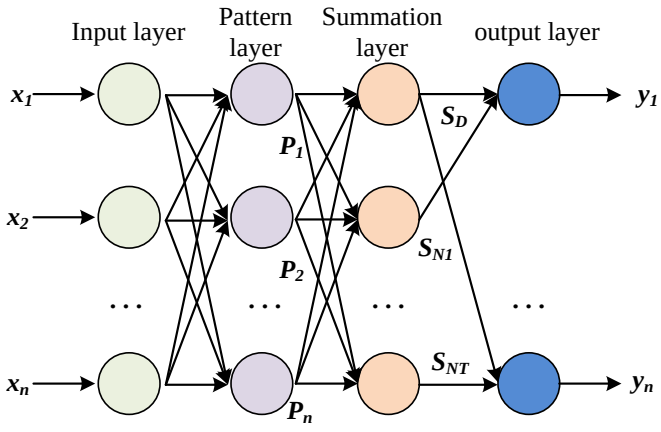

Fig. 7.7 Net structure schematics of the GRNN model

All the data sets in the established database, as well as the values of CRAC evaluated, were used for developing the GRNN model, as shown in Table 7.2. There were 186 data sets in the

established database, and it has been suggested that 75 % [Gerardo et al., 1999] or 80 % [Anderson et al., 1997] of data sets should be used for model training. Hence, 20 % (36 data sets) out of the total 186 data sets were selected randomly as the testing group for model testing, and the remaining 80 % (150 data sets) as the training group for model training. Besides, considering the size of the database, in order to improve the robustness and generalization ability of the GRNN model, Leave-One-Out cross validation method was applied to validate the GRNN mode. Leave-One-Out cross validation was a special case of the k-fold cross validation method, and the schematics of the k-fold validation are shown in Fig. 7.8. As seen, the date sets for model training may be equally divided into k subsets (i.e., k=5, 10, …). At each step of training, one subset out of the k subsets for training was used for testing and the remaining (k-1) subsets for training. In this way, a GRNN may be trained for k times till every subset for training was also tested for once. In the current study, k was set at 150, the same as the number of data sets used for training. The training results using the Leave-One-Out method was normally believed to be more accurate for those datasets with a relatively small number of data, as compared to other validation methods [Gerardo et al., 1999].

Table 7.2 Details of sample data for training and testing of the GRNN model

Input parameter				**Output parameter**	
T_a (℃)	RH (%)	t_A (min)	t_B (min)	$t_{f\text{-}d}$ (min)	CRAC (× 100 min^{-1})
0	70, 80, 90	6, 8, 10, 12	6, 8, 10, 12	46-94	2.7 - 4.4
2	70, 80, 85, 90	6, 8, 10, 12	6, 8, 10, 12, 15	52-119	1.02 - 2.31
4	70, 80, 90	6, 9, 12, 15	6, 9, 12, 15, 18	60-149	0.89 - 2.66
6	70, 80, 90	9, 12, 15, 18, 21	6, 9, 12, 15, 18, 21	68-162	0.78 - 2.16

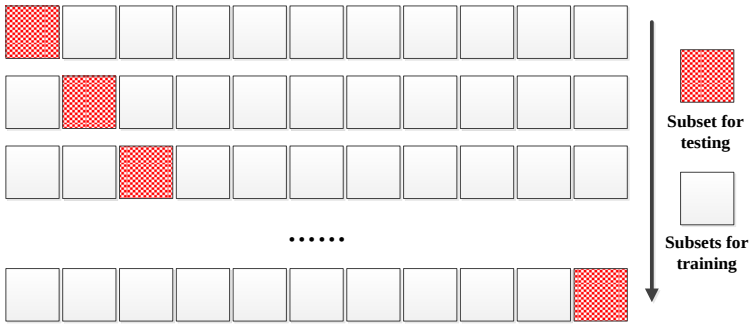

Fig. 7.8 Schematics of k-fold validation for training a GRNN model

7.3.1.2 Testing of the GRNN model

To test the developed GRNN model, some indexes were used to evaluate its performances [Wang et al., 2019]. Firstly, a smooth factor, σ, was used. A higher σ value would result in over smoothing of the data and a smaller σ overfitting of the data. An optimal σ may however be determined by using the *k*-fold cross validation process, based on the expected error percentage, EEP, as follows,

$$\mathrm{EEP} = \frac{\sqrt{\dfrac{\sum_{j=1}^{150}(\hat{y}_j - y_j)^2}{150}}}{|y_{\max}|} \times 100\% \tag{7.3}$$

Where $\hat{y}_j$ and y_j are the *j*th predicted and measured output parameters out of the total 150 data sets for training, respectively, and y_{max} the maximum measured value of output parameters. Assuming that σ was changed from 0.01 to 0.9 with an increment of 0.01, EEP would be calculated for each k value, the optimal σ value was determined when EEP was at its minimum value.

Besides, the relative error, RE, was calculated as follows,

$$\mathrm{RE} = \frac{|\hat{y}_j - y_j|}{y_j} \times 100\% \tag{7.4}$$

The mean absolute error, MAE, was as follows,

$$MAE = \frac{1}{36} \times \sum_{i=1}^{36} \left| \hat{y}_j - y_j \right| \tag{7.5}$$

Where $\hat{y}_j$ and y_j are defined in Equation (7.3).

Finally, the Pearson Correlation Coefficient, P, for evaluating the degree of correlation for the GRNN model developed, was as follows,

$$P = \frac{\sum_{j=1}^{n} \left(x_j - \bar{x} \right) \left(\hat{y}_j - \bar{y} \right)}{\sqrt{\sum_{j=1}^{n} \left(x_j - \bar{x} \right)^2} \sqrt{\sum_{j=1}^{n} \left(\hat{y}_j - \bar{y} \right)^2}} \tag{7.6}$$

where x_j is jth input parameter out of the total of 36 data sets for testing, $\bar{x}$ and $\bar{y}$ the mean values of x_j and $\hat{y}_j$, respectively. The range of P is [-1,1], and its absolute value $|P|$, represents the correlation level between parameters, the greater the $|P|$, the stronger the correlation.

With the above-mentioned indexes, the performances of the developed GRNN model were evaluated. The comparison between the predicted values using the GRNN model and the measured values in the testing group is shown in Fig. 7.9. As seen, both the predicted $t_{f\text{-}d}$ value and CRAC agreed well with the measured or evaluated data in the testing group, with a MAE of ± 5.9 % for $t_{f\text{-}d}$ and that of ± 5 % for CRAC, respectively. Besides, the Pearson correlation coefficients for $t_{f\text{-}d}$ and CRAC were at 0.978 and 0.983, respectively, and 94.5 % of the predicted results were within the ± 10 % error band. The optimal σ for the GRNN model was 0.17, with a minimum EEP of 4 %.

Therefore, the developed GRNN model was considered adequately accurate and may be used to predict $t_{f\text{-}d}$ and CRAC with an acceptable accuracy.

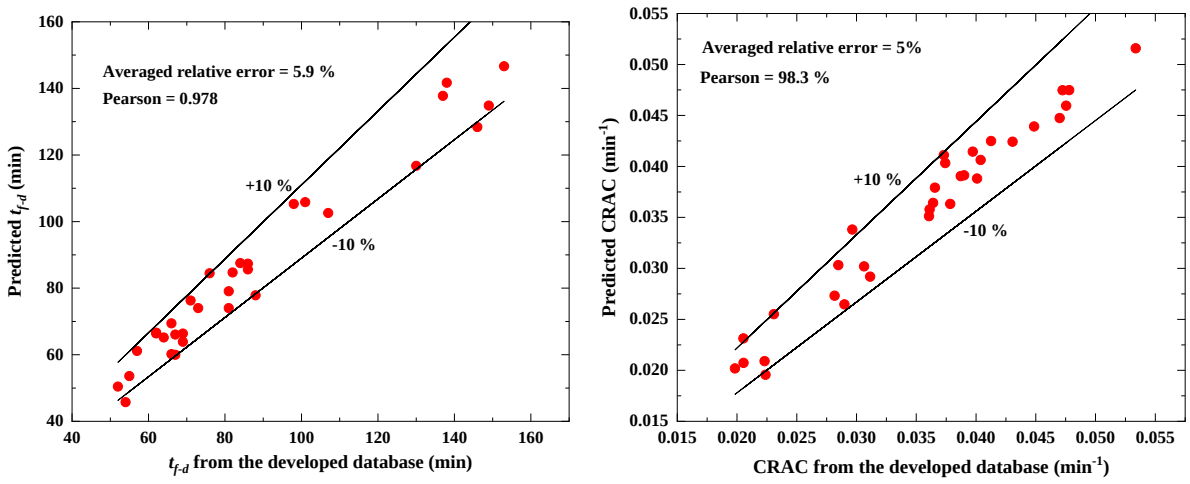

a) $t_{f\text{-}d}$ b) CRAC

Fig. 7.9 Comparisons between predicted and measured values in the testing group

7.3.2 The prediction and optimisation using the developed GRNN model

Based on the developed GRNN model, a new input matrix for the input layer for the developed GRNN model was built for prediction, and is shown in Table 7.3. As seen, the variation range for ambient air temperature was from 0 to 6 ℃ with an interval of 0.2 ℃, and that for *RH* from 70 % to 92 % with an interval of 2 %. Besides, for t_A and t_B, they were varied with an increment of 1 minute. Therefore, there were a total of 29016 combinations for T_a, *RH*, t_A and t_B in Table 7.3.

To obtain the optimal dual-fan operating modes at different ambient air conditions, which can result in the smallest CRAC, all the 29016 combinations in the new input matrix shown in Table 7.3 were input to the developed GRNN model to obtain the predicted values for both $t_{f\text{-}d}$ and CRAC, which are in the last two columns of Table 7.3 to form a complete GRNN-based predicted dataset. On the other hand, according to the analysis results presented in Section 7.2.1, at the same ambient air condition, a dual fan operating mode 't_A+t_B' that can lead to the

minimum predicted CRAC value was taken as an optimal one and thus selected. There were totally 372 optimal modes at different ambient air conditions so selected from the total 29016 combinations, and are listed in Table 7.4 to form an objective dataset. As seen, in Table 7.4, for all the optimal dual-fan operating modes, their corresponding T_a variation ranges were from 0 to 6 ℃ and that for *RH* from 70 % to 92 %, respectively. Therefore, at a given ambient condition, its matching optimal dual-fan operating mode may be easily identified from Table 7.4 for controlling the operation of the experimental ASHP / DFOC unit. Consequently, using Table 7.4, a dynamic control strategy applied to the experimental ASHP / DFOC unit under varying ambient air conditions can be developed.

Table 7.3 New input matrix for the GRNN model for predicting and the corresponding predicted $t_{f\text{-}d}$ and CRAC

New input matrix					Predicted output matrix	
No.	T_a (℃)	*RH* (%)	t_A (min)	t_B (min)	$t_{f\text{-}d}$ (min)	CRAC (min^{-1})
1	0	70	6	6	92.8	0.0288
2	0	70	6	7	90.4	0.0294
3	…	…	…	…	…	…
…	0.2	82	9	11	77.6	0.036
…	0.2	82	9	12	72.6	0.037
…	…	…	…	…	…	…
29016	6	92	21	21	77.2	0.041

Table 7.4 Objective dataset of optimal dual-fan operating modes at different ambient conditions

No.	T_a (℃)	*RH* (%)	t_A (min)	t_B (min)	$t_{f\text{-}d}$ (min)	CRAC (min^{-1})
1	0	70	6	6	92.8	0.0288
2	0	72	6	7	91.9	0.031
3	…	…	…	…	…	…
…	0.2	82	9	11	77.6	0.036
…	0.2	84	9	11	75.8	0.037
…					…	…
372	6	92	18	21	84.9	0.0376

7.4 Development and validation of an optimal control strategy

Following the establishment of Objective dataset as shown in Table 7.4, an optimal control strategy for the novel experimental DFOC used in the experimental ASHP units under varying ambient air conditions was developed, and validated via three experimental cases using the experimental ASHP / DFOC unit.

7.4.1 Development of an optimal control strategy for the novel DFOC used in the experimental ASHP unit

An optimal control strategy applied to the experimental ASHP / DFOC unit under varying ambient air conditions was developed, and its control logic is shown in Fig. 7.10.

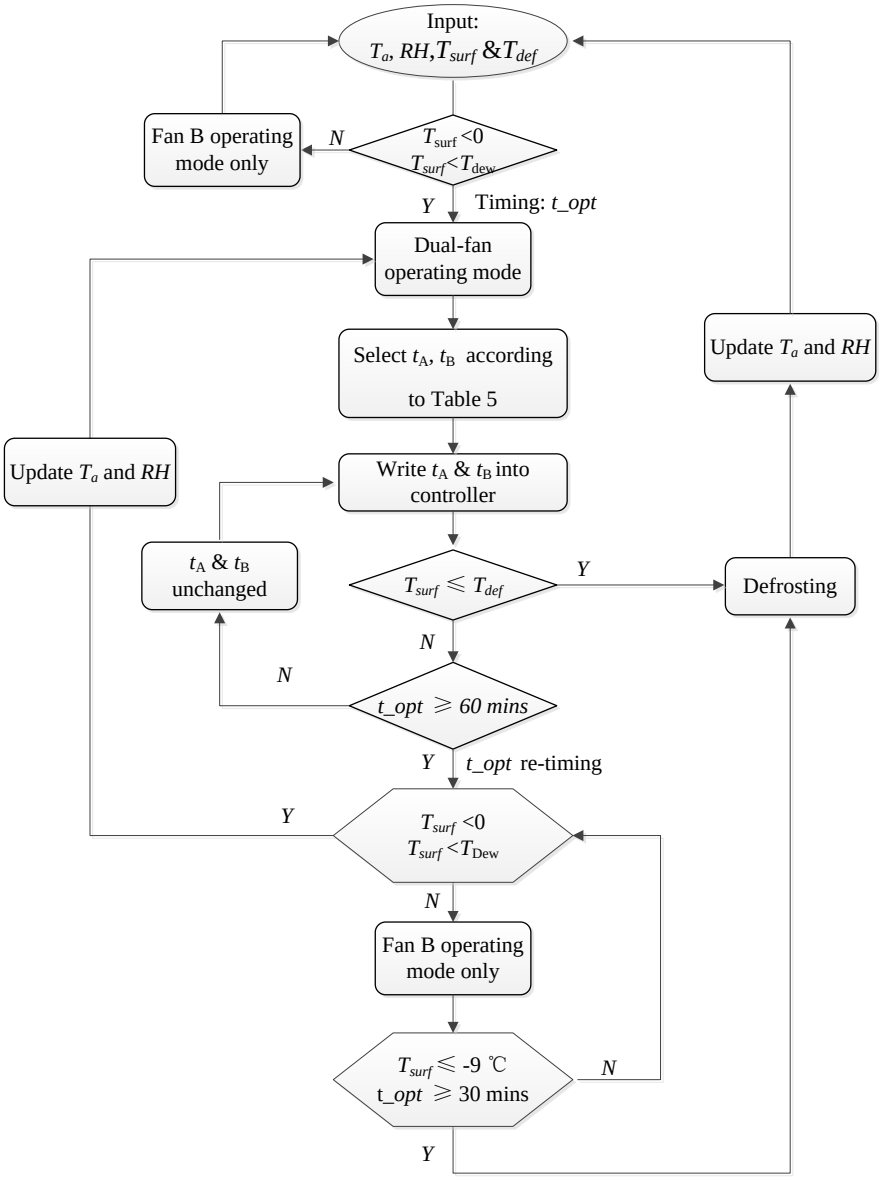

Fig. 7.10 Flow chart of the developed optimal control strategy for the experimental ASHP / DFOC unit

As seen in Fig. 7.10, under the developed optimal control strategy, when the experimental ASHP / DFOC unit was put into operation, the measured T_a and RH, surface temperature of the outdoor coil, T_{surf}, and the defrosting initiation setting temperature, T_{def}, were input to the control strategy. Under these inputs, the control strategy was implemented in the following four steps.

Step 1: It is necessary to check whether the experimental ASHP / DFOC was operated at

frosting conditions by examining if T_{surf} was lower than both 0 ℃ and the dew point of ambient air. If it was operated at a non-frosting condition, the traditional single-fan operating mode was used by using only Fan B. If however it was operated at a frosting condition, the dual-fan operating mode would be chosen and a timer, *t-opt*, started timing, and the setting values for Fan A and Fan B at the dual-fan operating mode would be selected from Table 7.4 to control the operation of the experimental DFOC.

Step 2: During operation, it was necessary to check in real-time whether defrosting initiation condition arrived, i.e., $T_{surf} \leqslant T_{def}$. If not, but *t-opt* reached 60 mins, the operation moved on to Step 3.

Step 3: When *t-opt* $\geqslant$ 60 mins, the timer was reset, and T_a and *RH* were measured in real-time again to see if the experimental ASHP / DFOC unit was still operated at frosting condition or not. If yes, dual-fan operating mode would be updated according to the currently measured ambient air condition, till defrosting was initiated. However, if not, the operation moved on to Step 4.

Step 4: the current dual-fan operating mode was switched to the single-fan operating mode, i.e., running Fan B only, in the subsequent duration of 30 mins. At this moment, if T_{surf} was also lower than -9 ˚C, defrosting would be initiated. Otherwise, the timer was reset, and T_a and *RH* were measured once again to update the fan operating mode if needed. If the experimental ASHP / DFOC unit was still operated at a frosting condition, Steps 1 - 3 would be repeated. Otherwise, Step 4 would be repeated till defrosting was initiated.

Moreover, in Fig. 7.10, the time interval in Step 2 and 3 for updating dual-fan operating mode under frosting conditions was set at 60 mins, because the changes in ambient air conditions were usually gradual and steady ambient conditions may be assumed within one hour. For

example, Zhu et al [2015b] and Bai et al [2018] have carried out extensive field studies for ASHP units operated in different regions of China. In their studies, it was observed that the ambient air temperature and humidity were relatively stable within one hour. Besides, frequent updating dual-fan operating mode may also lead to an unstable operation of the DFOC, which can be counter-productive to even frosting. Therefore, *t_op* was set at 60 mins in the current study.

7.4.2 Validation of the optimal control strategy using the experimental ASHP / DFOC unit

7.4.2.1 Experimental cases and conditions

The developed optimal control strategy was experimentally validated. There were 3 experimental cases with an experimental duration of 10 hours. The experimental cases and conditions are listed in Table 7.5.

Meteorological data for 10 hours in a typical day in January in Shanghai City from the Typical Meteorological Year Database (TMYD), as shown in Fig. 7.11, were selected [Zhang, 2006] and used as the experimental ambient conditions, as shown in Table 7.5. As seen, the hourly averaged T_a varied from 1.7 ˚C to 4.7 ˚C, and *RH* 74 % to 89 %. Based on the frosting map developed by Zhu et al [2015a], the selected experimental ambient conditions fell in the severer frosting zone, moderate frosting zone and mild frosting zone of the frosting map. Therefore, the selected experimental ambient air conditions shown in Fig. 7.11 were considered typical and appropriate to validate the developed dual-fan optimal control strategy.

Three experimental cases are detailed as follows. For Case 1, traditional single-fan operating mode using only Fan B was adopted. For Case 2, the fixed dual-fan operating mode of ‘6+7’

was employed throughout an experiment. In Case 3, the operating mode was controlled by the developed dual-fan optimal control strategy shown in Fig. 7.10. It was intended that the experimental results from Cases 1 and 2 were served as a basis for comparison to reflect the operating performances of the experimental ASHP / DFOC unit using the developed optimal control strategy.

Table 7.5 Experimental cases for validating the developed dual-fan optimal control strategy

<table>
<tr><th>Case No.</th><th>T_a (°C)</th><th>RH (%)</th><th>t_A (min)</th><th>t_B (min)</th><th>Duration (h)</th></tr>
<tr><td>1</td><td rowspan="3">1.7 - 4.7</td><td rowspan="3">74 % - 89 %</td><td>-</td><td>Only Fan B operated</td><td rowspan="3">10</td></tr>
<tr><td>2</td><td>Fixed at 6 mins</td><td>Fixed at 7 mins</td></tr>
<tr><td>3</td><td colspan="2">Under the developed optimal control strategy</td></tr>
</table>

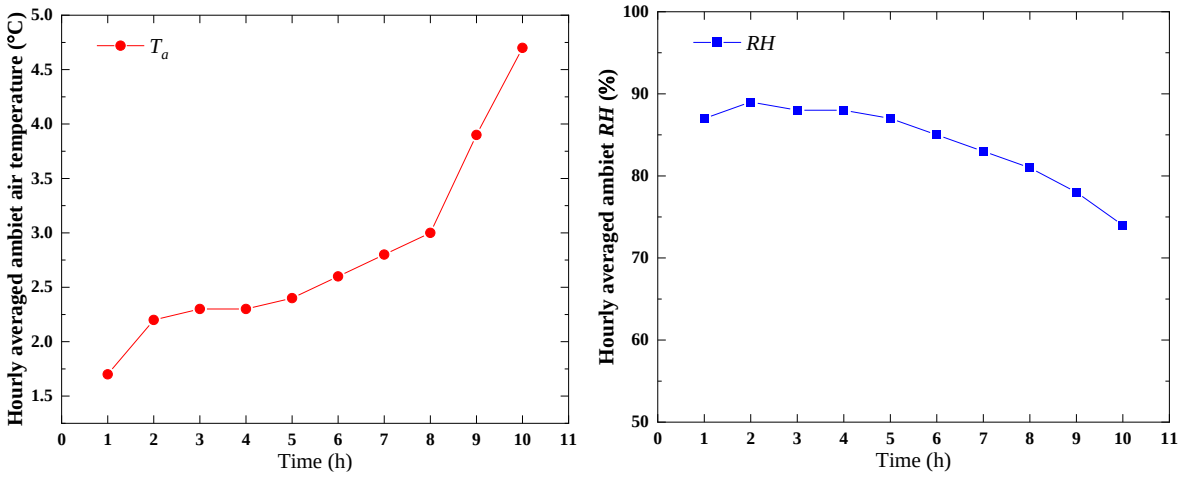

a) T_a b) *RH*

Fig. 7.11 Changes in hourly averaged T_a and *RH* used for experimental validation of the developed optimal control strategy

7.4.2.2 Comparison of experimental results

The optimal dual-fan operating modes used in Case 3 are shown in Table 7.6. As seen, as time went by, the dual-fan operating mode was automatically adjusted based on the optimal control logic developed in Fig. 11. It was noted that T_a and RH in the 2nd, 3rd and 4th hour were relatively stable, hence, the dual-fan operating mode during the three hours was same.

Table 7.6 Values for t_A and t_B during the different hours used in Case 3

Time (h) / *Fan mode*	*1*	*2*	*3*	*4*	*5*	*6*	*7*	*8*	*9*	*10*
t_A *(mins)*	6	6	6	6	7	8	8	9	10	12
t_B *(mins)*	7	9	9	9	8	9	10	11	12	14

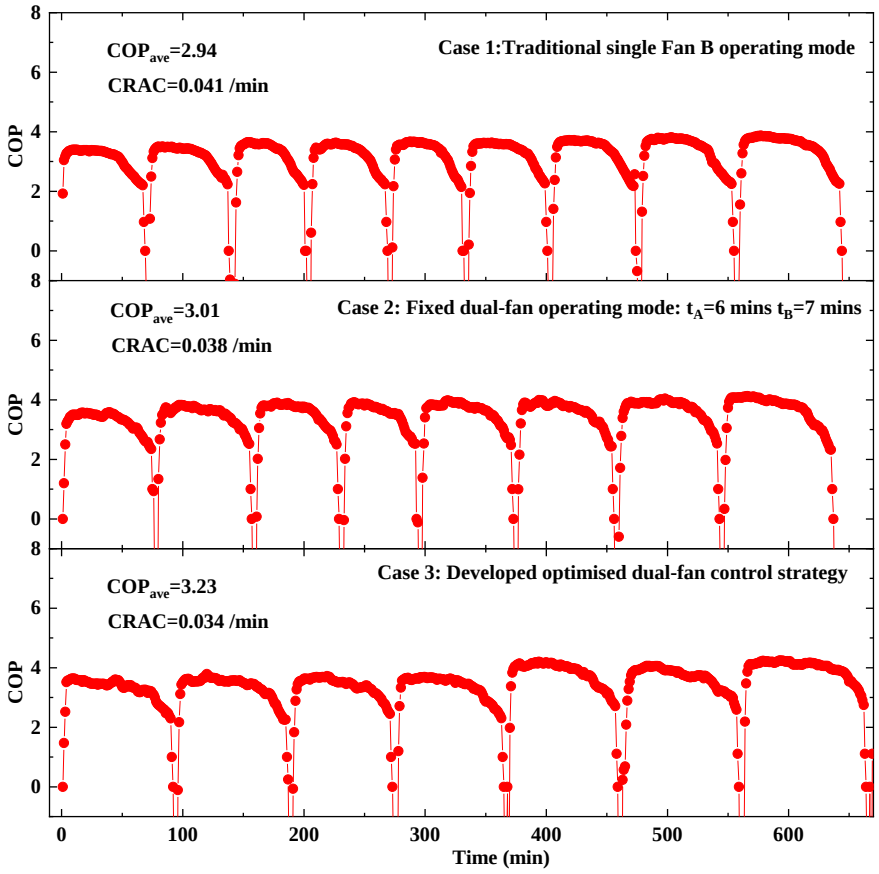

Fig. 7.12 Experimental values of COP and CRAC in the three experimental cases

The obtained experimental values of COP and CRAC in the three cases in the 10 hours long experimental multiple frosting - defrosting cycles are compared shown in Fig. 7.12. As seen in Fig. 7.12, there were totally 9 frosting - defrosting cycles in Case 1, with its COP_{ave} at 2.94 and CRAC 0.041 min-1, respectively. In Case 2 where the dual-fan operating mode was at '6 + 7', there were 8 frosting - defrosting cycles, with its COP_{ave} at 3.01 and CRAC at 0.038 min^{-1}, respectively. For Case 3 using the developed dual-fan optimal control strategy, its COP_{ave} was at 3.01 and CRAC at 0.038 min^{-1}, respectively. As compared to the experimental results in Case 1 and Case 2, the COP_{ave} in Case 3 was improved by 9.9 % and 6.8 %, respectively, and CRAC decreased by 17.1 % and 10.5 %, respectively. The experimental results suggested clearly that when the experimental ASHP / DOFC unit was under the developed optimal control strategy, a better operating performance in terms of a higher COP_{ave} and lower CRAC can be achieved, at typical frosting operating ambient air conditions.

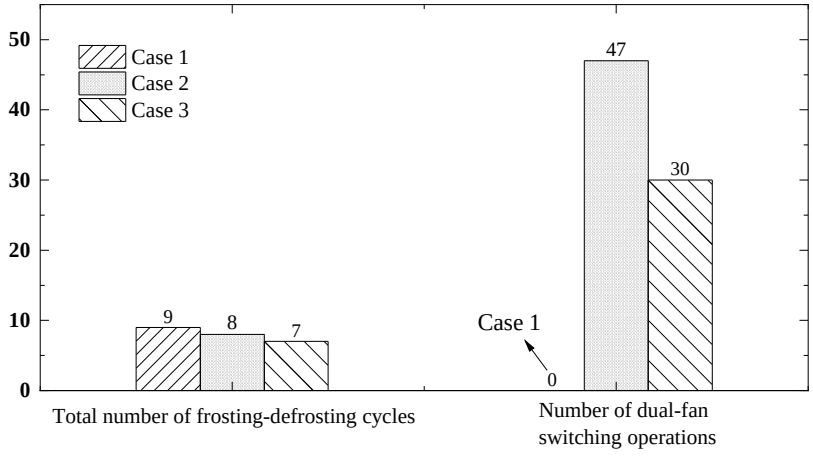

Fig. 7.13 Number of frosting - defrosting cycles and dual-fan switching in the three experimental cases during the 10 hours long experiment

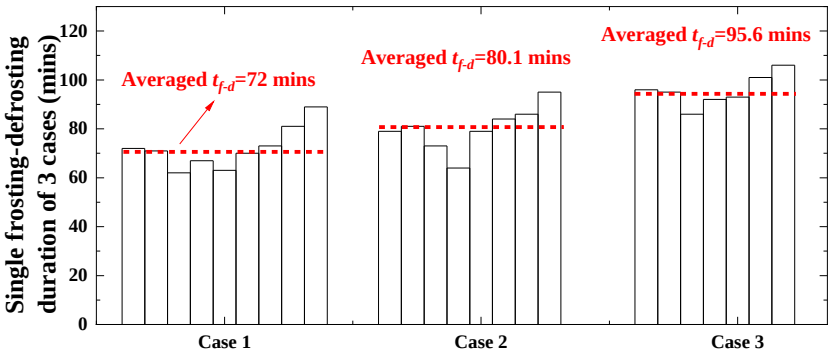

Fig. 7.14 The duration of each of the multiple frosting - defrosting cycles in the three experimental cases

The number of frosting - defrosting cycles and the number of dual-fan switching for the experimental ASHP / DFOC unit during the 10 hours long experiments in the three cases are shown in Fig. 7.13. As seen, frosting - defrosting number was 9 in Case 1, 8 in Case 2 and 7 in Case 3, and a 22.2 % and 12.5 % reduction in Case 3, relative to Case 1 and Case 2, respectively. In addition, the number of dual-fan switching in Case 2 was 47, in Case 3 only 30, or a 36.2 % reduction. This suggested that using the developed dual-fan optimal control strategy can avoid unnecessary switching operations of the novel DFOC to achieve higher operating performances.

Furthermore, Fig. 7.14 shows the durations of each of the multiple frosting - defrosting cycles in the three experimental cases. As seen, the averaged $t_{f\text{-}d}$ value for Case 1, Case 2 and Case 3 was at 72 mins, 80.1 mins and 95.6 mins, respectively. The averaged $t_{f\text{-}d}$ value in Case 3 was 32.8 % greater than that in Case 1 and 19.4 % greater than that Case 2. The results demonstrated that using the developed dual-fan optimal control strategy can significantly prolong the duration of a single frosting - defrosting cycle for the experimental ASHP / DFOC unit.

The experimental results demonstrated that using the developed dual-fan optimal control strategy, better operating performances of the experimental ASHP / DFOC unit in terms of a higher averaged COP and a smaller CRAC, a longer frosting - defrosting duration and a fewer number of dual-fan switching, may be achieved.

7.5. Conclusions

To enable an experimental ASHP / DFOC unit to operate at varying ambient air conditions with evener frosting along air flow direction and a higher operating efficiency, an optimal control strategy for the experimental ASHP / DFOC unit was developed using GRNN modelling approach and is presented in this Chapter. A database for developing the GRNN model was established first, and a new COP-related performance index, CRAC, was proposed after analysing the database. Then, based on the developed database and CRAC, a GRNN model was developed and validated, and the validated GRNN model was used to predict and search for the optimal dual-fan operating modes when the experimental ASHP / DFOC was operated at different ambient air conditions. Finally, an optimal control strategy for the experimental ASHP / DFOC unit based on identified optimal dual-fan operating modes was developed and experimentally validated. The conclusions of this Chapter are as follows:

1) The analysis results of the established database demonstrated that the ambient air temperature, relative humidity and the dual-fan operating mode can significantly impact the operating performance and heating efficiency of the experimental ASHP / DFOC unit. At a fixed ambient air condition, among all dual-fan operating modes, there existed one mode at which $t_{f\text{-}d}$ was the longest. The analysis results also indicated that existing individual operating parameters such as COP, $t_{f\text{-}d}$ or defrosting frequency for the multiple frosting - defrosting cycles, cannot be used to effectively evaluate both the operating performance and heating efficiency for the experimental ASHP / DFOC unit, at different dual-fan operating modes but at the same ambient air conditions;

2) The newly proposed COP-related performance index, CRAC, was able to

effectively reflect the comprehensive operating performances of the experimental ASHP / DFOC unit during multiple frosting - defrosting operating cycles. The smaller the CRAC, the better the frosting - defrosting operating performances of the experimental ASHP / DFOC unit. Therefore, CRAC can be used as a criteria to select the most suitable optimal dual-fan operating modes for the experimental ASHP / DFOC unit when operated under different ambient air conditions to achieve the best possible frosting - defrosting operating performances;

3) The developed GRNN model was validated and can be used to predict $t_{f\text{-}d}$ and CRAC with an acceptable accuracy, in terms of a minimum EEP of 4 % for GRNN model, and a mean absolute error between the predicted and measured values of ± 5.9 % for $t_{f\text{-}d}$ and that of ± 5 % for CRAC, respectively. Hence, based on the validated GRNN model and minimum CRAC, an objective dataset consisted of 372 optimal dual-fan operating modes at different ambient air conditions was established for guiding the development of an optimal control strategy for the experimental ASHP / DFOC unit;

4) The optimal control strategy for the experimental ASHP / DFOC unit was developed based on the objective dataset, and its experimental validation demonstrated that using the developed dual-fan optimal control strategy, better operating performances of the experimental ASHP / DFOC unit in terms of a higher averaged COP and a smaller CRAC, a longer frosting - defrosting duration and a fewer number of dual-fan switching, can be achieved. When using the optimal dual-fan control strategy, COP_{ave} was improved by 9.9 % and 6.8 %, CRAC decreased by 17.1 % and 10.5 %, the defrosting frequency was reduced

by 22.2 % and 12.5 %, and the averaged frosting - defrosting duration extended by 32.8 % and 19.4 %, respectively, when compared to those cases using the traditional single-fan operating mode and the fixed dual-fan operating mode. Besides, using the developed dual-fan optimal control strategy can also avoid unnecessary switching operations of the novel DFOC to achieve more reliable operating performances, at a reduction rate of 36.2 % for the number of dual-fan switching, as compared to that using the fixed dual-fan operating mode.

Chapter 8

Conclusion and future work

8.1 Conclusions

In the research project presented in this Thesis, in order to achieve even frosting along the airflow direction of the outdoor coil in ASHP units, firstly, a novel DFOC that can alternately reverse the airflow direction has been proposed, and the even frosting characteristics and heating performances of an experimental ASHP / DFOC unit have been experimentally evaluated. Secondly, a dynamic mathematical model for the experimental ASHP / DFOC setup has been developed and experimentally validated. Thirdly, based on the experimental and mathematical study results, an optimal control strategy for the experimental ASHP / DFOC unit based on GRNN modelling has been successfully developed and validated. The control strategy enabled the experimental ASHP / DFOC unit to be used at different operating ambient air conditions to achieve evener frosting and higher heating performances. The conclusions of the Thesis are as follows:

1) An experimental study on investigating the even frosting characteristics and heating performances of the ASHP / DFOC unit under different dual-fan operating modes has been carried out and reported in Chapter 5. The results demonstrated that the use of the novel dual-fan outdoor coil can help effectively achieve evener frosting on both sides of the FTHX, and hence a longer heating operation duration and a higher operating efficiency and output heating capacity, compared to the use of a traditional single fan outdoor coil.

2) The development and experimental validation of a dynamic physical-based mathematical

model for the experimental / DFOC unit are reported in Chapter 6. The model was validated using the experimental data reported in Chapter 5, with an acceptable predicting accuracy. Then a follow-up modelling study for different operating modes of the two fans, fin pitches and operating ambient conditions was carried out using the validated model. The modelling results demonstrated that by optimizing fan operating mode, the difference in frost thickness between the windward and leeward sides of the dual-fan outdoor coil can be reduced by up to 77.3 %, the averaged output heating capacity and COP improved by up to 11.1 % and 12.7 %, respectively, and the number of switching operation of the two fans decreased by 55.6 %. The model can also be used to provide recommendations for using the dual-fan outdoor coil at different operating modes of the two fans, different fin pitches and operating ambient conditions.

3) An optimal control strategy for ASHP units / DFOC for evener frosting along airflow direction based on GRNN modelling was developed and experimentally validated, as presented in Chapter 7. The experimental results demonstrated that the use of the developed optimal control strategy led to a higher heating efficiency, a longer frosting - defrosting duration and a fewer number of dual-fan switching for the experimental ASHP / DFOC unit, with its averaged COP improved by 9.9 % and 6.8 %, CRAC decreased by 17.1 % and 10.5 %, defrosting frequency reduced by 22.2 % and 12.5 %, and averaged frosting - defrosting duration extended by 32.8 % and 19.4 %, respectively, when compared to the use of traditional single-fan operating mode and a fixed dual-fan operating mode at varying ambient conditions.

The main outcomes of this research project reported in this These included: 1) the detailed developments of the novel DFOC used in an ASHP unit, including its experimental evaluations in achieving even frosting along the airflow direction with different dual-fan operating modes; 2) the experimentally validated dynamic mathematical model for the even frosting

characteristics of the experimental ASHP / DFOC unit at different fan operating modes, with different configurations and under different operating ambient conditions; 3) the optimal control strategy that enabled the experimental ASHP / DFOC unit to operate at different operating ambient air conditions with evener frosting along air flow direction and higher heating performances.

The successful carrying out of the research project has helped achieve even frosting on an outdoor coil along the airflow direction, so as to alleviate negative impacts of uneven frosting during both frosting and defrosting including a more stable operation, a longer heating operation duration, a lower defrosting frequency and higher heating performances, etc. The long-term significance of the research project is its contributions to sustainability by reducing the energy use for ASHP-based space heating while improving the thermal comfort of building occupants, and the advance of ASHP technology. In addition, the research project also provided new ideas on the novel design of ASHP / DFOC units, as compared to the design of traditional single fan outdoor units with fixed air flow direction. Therefore, the outcomes of this research project can help promote a wider application of ASHP technology.

8.2 Proposed future work

Following the successful completion of the research project reported in this Thesis, a number of future possible studies are proposed as follows:

1) The experimental study reported in Chapter 5 focused on investigating even frosting characteristics, and the study results demonstrated that the use of the novel DFOC in an ASHP unit can help achieve even frosting along airflow direction. However, a detailed investigation on defrosting performances for the experimental ASHP / DFOC unit with different frosting levels on both sides of the FTHX in the DFOC should be

carried out for developing a new defrosting initiation strategy specially for such a DFOC unit.

2) In this research project, a novel experimental DFOC was developed, and the even frosting characteristics of the experimental ASHP / DFOC unit were investigated in great detail. However, due to the dual-fan structure, it was inevitable to employ 4 dampers to enable changing airflow direction, which would nonetheless increase the dimension of the DFOC and control complexity. Therefore, it becomes necessary to simplify the configuration of the experimental DFOC unit, by using an outdoor air fan that can reverse its rotation for changing airflow direction, so that air dampers may no longer be needed, and the dimension of an DFOC reduced.

3) The developed optimal control strategy presented in Chapter 7 was based on a fixed compressor speed. In practical applications, ASHP units having a varied speed compressor have been widely used for building space heating and cooling. Therefore, a more comprehensive control strategy for use by varied speed ASHP / DFOC units should be further considered.

4) There were some other existing methods to mitigate uneven frosting on heat exchangers along airflow direction such as using unequal fin pitch for windward and leeward sides of FTHXs. Therefore in future, it is possible to use these existing methods in the proposed DFOC, which may be particular useful in dealing with the impact of fixed refrigerant flow direction on even frosting performances.

Appendix

Photo images of the experimental setup

Photo 1 The novel DFOC of the experimental ASHP / DFOC unit

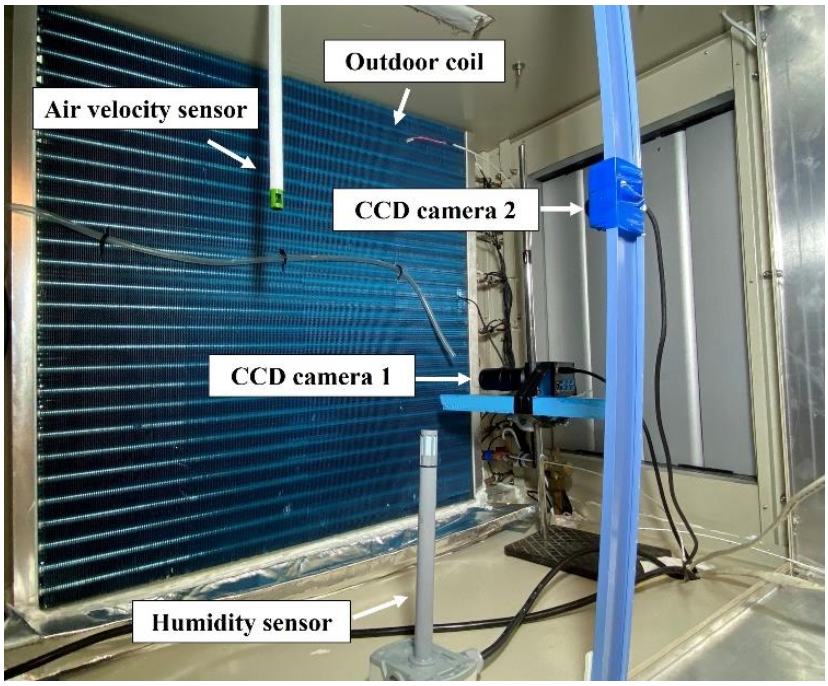

Photo 2 Side B of the FTHX in the experimental ASHP / DFOC unit

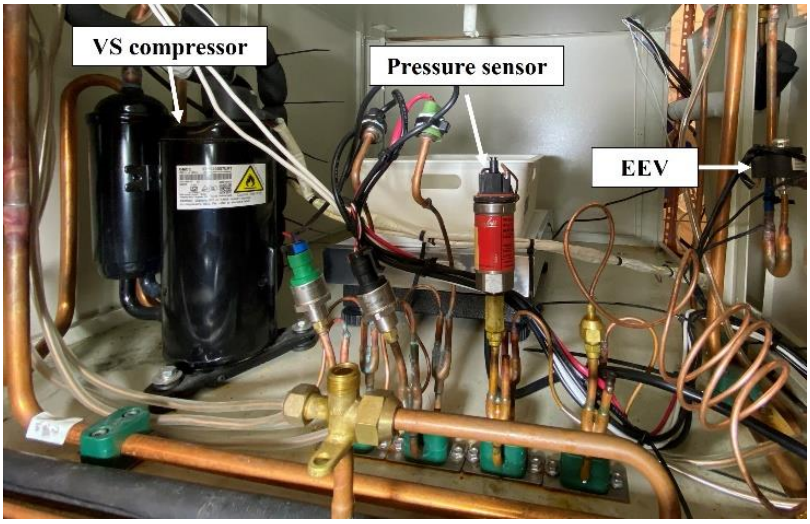

Photo 3 The refrigeration plant in the experimental ASHP / DFOC unit

Photo 4 The existing environmental chamber

References

1. Abbas and Park, 2021
   Abbas, S., Park, C. W.
   Frosting and defrosting assessment of carbon fiber reinforced polymer composite with surface wettability and resistive heating characteristics; International Journal of Heat and Mass Transfer, 169 (2021), 120883.

2. Akram et al., 2022
   Akram, M. W., Mohd Zublie, M. F., Hasanuzzaman, M., Rahim, N. A.
   Global Prospects, Advance Technologies and Policies of Energy-Saving and Sustainable Building Systems: A Review. Sustainability, 14, 3 (2022), 1316.

3. Anderson et al., 1997
   Anderson, C. W., Hittle, D. C., Katz, A. D., Kretchmar, R. M.
   Synthesis of reinforcement learning, neural networks and PI control applied to a simulated heating coil'; Artificial Intelligence in Engineering, 11, 4 (1997), 421–429.

4. Amer and Wang, 2020
   Amer, M., Wang, C.-C.
   Experimental investigation on defrosting of a cold flat plate via ultrasonic vibration under natural convection. Applied Thermal Engineering, 179 (2020), 115729.

5. American Society of Heating, Refrigerating, and Air Conditioning Engineers (ASHRAE), 2010. (2010, July 23). Retrieved 3 March 2023.

6. Bai et al., 2018
   Bai, X., Wang, W., Sun, Y., Liu, J., Ge, Y., Deng, S.
   Operating performances of an ASHP unit operated in a mild and humid region using tube-encircled photoelectric sensor based defrosting initiation strategy. Energy and Buildings, 177 (2018), 140–153.

7. Barbosa et al., 2009
Barbosa, J. R., Melo, C., Hermes, C. J. L., Waltrich, P. J.
A study of the air-side heat transfer and pressure drop characteristics of tube-fin 'no-frost' evaporators. Applied Energy, 86, 9 (2009), 1484–1491.

8. Bound et al., 2001
Bound, J., Brown, C., Mathiowetz, N.
Measurement error in survey data' (Handbook of Econometrics); Elsevier (2001), 3705–3843.

9. Boyina et al., 2019
Boyina, K. S., Mahvi, A. J., Chavan, S., Park, D., Kumar, K., Lira, M., et al. Condensation frosting on meter-scale superhydrophobic and superhydrophilic heat exchangers. International Journal of Heat and Mass Transfer, 145 (2019), 118694.

10. Brèque and Nemer, 2016
Brèque, F., Nemer, M.
Frosting modeling on a cold flat plate: Comparison of the different assumptions and impacts on frost growth predictions. International Journal of Refrigeration, 69 (2016),

11. Breque and Nemer, 2017
Breque, F., Nemer, M.
Modeling of a fan-supplied flat-tube heat exchanger exposed to non-uniform frost growth. International Journal of Refrigeration, 75 (2017), 129–140.

12. Brian et al., 1970
Brian, P. L. T., Reid, R. C., Shah, Y. T.
Frost Deposition on Cold Surfaces. Industrial & Engineering Chemistry Fundamentals, 9, 3 (1970), 375–380.

13. Brian et al., 2002
Brian, P. L. T., Reid, R. C., Shah, Y. T.
Frost Deposition on Cold Surfaces. (2002, May 1).

14. Carlson et al., 2001
Carlson, D. M., Hrnjak, P. S., Bullard, C. W.
Deposition, Distribution, and Effects of Frost on a Multi-Row Heat Exchanger Performance. Air Conditioning and Refrigeration Center TR-183 (2001).

15. Chen et al., 2003
Chen, H., Thomas, L., Besant, R. W.
Fan supplied heat exchanger fin performance under frosting conditions. International Journal of Refrigeration, 26, 1 (2003), 140–149.

16. Chen et al., 2018
Chen, W., Chan, M., Weng, W., Yan, H., Deng, S.
Development of a steady-state physical-based mathematical model for a direct expansion based enhanced dehumidification air conditioning system. International Journal of Refrigeration, 91 (2018), 55–68.

17. Chen and Deng, 2006
Chen, W., Deng, S.
Development of a dynamic model for a DX VAV air conditioning system. Energy Conversion and Management, 47, 18 (2006), 2900–2924.

18. Chen and Guo, 2009
Chen, Y., Guo, X.
Dynamic defrosting characteristics of air source heat pump and effects of outdoor air parameters on defrost cycle performance. Applied Thermal Engineering, 29, 13 (2009), 2701–2707.

19. Cheng and Shiu, 2002
Cheng, C.-H., Shiu, C.-C.
Frost formation and frost crystal growth on a cold plate in atmospheric air flow. International Journal of Heat and Mass Transfer, 45, 21 (2002), 4289–4303.

20. Cheung and Braun, 2014
Cheung, H., Braun, J. E.
Component-based, gray-box modeling of ductless multi-split heat pump systems. International Journal of Refrigeration, 38 (2014), 30–45.

21. Chi and Didion, 1982
Chi, J., Didion, D.
A simulation model of the transient performance of a heat pump. International Journal of Refrigeration, 5, 3 (1982), 176–184.

22. China 2015
Center of Science and Technology Development of The Ministry of Housing and Urban-Rural Development, People's Republic of China. Guidebook of Taking Air Thermal Energy as a Renewable Energy Source (In Chinese). (2015).

23. Choi et al., 2011
Choi, H.-J., Kim, B.-S., Kang, D., Kim, K. C.
Defrosting method adopting dual hot gas bypass for an air-to-air heat pump. Applied Energy, 88, 12 (2011), 4544–4555.

24. Choi and Kim, 2003
Choi, J. M., Kim, Y. C.
Capacity modulation of an inverter-driven multi-air conditioner using electronic expansion valves. Energy, 28, 2 (2003), 141–155.

25. Chung et al., 2017
Chung, M. H., Yang, Y. K., Lee, K. H., Lee, J. H., Moon, J. W.

Application of artificial neural networks for determining energy-efficient operating set-points of the VRF cooling system. Building and Environment, 125 (2017), 77–87.

26. Cui et al., 2011
Cui, J., Li, W. Z., Liu, Y., Zhao, Y. S.
A new model for predicting performance of fin-and-tube heat exchanger under frost condition. International Journal of Heat and Fluid Flow, 32, 1 (2011), 249–260.

27. D, 1967
D, Y. J.
An investigation of the thermal conductivity of frost while forming on a flat horizontal plate. ASHRAE Transactions, 73, 2 (1967), 1.1-1.11.

28. Da Silva et al., 2011
Da Silva, D. L., Hermes, C. J. L., Melo, C.
First-principles modeling of frost accumulation on fan-supplied tube-fin evaporators. Applied Thermal Engineering, 31, 14 (2011), 2616–2621.

29. Damasceno et al., 1990
Damasceno, G. S., Goldschmidt, V. W., Rooke, S. P.
Comparison of three steady-state heat pump computer models. ASHRAE Transactions (American Society of Heating, Refrigerating and Air-Conditioning Engineers); (United States), 96:2 (1990).

30. Deng, 2000
Deng S.
A dynamic mathematical model of a direct expansion (DX) water-cooled air-conditioning plant. Building and Environment, 35, 7 (2000), 603–613.

31. Ding 2007
Ding G.l.

Recent developments in simulation techniques for vapour-compression refrigeration systems. International Journal of Refrigeration, 30 (2007): 1119-1133.

32. Ding et al., 2004
Ding, Y., Ma, G., Chai, Q., Jiang, Y.
Experiment investigation of reverse cycle defrosting methods on air source heat pump with TXV as the throttle regulator. International Journal of Refrigeration, 27, 6 (2004), 671–678.

33. Domanski, 1991
Domanski, P. A.
Simulation of an Evaporator with Nonuniform One-Dimensional Air Distribution. NIST (1991).

34. Dutta et al., 2001
Dutta, A. K., Yanagisawa, T., Fukuta, M.
An investigation of the performance of a scroll compressor under liquid refrigerant injection. International Journal of Refrigeration, 24, 6 (2001), 577–587.

35. Eckert and Drake, 1987
Eckert, E. R. G., Drake, J.
Analysis of heat and mass transfer. (1987).

36. European 2009
Directive 2009/28/EC of the European Parliament and of the Council of 23 April 2009 on the promotion of the use of energy from renewable sources and amending and subsequently repealing Directives 2001/77/EC and 2003/30/EC. Official Journal of the European Union.http://eur-lex.europa. eu/legal-content/EN/TXT/PDF/?uri=CELEX:32009L0028&from=EN.(2009).

37. Fossa and Tanda, 2002
Fossa, M., Tanda, G.

Study of free convection frost formation on a vertical plate. Experimental Thermal and Fluid Science, 26, 6 (2002), 661–668.

38. Gao and Gong, 2011
Gao, T., Gong, J.
Modeling the airside dynamic behavior of a heat exchanger under frosting conditions. Journal of Mechanical Science and Technology, 25, 10 (2011), 2719.

39. Ge et al., 2016
Ge, Y., Sun, Y., Wang, W., Zhu, J., Li, L., Liu, J.
Field test study of a novel defrosting control method for air-source heat pumps by applying tube encircled photoelectric sensors. International Journal of Refrigeration, 66 (2016), 133–144.

40. Gerardo et al., 1999
Gerardo Díaz,Mihir Sen,K. T. Yang &Rodney L. McClain
Simulation of heat exchanger performance by artificial neural networks, 1999. Hvac&r Research, 5, 3 (1999), 195–208.

41. Gokhale et al., 2022
Gokhale, G., Claessens, B., Develder, C.
Physics informed neural networks for control oriented thermal modeling of buildings. Applied Energy, 314 (2022), 118852.

42. Gupta et al., 2007
Gupta, J. K., Ram Gopal, M., Chakraborty, S.
Modeling of a domestic frost-free refrigerator. International Journal of Refrigeration, 30, 2 (2007), 311–322.

43. Hadid, 2011
Hadid, Z.

Modeling Ice Formation On Heat exchangers Fins. (2011).

44. Han and Ro, 1999
Han, H. D., Ro, S. T.
The characteristics of frost growth on parallel plates; In K. Hutter, Y. Wang & H. Beer (Eds.), Advances in Cold-Region Thermal Engineering and Sciences. Berlin, Heidelberg: Springer (1999), 55–64.

45. HAYASHI et al., 1977
HAYASHI, Y., K, A., H, Y.
Study of frost formation based on a theoretical model of the frost layer. (1977).

46. Hermes et al., 2014
Hermes, C. J. L., Loyola, F. R., Nascimento, V. S.
A semi-empirical correlation for the frost density. International Journal of Refrigeration, 46 (2014), 100–104.

47. Hewitt and Huang, 2008
Hewitt, N., Huang, M. J.
Defrost cycle performance for a circular shape evaporator air source heat pump. International Journal of Refrigeration, 31, 3 (2008), 444–452.

48. Hoffenbecker et al., 2005
Hoffenbecker, N., Klein, S. A., Reindl, D. T.
Hot gas defrost model development and validation. International Journal of Refrigeration, 28, 4 (2005), 605–615.

49. Hongliang et al., 2009
Hongliang, L., Huanxin, C., Junlong, X., Hongge, T., Yunpeng, H.
Refrigerant flow distributary disequilibrium caused by configuration of two phase fluid pipe network. Energy Conversion and Management, 50, 3 (2009), 730–738.

50. Hu et al., 2021
Hu, J., Zheng, W., Zhang, S., Li, H., Liu, Z., Zhang, G., Yang, X.
Thermal load prediction and operation optimization of office building with a zone-level artificial neural network and rule-based control. Applied Energy, 300 (2021), 117429.

51. Huang et al., 2009a
Huang, D., Li, Q., Yuan, X.
Comparison between hot-gas bypass defrosting and reverse-cycle defrosting methods on an air-to-water heat pump. Applied Energy, 86, 9 (2009a), 1697–1703.

52. Huang et al., 2014
Huang, D., Ri-Jing, Z., Liu, Y., Yi, D.-B.
Effect of fin types of outdoor fan-supplied finned-tube heat exchanger on periodic frosting and defrosting performance of a residential air-source heat pump. Applied Thermal Engineering, 69, 1 (2014), 251–260.

53. Huang et al., 2004
Huang, D., Yuan, X., Zhang, X.
Effects of fan-starting methods on the reverse-cycle defrost performance of an air-to-water heat pump. International Journal of Refrigeration, 27, 8 (2004), 869–875.

54. Huang et al., 2009b
Huang, L., Liu, Z., Liu, Y., Gou, Y., Wang, J.
Experimental study on frost release on fin-and-tube heat exchangers by use of a novel anti-frosting paint. Experimental Thermal and Fluid Science, 33, 7 (2009b), 1049–1054.

55. Huang et al., 2019
Huang, S., Zuo, W., Lu, H., Liang, C., Zhang, X.
Performance comparison of a heating tower heat pump and an air-source heat pump: A comprehensive modeling and simulation study. Energy Conversion and Management, 180 (2019), 1039–1054.

56. Hwang and Cho, 2014
Hwang, J., Cho, K.
Numerical prediction of frost properties and performance of fin–tube heat exchanger with plain fin under frosting. International Journal of Refrigeration, 46 (2014), 59–68.

57. Ismail et al., 1997
Ismail, K. A. R., Salinas, C., Gonçalves, M. M.
Frost growth around a cylinder in a wet air stream. International Journal of Refrigeration, 20, 2 (1997), 106–119.

58. Ismail and Salinas, 1999
Ismail, K. A. R., Salinas, C. S.
Modeling of frost formation over parallel cold plates. International Journal of Refrigeration, 22, 5 (1999), 425–441.

59. Jia et al., 2006
Jia, C. X., Dai, Y. J., Wu, J. Y., Wang, R. Z.
Analysis on a hybrid desiccant air-conditioning system. Applied Thermal Engineering, 26, 17 (2006), 2393–2400.

60. Jia et al., 2007
Jia, C. X., Dai, Y. J., Wu, J. Y., Wang, R. Z.
Use of compound desiccant to develop high performance desiccant cooling system. International Journal of Refrigeration, 30, 2 (2007), 345–353.

61. Jia et al., 1995
Jia, X., Tso, C. P., Chia, P. K., Jolly, P.
A distributed model for prediction of the transient response of an evaporator. International Journal of Refrigeration, 18, 5 (1995), 336–342.

62. Jiang et al., 2006

Jiang, W., Khan, J., Dougal, R. A.
Dynamic centrifugal compressor model for system simulation. Journal of Power Sources, 158, 2 (2006), 1333–1343.

63. Jing et al., 2013
Jing, T., Kim, Y., Lee, S., Kim, D., Kim, J., Hwang, W.
Frosting and defrosting on rigid superhydrohobic surface. Applied Surface Science, 276 (2013), 37–42.

64. Joppolo et al., 2012
Joppolo, C. M., Molinaroli, L., De Antonellis, S., Merlo, U.
Experimental analysis of frost formation with the presence of an electric field on fin and tube evaporator. International Journal of Refrigeration, 35, 2 (2012), 468–474.

65. Kandula, 2011
Kandula, M. Frost growth and densification in laminar flow over flat surfaces. International Journal of Heat and Mass Transfer, 54, 15 (2011), 3719–3731.

66. Kim et al., 2015a
Kim, D., Kim, H., Kim, S. W., Kim, D. R., Lee, K.-S.
Experimental investigation of frost retardation for superhydrophobic surface using a luminance meter. International Journal of Heat and Mass Transfer, 87 (2015a), 491–496.

67. Kim and Cho, 2022
Kim, H.-J., Cho, Y.-H.
Optimization of supply air flow and temperature for VAV terminal unit by artificial neural network. Case Studies in Thermal Engineering, 40 (2022), 102511.

68. Kim et al., 2015b
Kim, J., Choi, H.-J., Kim, K. C.

A combined Dual Hot-Gas Bypass Defrosting method with accumulator heater for an air-to-air heat pump in cold region. Applied Energy, 147 (2015b), 344–352.

69. Kim et al., 2013
Kim, K., Kim, D. R., Lee, K.-S.
Local frosting behavior of a plated-fin and tube heat exchanger according to the refrigerant flow direction and surface treatment. International Journal of Heat and Mass Transfer, 64 (2013), 751–758.

70. Kim and Lee, 2011a
Kim, K., Lee, K.-S.
Effects of Surface Treatment on Frost Formation and Defrosting. Presented at the ASME/JSME 2011 8th Thermal Engineering Joint Conference, American Society of Mechanical Engineers Digital Collection (2011a).

71. Kim and Lee, 2011b
Kim, K., Lee, K.-S.
Frosting and defrosting characteristics of a fin according to surface contact angle. International Journal of Heat and Mass Transfer, 54, 13 (2011b), 2758–2764.

72. Kim and Lee, 2013
Kim, K., Lee, K.-S.
Frosting and defrosting characteristics of surface-treated louvered-fin heat exchangers: Effects of fin pitch and experimental conditions. International Journal of Heat and Mass Transfer, 60 (2013), 505–511.

73. Kim et al., 2017
Kim, M.-H., Kim, D. R., Lee, K.-S.
Stochastic approach to the anti-freezing behaviors of superhydrophobic surfaces. International Journal of Heat and Mass Transfer, 106 (2017), 841–846.

74. Klein and Alvarado 2002

Klein S. and Alvarado F.
EES-Engineering Equation Solver. F-Chart Software.

75. Kondepudi and O'Neal, 1989
Kondepudi, S. N., O'Neal, D. L.
Effect of frost growth on the performance of louvered finned tube heat exchangers. International Journal of Refrigeration, 12, 3 (1989), 151–158.

76. Kondepudi and O'Neal, 1993
Kondepudi, S. N., O'Neal, D. L.
Performance of finned-tube heat exchangers under frosting conditions: I. Simulation model. International Journal of Refrigeration, 16, 3 (1993), 175–180.

77. Kondepudi et al., 1995
Kondepudi, S., Murali, K., Lorsch, H., & Bhalerao, A. (1995).
Voiding HP evaporator frost through the use of desiccants. In ASME-JSESJSME International Solar Energy Conference (pp. 25-29).

78. Kwak and Bai, 2010
Kwak, K., Bai, C.
A study on the performance enhancement of heat pump using electric heater under the frosting condition: Heat pump under frosting condition. Applied Thermal Engineering, 30, 6 (2010), 539–543.

79. Kwon et al., 2006
Kwon, J.-T., Lim, H. J., Kwon, Y.-C., Koyama, S., Kim, D.-H., Kondou, C.
An experimental study on frosting of laminar air flow on a cold surface with local cooling. International Journal of Refrigeration, 29, 5 (2006), 754–760.

80. Le Gall et al., 1997
Le Gall, R., Grillot, J. M., Jallut, C.

Modelling of frost growth and densification. International Journal of Heat and Mass Transfer, 40, 13 (1997), 3177–3187.

81. Lee et al., 2004
Lee, H., Shin, J., Ha, S., Choi, B., Lee, J.
Frost formation on a plate with different surface hydrophilicity. International Journal of Heat and Mass Transfer, 47, 22 (2004), 4881–4893.

82. Lee and Lee, 2018
Lee, J., Lee, K.-S.
The behavior of frost layer growth under conditions favorable for desublimation. International Journal of Heat and Mass Transfer, 120 (2018), 259–266.

83. Lee et al., 1994
Lee, K. S., Lee, T. H., Kim, W. S.
Heat and Mass Transfer of Parallel Plate Heat Exchanger under Frosting Condition. Korean Journal of Air-Conditioning and Refrigeration Engineering, 6, 2 (1994), 155–165.

84. Lee et al., 2003
Lee, K.-S., Jhee, S., Yang, D.-K.
Prediction of the frost formation on a cold flat surface. International Journal of Heat and Mass Transfer, 46, 20 (2003), 3789–3796.

85. Lee et al., 1997
Lee, K.-S., Kim, W.-S., Lee, T.-H.
A one-dimensional model for frost formation on a cold flat surface. International Journal of Heat and Mass Transfer, 40, 18 (1997), 4359–4365.

86. Lee and Ro, 2001
Lee, Y. B., Ro, S. T.

An experimental study of frost formation on a horizontal cylinder under cross flow. International Journal of Refrigeration, 24, 6 (2001), 468–474.

87. Lee and Ro, 2002
Lee, Y. B., Ro, S. T.
Frost formation on a vertical plate in simultaneously developing flow. Experimental Thermal and Fluid Science, 26, 8 (2002), 939–945.

88. Lemmon et al., 2013
Lemmon, E. W., Huber, M. L., McLinden, M. O.
NIST Standard Reference Database 23: Reference Fluid Thermodynamic and Transport Properties-REFPROP, Version 9.1. NIST (2013).

89. Li et al., 2022
Li, F., Wu, S., Ma, Z., Zhao, R., Huang, D.
Effect of surface coating on defrosting water drainage characteristics of vertical-fin microchannel frosting evaporator. Applied Thermal Engineering, 208 (2022), 118220.

90. Li, 2013
Li, W.
Simplified modeling analysis of mass flow characteristics in electronic expansion valve. Applied Thermal Engineering, 53, 1 (2013), 8–12.

91. Li et al., 2020
Li, Z., Wang, W., Sun, Y., Liang, S., Deng, S., Lin, Y., Wu, X.
A novel defrosting initiating method for air source heat pumps based on the optimal defrosting initiating time point. Energy and Buildings, 222 (2020), 110064.

92. Liang et al., 2020
Liang, S., Wang, W., Sun, Y., Lin, Y., Luo, Q., Deng, S.

Field investigations on frosting suppression for variable-capacity ASHPs through optimizing their operations and configurations. Energy and Buildings, 224 (2020), 110266.

93. Liang and Wu, 2022
Liang, X., Wu, L.
A brief review: The mechanism; simulation and retardation of frost on the cold plane and evaporator surface. Energy and Buildings, 272 (2022), 112366.

94. Lin et al., 2019
Lin, Y., Wang, W., Sun, Y., Liu, J., Deng, S.
A field study on the effects of outdoor coil fouling at different ambient air temperatures on the operating performances of a space cooling ASHP unit. Energy and Buildings, 183 (2019), 639–649.

95. Liu et al., 2007a
Liu, D., Zhao, F.-Y., Tang, G.-F.
Frosting of heat pump with heat recovery facility. Renewable Energy, 32, 7 (2007a), 1228–1242.

96. Liu et al., 2004
Liu, J., Wei, W., Ding, G., Zhang, C., Fukaya, M., Wang, K., Inagaki, T.
A general steady state mathematical model for fin-and-tube heat exchanger based on graph theory. International Journal of Refrigeration, 27, 8 (2004), 965–973.

97. Liu et al., 2023
Liu, K., Lin, T., Zhong, T., Ge, X., Jiang, F., Zhang, X.
New methods based on a genetic algorithm back propagation (GABP) neural network and general regression neural network (GRNN) for predicting the occurrence of trihalomethanes in tap water. Science of The Total Environment (2023), 161976.

98. Liu et al., 2006

Liu, Z., Wang, H., Zhang, X., Meng, S., Ma, C.
An experimental study on minimizing frost deposition on a cold surface under natural convection conditions by use of a novel anti-frosting paint. Part I. Anti-frosting performance and comparison with the uncoated metallic surface. International Journal of Refrigeration, 29, 2 (2006), 229–236.

99. Liu et al., 2007b
Liu, Z., Zhang, X., Wang, H., Meng, S., Cheng, S.
Influences of surface hydrophilicity on frost formation on a vertical cold plate under natural convection conditions. Experimental Thermal and Fluid Science, 31, 7 (2007b), 789–794.

100. Lu et al., 2022
Lu, H., Fang, N., Wang, L.
Signal identification based on modified filter bank feature and generalized regression neural network for optical fiber perimeter sensing. Optical Fiber Technology, 72 (2022), 102993.

101. Lüer and Beer, 2000
Lüer, A., Beer, H.
Frost deposition in a parallel plate channel under laminar flow conditions. International Journal of Thermal Sciences, 39, 1 (2000), 85–95.

102. MacArthur and Grald, 1987
MacArthur, J. W., Grald, E. W.
Prediction of cyclic heat pump performance with a fully distributed model and a comparison with experimental data. ASHRAE Trans.; (United States), 93:2 (1987).

103. Mago and Sherif, 2003
Mago, P. J., Sherif, S. A.
Heat and mass transfer on a cylinder surface in cross flow under supersaturated frosting conditions. International Journal of Refrigeration, 26, 8 (2003), 889–899.

104. Mei and Levermore 2002
Mei L. and Levermore G.
Simulation and validation of a VAV system with an ANN fan model and a non-linear VAV box model. Building and Environment, 37 (2002): 277-284.

105. Min et al., 2000
Min, J., Webb, R. L., Bemisderfer, C. H.
Long-Term Hydraulic Performance of Dehumidifying Heat-Exchangers With and Without Hydrophilic Coatings. HVAC&R Research, 6, 3 (2000), 257–272.

106. Minglu et al., 2010
Minglu, Q., Liang, X., Deng, S., Yiqiang, J.
Improved indoor thermal comfort during defrost with a novel reverse-cycle defrosting method for air source heat pumps. Building and Environment, 45, 11 (2010), 2354–2361.

107. Moallem et al., 2012a
Moallem, E., Cremaschi, L., Fisher, D. E., Padhmanabhan, S.
Experimental measurements of the surface coating and water retention effects on frosting performance of microchannel heat exchangers for heat pump systems. Experimental Thermal and Fluid Science, 39 (2012a), 176–188.

108. Moallem et al., 2012b
Moallem, E., Padhmanabhan, S., Cremaschi, L., Fisher, D. E. Experimental investigation of the surface temperature and water retention effects on the frosting performance of a compact microchannel heat exchanger for heat pump systems. International Journal of Refrigeration, 35, 1 (2012b), 171–186.

109. Na and Webb, 2003
Na, B., Webb, R. L.

A fundamental understanding of factors affecting frost nucleation. International Journal of Heat and Mass Transfer, 46, 20 (2003), 3797–3808.

110. Negrelli and Hermes, 2015
Negrelli, S., Hermes, C. J. L.
A semi-empirical correlation for the thermal conductivity of frost. International Journal of Refrigeration, 58 (2015), 243–252.

111. Nielsen et al., 2009
Nielsen, T. R., Rose, J., Kragh, J.
Dynamic model of counter flow air to air heat exchanger for comfort ventilation with condensation and frost formation. Applied Thermal Engineering, 29, 2 (2009), 462–468.

112. Okoroafor and Newborough, 2000
Okoroafor, E. U., Newborough, M.
Minimising frost growth on cold surfaces exposed to humid air by means of crosslinked hydrophilic polymeric coatings. Applied Thermal Engineering, 20, 8 (2000), 737–758.

113. Oskarsson et al., 1990
Oskarsson, S. P., Krakow, K. I., Lin, S. (1990).
Evaporator Models for Operation with Dry, Wet, and Frosted Finned Surfaces, Part II: Evaporator Models and Verification. ASHRAE Transactions, 96(1), 381-392.

114. O'Neal et al., 1991
O'Neal, D. L., Peterson, K., Anand, N. K.
Effect of short-tube orifice size on the performance of an air source heat pump during the reverse-cycle defrost. International Journal of Refrigeration, 14, 1 (1991), 52–57.

115. O'Neal and Tree, 1984
O'Neal, D., Tree, D. R.

Measurement of frost growth and density in a parallel plate geometry. ASHRAE Transactions, 90 (1984), 278–290.

116. Östin and Andersson, 1991
Östin, R., Andersson, S.
Frost growth parameters in a forced air stream. International Journal of Heat and Mass Transfer, 34, 4 (1991), 1009–1017.

117. P, 1990
P, O. S.
Evaporator models for operation with dry, wet, and frosted finned surfaces. ASHRAE Trans, 96, 1 (1990), 373–380.

118. Pan et al., 2012
Yan, P., Xiangguo, X., Liang, X., Shiming, D.
A modeling study on the effects of refrigerant pipeline length on the operational performance of a dual-evaporator air conditioning system. Applied Thermal Engineering, 39 (2012), 15–25.

119. Park et al., 2007
Park, C., Cho, H., Lee, Y., Kim, Y.
Mass flow characteristics and empirical modeling of R22 and R410A flowing through electronic expansion valves. International Journal of Refrigeration, 30, 8 (2007), 1401–1407.

120. Park et al., 2016
Park, J.-S., Kim, D. R., Lee, K.-S.
Frosting behaviors and thermal performance of louvered fins with unequal louver pitch. International Journal of Heat and Mass Transfer, 95 (2016), 499–505.

121. Pedrycz, 1993

Pedrycz, W.

Fuzzy control and fuzzy systems. Research Studies Press Ltd..

122. Piucco et al., 2008

Piucco, R. O., Hermes, C. J. L., Melo, C., Barbosa, J. R.

A study of frost nucleation on flat surfaces. Experimental Thermal and Fluid Science, 32, 8 (2008), 1710–1715.

123. Polat and Yıldırım., 2008

Polat, Ö., Yıldırım, T.

Genetic optimization of GRNN for pattern recognition without feature extraction. Expert Systems with Applications, 34, 4 (2008), 2444–2448.

124. Qin et al., 2014

Qin HJ, Li WZ, Zhu WY.

Simulation and experiment on the performances of an air cooler with variable fin pitch in frosting conditions. Journal of Thermal Science and Technology (in Chinese) 2014 (13) 206-212.

125. Qu et al., 2020

Qu, C., Qin, J., Guo, Q.

Urban Ecological Risk Assessment Based on Improved Analytic Hierarchy Process. In 2020 16th Dahe Fortune China Forum and Chinese High-educational Management Annual Academic Conference (DFHMC) (2020), 35–41.

126. Qu et al., 2006

Qu, K., Komori, S., Jiang, Y.

Local variation of frost layer thickness and morphology. International Journal of Thermal Sciences, 45, 2 (2006), 116–123.

127. Rasmussen et al., 2002

Rasmussen, B. P., Shah, R., Musser, A. B., Alleyne, A. G., Bullard, C. W., Hrnjak, P. S., Miller, N. R.

Control-Oriented Modeling of Transcritical Vapor Compression Systems. Air Conditioning and Refrigeration Center TR-204 (2002).

128. Rite, 1990

Rite, R. W.

The Effect of Frosting on the Performance of Domestic Refrigerator-Freezer Finned Tube Evaporator Coils. Air Conditioning and Refrigeration Center TR-01 (1990).

129. Ross, 2015.

Ross, I. M.

A primer on Pontryagin's principle in optimal control. Collegiate publishers.

130. Sanders, 1974

Sanders, C. T.

The influence of frost formation and defrosting on the performance of air coolers. PhD. Thesis (1974, September 1).

131. Savadkoohi et al., 2023

Savadkoohi, M., Macarulla, M., Casals, M.

Facilitating the implementation of neural network-based predictive control to optimize building heating operation. Energy, 263 (2023), 125703.

132. Seker et al., 2004

Seker, D., Karatas, H., Egrican, N.

Frost formation on fin-and-tube heat exchangers. Part I—Modeling of frost formation on fin-and-tube heat exchangers. International Journal of Refrigeration, 27, 4 (2004), 367–374.

133. Shah et al., 2003
Shah, R., Alleyne, A. G., Bullard, C. W., Rasmussen, B. P., Hrnjak, P. S.
Dynamic Modeling And Control of Single and Multi-Evaporator Subcritical Vapor Compression Systems. Air Conditioning and Refrigeration Center TR-216 (2003).

134. Shangwen et al., 2022
Shangwen, L., Mengjie, S., Chaobin, D., Yingjie, X., Keke, S.
Experimental study on the effect of surface temperature on the frost characteristics of an inverted cold plate under natural convection. Applied Thermal Engineering, 211 (2022), 118470.

135. Shapiro et al., 2012
Shapiro, C., Puttagunta, S., Owens, D.
Measure Guideline: Heat Pump Water Heaters in New and Existing Homes' (No. NREL/SR-5500-53184; DOE/GO-102012-3456); National Renewable Energy Lab. (NREL), Golden, CO (United States) (2012).

136. Sommers et al., 2018
Sommers, A. D., Gebhart, C. W., Hermes, C. J. L.
The role of surface wettability on natural convection frosting: Frost growth data and a new correlation for hydrophilic and hydrophobic surfaces. International Journal of Heat and Mass Transfer, 122 (2018), 78–88.

137. Song et al., 2016a
Song, M., Chen, A., Mao, N.
An experimental study on defrosting performance of an air source heat pump unit with a multi-circuit outdoor coil at different frosting evenness values. Applied Thermal Engineering, 94 (2016a), 331–340.

138. Song and Dang, 2018
Song, M., Dang, C.
Review on the measurement and calculation of frost characteristics. International Journal of Heat and Mass Transfer, 124 (2018), 586–614.

139. Song et al., 2016b
Song, M., Deng, S., Mao, N., Ye, X.
An experimental study on defrosting performance for an air source heat pump unit with a horizontally installed multi-circuit outdoor coil. Applied Energy, 165 (2016b), 371–382.

140. Song et al., 2017
Song, M., Liu, S., Deng, S., Sun, Z., Yan, H.
Experimental investigation on reverse cycle defrosting performance improvement for an ASHP unit by evenly adjusting the refrigerant distribution in its outdoor coil. Applied Thermal Engineering, 114 (2017), 611–620.

141. Song et al., 2016c
Song, M., Mao, N., Deng, S., Xia, Y., Chen, Y.
An experimental study on defrosting performance for an air source heat pump unit at different frosting evenness values with melted frost local drainage. Applied Thermal Engineering, 99 (2016c), 730–740.

142. Song et al., 2016d
Song, M., Xia, L., Deng, S.
A modeling study on alleviating uneven defrosting for a vertical three-circuit outdoor coil in an air source heat pump unit during reverse cycle defrosting. Applied Energy, 161 (2016d), 268–278.

143. Song et al., 2016e
Song, M., Xia, L., Mao, N., Deng, S.

An experimental study on even frosting performance of an air source heat pump unit with a multi-circuit outdoor coil. Applied Energy, 164 (2016e), 36–44.

144. Storey and Jacobi, 1999
Storey, B. D., Jacobi, A. M.
The effect of streamwise vortices on the frost growth rate in developing laminar channel flows. International Journal of Heat and Mass Transfer, 42, 20 (1999), 3787–3802.

145. Su et al., 2017
Su, W., Li, W., Zhang, X.
Simulation analysis of a novel no-frost air-source heat pump with integrated liquid desiccant dehumidification and compression-assisted regeneration. Energy Conversion and Management, 148 (2017), 1157–1169.

146. Taleizadeh et al., 2013
Taleizadeh, A. A., Niaki, S. T. A., Aryanezhad, M.-B., Shafii, N.
A hybrid method of fuzzy simulation and genetic algorithm to optimize constrained inventory control systems with stochastic replenishments and fuzzy demand. Information Sciences, 220 (2013), 425–441.

147. Tao et al., 1993
Tao, Y.-X., Besant, R. W., Rezkallah, K. S.
A mathematical model for predicting the densification and growth of frost on a flat plate. International Journal of Heat and Mass Transfer, 36, 2 (1993), 353–363.

148. Tokura et al., 1988
Tokura, I., Saito, H., Kishinami, K.
Prediction of growth rate and density of frost layer developing under forced convection. Wärme - Und Stoffübertragung, 22, 5 (1988), 285–290.

149. Trammel et al., 1968
Trammel, G. J., Little, D. C., Killgore, E. M.

A study of frost formed on a flat plate held at sub-freezing temperature. ASHRAE Journal, 10(7), 42-47.

150. Tudor and Ohadi, 2006
Tudor, V., Ohadi, M.
The effect of stationary and sweeping frequency AC electric fields on frost crystal removal on a cold plate. International Journal of Refrigeration, 29, 4 (2006), 669–677.

151. Turaga et al., 1988
Turaga, M., Lin, S., Fazio, P. P.
Correlations for heat transfer and pressure drop factors for direct expansion air cooling and dehumidifying coils. ASHRAE Transactions, 94 (1988), 616–630.

152. Vargas and Parise, 1995
Vargas, J. V. C., Parise, J. A. R.
Simulation in transient regime of a heat pump with closed-loop and on-off control. International Journal of Refrigeration, 18, 4 (1995), 235–243.

153. Wang et al., 2002
Wang, C.-C., Hwang, Y.-M., Lin, Y.-T.
Empirical correlations for heat transfer and flow friction characteristics of herringbone wavy fin-and-tube heat exchangers. International Journal of Refrigeration, 25, 5 (2002).

154. Wang et al., 2004
Wang, C.-C., Huang, R.-T., Sheu, W.-J., Chang, Y.-J.
Some observations of the frost formation in free convection: with and without the presence of electric field. International Journal of Heat and Mass Transfer, 47, 14 (2004), 3491–3505.

155. Wang et al., 2015
Wang, F., Liang, C., Yang, M., Fan, C., Zhang, X.

Effects of surface characteristic on frosting and defrosting behaviors of fin-tube heat exchangers. Applied Thermal Engineering, 75 (2015), 1126–1132.

156. Wang et al., 2018
Wang, F., Liang, C., Zhang, X.
Experimental study on frost suppression for ASHP combining superhydrophobic heat exchanger and air flow. Applied Thermal Engineering, 136 (2018), 666–673.

157. Wang and Touber, 1991
Wang, H., Touber, S.
Distributed and non-steady-state modelling of an air cooler. International Journal of Refrigeration, 14, 2 (1991), 98–111.

158. Wang and Liu, 2005
Wang, S. W., Liu, Z. Y.
A new method for preventing HP from frosting. Renewable Energy, 30, 5 (2005), 753–761.

159. Wang et al., 2019
Wang, W., Cui, Y., Sun, Y., Deng, S., Wu, X., Liang, S.
A new performance index for constant speed air-source heat pumps based on the nominal output heating capacity and a related modeling study. Energy and Buildings, 184 (2019), 205–215.

160. Wang et al., 2013a
Wang, W., Feng, Y. C., Zhu, J. H., Li, L. T., Guo, Q. C., Lu, W. P.
Performances of air source heat pump system for a kind of mal-defrost phenomenon appearing in moderate climate conditions. Applied Energy, 112 (2013a), 1138–1145.

161. Wang et al., 2013b
Wang, W., Xiao, J., Feng, Y., Guo, Q., Wang, L.

Characteristics of an air source heat pump with novel photoelectric sensors during periodic frost–defrost cycles. Applied Thermal Engineering, 50, 1 (2013b), 177–186.

162. Wang et al., 2011
Wang, W., Xiao, J., Guo, Q. C., Lu, W. P., Feng, Y. C.
Field test investigation of the characteristics for the air source heat pump under two typical mal-defrost phenomena. Applied Energy, 88, 12 (2011), 4470–4480.

163. Wang et al., 2017
Wang, Z., Wang, F., Wang, X., Ma, Z., Wu, X., Song, M.
Dynamic character investigation and optimization of a novel air-source heat pump system. Applied Thermal Engineering, 111 (2017), 122–133.

164. Wu and Webb, 2001
Wu, X. M., Webb, R. L.
Investigation of the possibility of frost release from a cold surface. Experimental Thermal and Fluid Science, 24, 3 (2001), 151–156.

165. Winkler et al. 2008
Winkler J., Aute V. and Radermacher R.
Comprehensive investigation of numerical methods in simulating a steady-state vapor compression system. International Journal of Refrigeration, 31 (2008): 930-942.

166. Xiao et al., 2010
Xiao, J., Wang, W., Guo, Q. C., Zhao, Y. H.
An experimental study of the correlation for predicting the frost height in applying the photoelectric technology. International Journal of Refrigeration, 33, 5 (2010), 1006–1014.

167. Xiao et al., 2009
Xiao, J., Wang, W., Zhao, Y. H., Zhang, F. R.

An analysis of the feasibility and characteristics of photoelectric technique applied in defrost-control. International Journal of Refrigeration, 32, 6 (2009), 1350–1357.

168. Yamakawa et al., 1972

Yamakawa, N., Takahashi, N., Ohtani, S. (1972).
Forced convection heat and mass transfer under frost conditions. Heat transfer-Japanese research, 1(2), 1-10.

169. Yan et al., 2003

Yan, W.-M., Li, H.-Y., Wu, Y.-J., Lin, J.-Y., Chang, W.-R.
Performance of finned tube heat exchangers operating under frosting conditions. International Journal of Heat and Mass Transfer, 46, 5 (2003), 871–877.

170. Yang et al., 2006

Yang, D.-K., Lee, K.-S., Cha, D.-J.
Frost formation on a cold surface under turbulent flow. International Journal of Refrigeration, 29, 2 (2006), 164–169.

171. Yao et al., 2004

Yao, Y., Jiang, Y., Deng, S., Ma, Z.
A study on the performance of the airside heat exchanger under frosting in an air source heat pump water heater/chiller unit. International Journal of Heat and Mass Transfer, 47, 17 (2004), 3745–3756.

172. Ye and Lee, 2013

Ye, H.-Y., Lee, K.-S.
Performance prediction of a fin-and-tube heat exchanger considering air-flow reduction due to the frost accumulation. International Journal of Heat and Mass Transfer, 67 (2013), 225–233.

173. Yun et al., 2002

Yun, R., Kim, Y., Min, M.
Modeling of frost growth and frost properties with airflow over a flat plate. International Journal of Refrigeration, 25, 3 (2002), 362–371.

174. Zhang et al., 2010
Zhang, L., Dang, C., Hihara, E.
Performance analysis of a no-frost hybrid air conditioning system with integrated liquid desiccant dehumidification. International Journal of Refrigeration, 33, 1 (2010), 116–124.

175. Zhang et al., 2012a
Zhang, L., Fujinawa, T., Saikawa, M.
A new method for preventing air-source heat pump water heaters from frosting. International Journal of Refrigeration, 35, 5 (2012a), 1327–1334.

176. Zhang et al., 2012b
Zhang, L., Hihara, E., Saikawa, M.
Combination of air-source heat pumps with liquid desiccant dehumidification of air. Energy Conversion and Management, 57 (2012b), 107–116.

177. Zhang et al., 2018
Zhang, L., Jiang, Y., Dong, J., Yao, Y., Deng, S.
An experimental study of frost distribution and growth on finned tube heat exchangers used in air source heat pump units. Applied Thermal Engineering, 132 (2018), 38–51.

178. Zhang et al., 2022
Zhang, L., Song, M., Mao, N., Dong, J.
Temporal and spatial frost growth prediction of a tube-finned heat exchanger considering frost distribution characteristics. International Journal of Heat and Mass Transfer, 183 (2022), 122192.

179. Zhang et al., 2023
Zhang, T., Chen, L., Wang, J.
Multi-objective optimization of elliptical tube fin heat exchangers based on neural networks and genetic algorithm. Energy, 269 (2023), 126729.

180. Zhang, 2006
Zhang, Q.
Development of the typical meteorological database for Chinese locations. Energy and Buildings, 38, 11 (2006), 1320–1326.

181. Zhu et al., 2015a
Zhu, J. H., Sun, Y. Y., Wang, W., Deng, S. M., Ge, Y. J., Li, L. T.
Developing a new frosting map to guide defrosting control for air-source heat pump units. Applied Thermal Engineering, 90 (2015a), 782–791.

182. Zhu et al., 2015b
Zhu, J., Sun, Y., Wang, W., Ge, Y., Li, L., Liu, J.
A novel Temperature–Humidity–Time defrosting control method based on a frosting map for air-source heat pumps. International Journal of Refrigeration, 54 (2015b), 45–54.

183. Zuo et al., 2017
Zuo, Z., Liao, R., Zhao, X., Song, X., Qiao, Z., Guo, C., et al.
Anti-frosting performance of superhydrophobic surface with ZnO nanorods. Applied Thermal Engineering, 110 (2017), 39–48.